Influence of alternative raw materials on autoclaved aerated concrete

Boesten, E.P.M.

Award date:
2012

Technische Universiteit
Eindhoven
University of Technology

Influence of alternative raw materials on autoclaved aerated concrete

August 27, 2012

Author
E.P.M. (Ellen) Boesten
Student number: 0726532
/ Department of the Built Environment at Eindhoven University of Technology
/ Unit Building Physics and Services

Where innovation starts

Influence of alternative raw materials on autoclaved aerated concrete

Author
E.P.M. (Ellen) Boesten
Student number: 0726532

Supervisors University
prof. dr. ir. H.J.H. (Jos) Brouwers
G. (George) Quercia Bianchi (PhD candidate)
/ Department of the Built Environment at Eindhoven University of Technology
/ Unit Building Physics and Services

Supervisors Company
H. (Hans) van den Broek
L. (Ladislaus) Heinz
/ HESS AAC Systems B.V.

Address Eindhoven University of Technology

Department of the Built Environment
Den Dolech 2, 5612 AZ Eindhoven
Postbus 513, 5600 MB Eindhoven
The Netherlands

In collaboration with

HESS AAC Systems B.V.
Aluminiumsteden 10
7547 TN Enschede
The Netherlands

I PREFACE

I would like to thank my supervisors, starting with: Prof. Dr. ir Jos Brouwers, for the opportunity to participate in this project; Ladislaus Heinz and Hans van den Broek of HESS AAC Systems B.V. for supporting and motivating me in every practical way; George Quercia Bianchi, for his valuable advice and helping me with the field emission scanning electron microscopy and X-ray diffraction measurements; Mr. Peter Cappon and Mr. Geert-Jan Maas for the technical support in the laboratory; Dipl. Eng. Miruna Florea for sharing her knowledge regarding several additives and finally I would like to thank drs. Arno Keulen for his advice regarding paper sludge ash.

Ellen Boesten

Eindhoven, August 2012

II SUMMARY

This research is formulated in cooperation with HESS AAC Systems B.V., a manufacturer of machines and plants for producing autoclaved aerated concrete (AAC) and sand-lime bricks. The subject of this research was to investigate the possibility of the partly replacement of the raw materials quartz and Portland cement in AAC, within the current process constraints. AAC is produced of cement, lime, gypsum, quartz and the rising agent aluminum which are all mixed together with water. The mixture cures at ambient temperature and autoclaved later on. A characteristic property of AAC is the low density, due to a high porosity of 70-80 %, which results in excellent thermal insulation properties and a reasonable compressive strength (CS).

In this study, waste products of other industrial processes in The Netherlands were used as additives, the used waste products are: cyclone ash, paper sludge ash, bio ash, bottom ash and fly ash. Additionally, the waste material Indian fly ash, which has already been used in AAC production, was applied. A literature review was conducted prior to the experimental work to define the impact of the partly substitution of additives on the AAC performance and is reported up front. A separated literature review introduces the involved reaction equations for AAC and the substituted additives.

The AAC process consists of the following phases: (I) mixing, (II) curing and, (III) autoclaving. Tests were conducted on the mixture, during the curing and after autoclaving (on the final product). These measurements define the composition, performance of curing and the physical and chemical properties of the final product. To obtain a satisfactory product it is essential that the rising and stiffening development during the curing period are within predefined limits. A balanced mixture is needed to get the required reaction rate which is controlled and adapted by changing the aluminum powder and water/solid (w/s) ratio. Experiments were conducted with different substitution ratios.

It is seen that an optimal mixture composition and optimal development reaction rate are essential for producing AAC with a potentially high CS for all the additives. Based on the semi-quantitative analysis by field emission scanning electron microscopy (FESEM) it can be concluded that the influence of the pore diameter and the homogeneity of the macropores formation are of significant importance. All additives resulted in a different crystal grow at the surface of the pores.

Paper sludge ash used as substitution shows the best performance because of the highest CS, low porosity and high homogeneity of the AAC pore distribution. Paper sludge ash can replace Portland cement at least up to 50 %, yielding similar CS with slightly higher density, compared to the reference. Bottom ash substitution results in a relatively sufficient CS. Cyclone ash produces a low CS and the highest porosity. All other used ashes, give poor CS due to the not optimal mixture composition and reaction conditions (curing and autoclaving). Bio ash delivers a specific problem due to the formation of phosphates. The color of the final products of all substitutions was similar to the reference color, except for the bio ash and bottom ash substitution samples.

In general, it can be said that the additive has an impact on the quality and performance of CS and porosity, while it is of major importance to have a constant (oxide) composition and particle size distribution (PSD). More substantial research is needed to optimize the reaction mixture and processing conditions during curing and autoclaving.

The replacement of quartz by additives seems only relevant with respect to sustainability (immobilizing solid waste, reducing landfill). All additives however are potential substitutes for quartz, but more research is needed to optimize the reaction mixture and processing conditions during curing and autoclaving. Applying bio ash requires upfront phosphate removal to be sustainable and successful in AAC.

It is advisable to optimizing one promising additive based on the currently generated data, after a thorough review of the origin and economics of the particular additive. It is recommended to using paper sludge ash at a low concentration as a substitute for Portland cement in the production process of AAC. Finally, research to optimize cyclone ash as a quartz substitution should be undertaken.

TABLE OF CONTENTS

1. INTRODUCTION

1.1 BACKGROUND

This research is formulated in cooperation with HESS AAC Systems B.V., a manufacturer of machines and plants to produce AAC and sand-lime bricks. About thirty years ago HESS AAC Systems B.V. became active on the AAC market, concentrating mainly on manufacturing, installing and maintaining the production machinery for the world market leaders in AAC. Nowadays, AAC is increasingly used by developers, architects, and home builders.

AAC products are used for both internal and external construction such as blocks, walls, floor and roof panels, and lintels. AAC is made of cement, lime, quartz, gypsum or anhydrite, and water. Aluminum powder is added to the mixture to let it rise, resulting in 70-80 % air voids, which are responsible for the two most essential characteristics of AAC, namely light-weight and excellent thermal insulation properties. The industrial production of AAC takes place as follows: firstly, all raw materials are mixed in water and are left to cure at ambient temperature in a mould. Afterwards the mixture is autoclaved at a temperature reaching 180 °C with a pressure up till ± 12 bar for in total of 12 h. During the autoclaving period quartz (SiO_2) reacts with calcium hydroxide ($Ca(OH_2)$) to form calcium silica hydrates (C-S-H). C-S-H is a gel phase which can be transformed into tobermorite during autoclaving. Tobermorite contains a stronger crystal structure compared to C-S-H gel.

AAC is one of building materials that follows the recent trend to use alternative raw materials, since they are less expensive than primary raw materials and they may reduce the CO_2 footprint of the product. In this research alternative material, by-products from different industries, are evaluated. The most common alternative materials are fly ash, bottom ash, and slag. These materials are reactive (pozzolanic) materials and some of these have cementitious properties.

1.2 STATE OF THE ART

This research has a relation with previous scientific articles regarding secondary materials in the production of AAC and with the preliminary study of Boesten (2012) which describes the state-of-the-art, delineated to this topic. The preliminary research gives a qualitative overview of the state-of-the-art of physical, functional and chemical properties, and an overview of substitution materials already used in AAC recipes.

Important aspects, found in literature, influencing the formation of C-S-H (I) gel and tobermorite 11.30 Å are as follows: chemical composition, particle size distribution (PSD), specific surface and water absorbance ability. These all have a significant influence on the hydration. The reaction rate is mainly influenced by the nature and distribution of the raw material and the processing temperature. The C-S-H crystallinity increases, resulting in either higher or lower strength depending on the amount of unreacted quartz (Mitsuda et al., 1992). Also, finer quartz will reduce the processing time, which can have economical benefits (Mitsuda et al., 1992); (Isu et al., 1995); (Chan et al., 1987). Next, finer quartz could supply larger amounts of dissolved silica, resulting in the formation of smaller crystals with lower crystallinity (Aroni, 1993). Additional, the hydrothermal reaction in the Ca/Si ratio are controlled by the dissolution of quartz (Isu et al., 1995); (Aroni, 1993); (Mitsuda et al., 1992); (Okada et al., 1990); (Chan et al., 1987); (Kondo, 1967). On the other hand, water is a key component in the dissolving of silica and lime (Chan et al., 1987). The optimum water ratio is depending on the water absorption capacity and surface area of the raw materials. The mixture will not rise sufficiently during the hydration phase if the water amount is too little.

The objective of scientific articles concerning the substitution of primary materials by alternative materials is to analyze the overall microstructural properties and phase compositions. This in order to obtain a shorter autoclaving time and/or lower autoclaving temperature, resulting in the reduction of production costs and in some cases a higher CS of the AAC. So far, the following alternative materials were implemented in the AAC mixtures: water cooled ground granulate blast furnace slag (GGBFS), wet-bottom boiler slag (WBBS), alkali-activated slag (AAS), air-cooled blast furnace slag (ACBFS), metakaolin (MK), dry coal bottom ash (CBA) and fly ash (FA). These materials can replace either cement or quartz, depending on their chemical composition, PSD,

physical properties, color and method of preparing like grinding. FA and MK have comparable, (almost the same), specific surfaces as cement. The specific surface of GGBS, BFS, WBBS are higher in comparison with cement. Based on the found chemical composition, FA and MK have the properties to substitute quartz, since they have a high SiO_2 level. Secondly, based on the high calcium level, GGBS and BFWS are perhaps potential substitution products. Finally, a disadvantage could be the change in color of the end product compared to the reference.

1.3 AIM AND PROBLEM STATEMENT

AIM

HESS AAC Systems B.V. sells AAC factories and, advises and assists buyers to optimize the AAC manufacturing process. They like to know how the AAC mixture can be optimized with economical benefits. For this research the Dutch market is taken as a reference. The main goal of the present research is to discover which alternative materials of Dutch origin can replace a conventional raw material, while maintaining or preferably improving the specific characteristics. The following characteristics will be analyzed: CS, dry density, porosity, thermal conductivity, color, crystallographic structure, surface topography and composition. This could lead to an improvement of the quality and reduce recipe costs. The characteristics of the new product should be in line with the requirements of the original product. The practical relevance of this research is to create a sustainable product.

PROBLEM STATEMENT

The present research is restricted to economically improve the sustainability, but most of all, to optimize the current AAC recipe. The Dutch market, however, is very critical and not tolerant if it comes to product changes. One of the contradictions of the Dutch market is that a less expensive sustainable product is interesting but it is expected to have similar qualities as the original product. For example, a change of the product color, or a decrease in quality such as a reduction of CS or an increase in density is not desirable. The question is “How to deal with these restrictions”.

First the color change of the product is affected by the choice, the quantity and the composition of ingredients in the recipe. Color changes can be foreseen and taken into account, and be solved before preparing the recipe. Darker colored materials of secondary sources can lead to a darker final product.

The second constraint, a reduction of product quality is also affected by the choice of the ingredients and the quantity of the composition of the ingredients in the overall recipe. It is important to know the chemical composition, particle size distribution and physical characteristics of all the ingredients before mixing. In this case one variable, the desired C-S-H phase formation (tobermorite) calculated by the Ca/Si ratio, ranging between 0.8-1.0, can be calculated before mixing. However the actual tobermorite formation, which influences the strength, cannot be calculated beforehand. Unfortunately, the desired strength is only measurable after having produced the product.

Thirdly, the density needs to be, desirably, within range of 300-500 kg/m^3, since this is the target value for the Dutch market. The porosity is achieved by aluminum powder, which reacts with calcium hydroxide and water to form hydrogen gas, and thus creating voids in the mixture. And as mentioned above the Ca/Si ratio is very critical. In summary, the chemical composition of all the ingredients might affects the final density.

1.4 OBJECTIVE AND RESEARCH QUESTIONS

This experimental study is embedded within the strive for developing a sustainable and cheaper AAC product focusing on the Dutch market. The primary objective of this study is to determine the advantages and disadvantages of the substitution of quartz and Portland cement by materials of secondary sources in order to create a sustainable and more economically AAC product. In order to fulfill this objective, the following research questions need to be dealt with:

1. What are the possibilities and restrictions of materials of secondary source incorporated into AAC?
2. What is the performance of the new product?
3. What role can the new product play in sustainability and promoting future developments?

The following research question is formed:

Which materials of secondary source produced in The Netherlands can partly replace a primary binding agent in the AAC recipe while remaining the original product properties with a density range of 300-500 kg/m^3, thereby showing little to no discoloration and being in line with Dutch regulations?

1.5 METHODOLOGY

MEASUREMENTS

The original product specification criteria are: color, density, porosity, CS and thermal conductivity. These aspects will be measured. The samples are analyzed and compared as to which kind of substitution material and substitution level is the most promising. Additionally, the tobermorite structure of each test sample will be analyzed by X-ray diffraction (XRD) and FESEM.

SUBSTITUTION MATERIALS AND DISTRIBUTION

The choice of substitution materials is based on their availability and properties such as specific surface, color, calcium and silica content. The following substitution materials are selected: cyclone ash (HVC), paper sludge ash, bottom ash, bio ash (SNB), Dutch fly ash and Indian fly ash. The composition of the test samples recipe including the substitution materials are varied in a range between 0-15 in steps of 5 %, (by dry mass).

1.6 OUTLINE OF THE THESIS

The research is structured into two parts. Firstly, Chapters 2 is the theory based on literature study introducing the reactions, information regarding additives used in AAC and their influence.

Secondly, the characterization of the used additives is given in Chapter 3. Partial experimental program including test method is illustrated in Chapter 4. This chapter describes the substitutions of quartz and Portland cement. The experimental result, comparison and conclusions concerning the quartz replacement are described in Chapter 5-10. Chapter 11 and 12 shows all experimental results and conclusion of partly Portland cement replacement by paper sludge ash. Chapter 13 gives the overall discusion and conclusions. Finally, recommendations and further research are elucitated in Chapter 14.

2. LITERATURE REVIEW

This literature review gives an introduction of the process and the involved reaction equations for AAC and the substituted additives. The influence of the different additives on AAC production is given in preliminary study: Alternative raw materials in AAC production written by Boesten (2012).

2.1 HYDRATION AND PRODUCTION OF AAC

AAC is normally manufactured from CaO containing materials (cement and quick lime) and siliceous materials (quartz, crushed silica rock and/or stone) with a trace of aluminum as the foaming agent. Silica and calcium oxide can also be obtained from waste materials of other processes. Gypsum and anhydrite have similar function and are used as a catalyst for optimizing the properties of AAC. The average ratio of raw materials used in the laboratory of the company HESS AAC Systems B.V. is shown Tab. 1. The percentages vary slightly depending on the desired density.

Table 1: Example laboratory formula of AAC (Heinz, 2012)

Raw materials	Values [mass %]
Quartz	± 66
Portland cement	± 20
Lime	± 8
Lime hydrate	± 3
Gypsum	± 3
Aluminum powder	± 0.05

The final properties of AAC are depending on the recipe (production), the chemical composition, the PSD and the physical properties of the raw materials, but also on the method of preparing/ pulverizing/ mixing of raw materials, the method of pore-formation, curing and of autoclaving the products.

The chemical composition of each raw material is crucial for the reaction during the curing period (hydration phase). The mixing period is when the raw materials, including water, are mixed. As a result the product (also called the green cake) will rise and become stiff (at ambient temperature) during the so called curing period. Next, the stiff mixture is autoclaved. During autoclaving, the fine siliceous material reacts chemically with the calcareous raw materials (such as lime) to form C-S-H gel which will transform later on into tobermorite.

2.2 CHEMICAL PROCESS

REACTIONS DURING CURING PERIOD (FAST REACTIONS)

The highly exothermic processes take place at atmospheric pressure during the mixing and curing phase. The exothermic reactions of quicklime [1] and aluminum [2] with water occur instantaneous, resulting in a significant temperature increase. The reaction of aluminum with water generates the hydrogen required for the rising process. This reaction takes place simultaneous with the reaction of aluminum with portlandite and water to form tricalcium aluminate.

Quicklime + Water → Portlandite + 65.2 kJ/mol [1]

$CaO + H_2O \rightarrow Ca(OH)_2 + 65.2\ kJ/mol$

Metallic aluminum + Portlandite + Water → Tricalcium aluminate + Hydrogen [2]

$2Al + Ca(OH)_2 + 6H_2O \rightarrow Ca[Al(OH)_4]_2 + 3H_2$

REACTIONS DURING AUTOCLAVING (SLOW REACTIONS)

During autoclaving is steam of 11 bar and 190 °C added to the close system with cured product, which reacts. Several parallel and serie reaction occur at these high temperatures and high moisture content.

1. Gypsum is dehydrated due to the high temperature [3].
2. The Portland cement reacts relative fast with water to form the reactive intermediate calcium silicate hydrate (C-S-H gel) and portlandite [4a-d].
   2a. Tricalcium silicate [4a], dicalcium silicate [4b], tricalcium aluminate [4c], tetracalcium aluminoferrite [4d] present in Portland cement will reacted with water and/or anhydrite and/or portlandite to form C-S-H gel.
3. The added portlandite (raw material) reacts with quartz to form C-S-H gel [5]. Finally, C-S-H gel will form tobermorite [6].

Gypsum + heat → $CaSO_4 \cdot 2H_2O$ →	Anhydrite (calcium sulfate) + water $CaSO_4 \cdot 0.5H_2O + 1.5H_2O$	[3]

Cement reactions

Tricalcium silicate + water → $2\ (3\ CaO \cdot SiO_2) + 6\ H_2O$ →	Tricalcium silicate hydrate (C-S-H gel) + Portlandite $(3\ CaO \cdot 2\ SiO_2 \cdot 3\ H_2O) + 3\ Ca(OH)_2$	[4a]
Dicalcium silicate + water → $2\ (2\ CaO \cdot SiO_2) + 4\ H_2O$ →	Tricalcium silicate hydrate (C-S-H gel) + Portlandite $(3\ CaO \cdot 2\ SiO_2 \cdot 3\ H_2O) + Ca(OH)_2$	[4b]
Tricalcium aluminate + water → $(3\ CaO \cdot Al2O_3) + Ca(OH)_2 + 12H_2O$ →	Tetracalcium aluminate hydrate (C-A-H gel) $(4\ CaO \cdot Al2O_3 \cdot 13\ H_2O)$	[4c]
Tetracalcium aluminoferrite + water → $(4\ CaO \cdot Al_2O_3 \cdot Fe_2O_3) + 13\ H_2O$ →	Tetracalcium aluminoferrite hydrate (C-A-F-H gel) $(4\ CaO \cdot Al_2O_3 \cdot Fe_2O_3 \cdot 13\ H_2O)$	[4d]

Other reactions

Quartz + Portlandite → $SiO_2 + Ca(OH)_2$ →	Calcium silicate hydrate (C-S-H gel) $CaSiO_3 \cdot\ H_2O$	[5]
C-S-H gel + autoclave → $5\ CaO \cdot 6\ SiO_2 \cdot 5\ H_2O$ →	11.30 Å Tobermorite $Ca_5Si_6O_{16}(OH)_2 \cdot 4H_2O$	[6]

2.3 Additional reaction due to additives substitution

The additives contain substances which are already present (e.g. quicklime, quartz, calcite) in the processed mixture and influence and involved reactions. Also new components can be present (e.g. metakaolin [7-8], metal oxides and phosphates [9]).

Reactions during autoclaving (Slow reactions)

The presence of metakaolin generates different reaction products, as can be seen in the following reactions: (C-S-A-H gel: Calcium Aluminosilicates Hydrate (strattlingite).

Metakaolin + Quicklime + Water→ $Al_2O_3 \cdot SiO_2 + 3\ CaO + 6\ H_2O$ → $Al_2O_3 \cdot SiO_2 + 2\ CaO + 8\ H_2O$ → $Al_2O_3 \cdot SiO_2 + 4\ CaO + 13\ H_2O$ →	C-S-A-H gel + C-S-H gel $3\ CaO \cdot Al_2O_3 \cdot SiO_2 \cdot 6\ H_2O$ $2\ CaO \cdot Al_2O_3 \cdot SiO_2 \cdot 8\ H_2O$ $4\ CaO \cdot Al_2O_3 \cdot SiO_2 \cdot 13\ H_2O$	[7]
Metakaolin + Portlandite → $2\ Al_2O_3 \cdot SiO_2 + 4\ Ca(OH)_2$ →	C-A-S-H gel + C-S-H gel $2\ CaO \cdot 2\ Al_2O_3 \cdot 2\ SiO_2 \cdot 4\ H_2O$	[8]

Bio ash contains phosphates which gives the following reaction with portlandite:

Portlandite + Phosphate → $5\ Ca(OH)_2 + 3\ PO_4^{-3}$ →	Calcium hydroxyapatite + Hydroxyl $Ca_5(PO_4)_3OH + 9\ OH^-$	[9]

Remark

All additives contain also numerous low concentration other metal oxides, which can reacts comparable to the present Al, Fe, Si oxides, thereby influencing the total process in different ways (negative, positive, neutral). Also different salt are present such as NaCl. These will also influence the total process.

3. CHARACTERIZATION OF ADDITIVES

The characterization of the used additives is elucidated in: (I) background information, (II) oxide composition, (III) mineral phase, (IV) physical properties and particle size distribution and, (V) FESEM.

For comparison purposes Indian fly ash is tested. All other used additives were produced in The Netherlands. Tab. 2 illustrates the origin of the additives and Fig. 1 shows the color. It should be noted in Fig. 1 that the bottom ash is ground (for AAC production purpose).

Table 2: Origin of additives

Additives	Burning material	Factory
Cyclone ash	Wood	Power plant
Paper sludge ash	Paper	Paper recycling plant
Bio ash	Waste water sludge*	Sludge incineration
Bottom ash	Municipal waste	Power plant
Dutch fly ash	Wood and municipal waste	Power plant
Indian fly ash	Coal	Power plant

*In Dutch: Slib

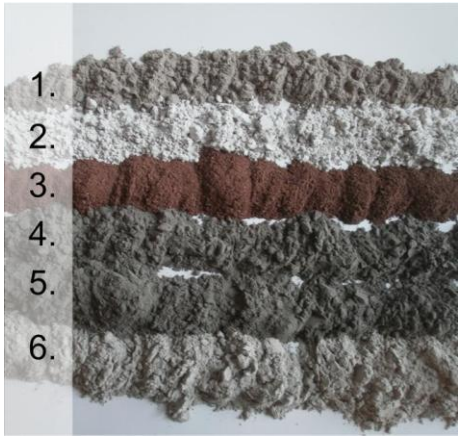

Figure 1: Color additives: 1. Cyclone ash, 2. Paper sludge ash, 3. Bio ash, 4. Ground bottom ash, 5. Dutch fly ash and, 6. Indian fly ash

BACKGROUND INFORMATION

In general, the consistency of the used materials (input) is crucial for a constant quality additive. The precise composition is highly depending on the type of incineration and thermal conditions applied. The composition is therefore no constant value and ranging.

The **cyclone ash** is a bio ash resulting from burning wood coming from the HVC power plant in Alkmaar. Cyclone ash is a type of product from a coal combustor, commonly used in large industrial boilers. Yearly, 170.000 ton of wood incinerated as a source of green energy (HCV, 2011). No extra CO_2 is added to the atmosphere by burning this material for energy generation. The cyclone ash is an inorganic material derived from municipal waste, wood or cane. The main components are calcium oxide and silicon oxide. Cyclone ash has a large quantity of bounded aluminum oxide. This aluminum oxide is not metallic like the aluminum which is specially fabricated for AAC production (Heinz, 2012).

The **Paper sludge ash** is the industrial name of the residue from the combustion of paper sludge coming from the paper industry. The commercial name is called Topcrete®. Paper sludge ash is a white non-toxic pozzolanic material, which is already used as a cement and quicklime replacement in the concrete industry, as an admixture to Portland cement. The material is mainly composed of metakaolin, quicklime, calcite and portlandite. Because of the large specific surface area, quicklime, as well as metakaolin are quickly fully utilized. Paper sludge ash has a high binding reactivity therefore it is advisable to slightly increase the water to binder ratio. The PSD of paper sludge ash is similar to that of Portland cements, allowing it to be a possible substitution. Finally, paper sludge ash has a high specific surface area due to the porosity of the particles.

The **Bio ash** is a reddish ash from incineration of waste water sludge in Moerdijk (Wijs, 2008). Results show that, if bio ash is mixed with water, temperature rises because of hydration. Bio ash contains phosphates. The Interim Report (2012): Assessment of Potential Phosphate Ion-Concrete Interactions provides an indication that there are harmful interactions between phosphate ions, cementitious materials and the phosphate solutions in concrete. This research concludes that phosphate could react with calcium hydroxide ($Ca(OH)_2$) to form calcium hydroxyapatite ($Ca_5(PO_4)_3OH$) [9]. Ferric oxide (Fe_2O_3) is also present and occurs naturally as the mineral hematite. Neither oxide is protective at pHs below approximately 11. This could affect the tetracalcium aluminoferrite (ferrite phase, $4CaO \cdot Al_2O_3 \cdot Fe_2O_3$ C_4AF) of Portland cement.

The used **Bottom ash** is produced by burning municipal waste. It consists of ash particles derived from natural minerals that are found in coal and is therefore dark gray colored (Vliegasunie, 2011). From mineralogical point of view, bottom ashes consist predominantly of glass and to a smaller extent of quartz and feldspar. The material is comparable with sand with a predominantly angular granular form. It consists largely of aluminum silicate compounds and is inert (Vliegasunie, 2011). To conclude, bottom ash contains aluminum silicate compounds which are also present in Portland cement reactions. These compounds could enhance the binder content.

In **Dutch fly ash and Indian fly ash** SiO_2, and Al_2O_3 are the main components, with next to a lesser extent Fe_2O_3, and CaO. The most important mineral phase is a glass-like compound which forms the greater part of the observed SiO_2, and Al_2O_3. In addition, mineral phases such as mullite, quartz, hematite and magnetite are present in Dutch fly ash (Vliegasunie, 2011). The fly ash contains pozzolans, which react with portlandite. The pozzolanic properties ar due to glassy phases in fly ash. In the alkalic environment in AAC these glassy phases are broken down reacting with portlandite to form C-S-H gels. Only a small proportion of the inorganic element is initially organically bound. Important minerals in coal are kaolinite ($Al_2Si_2O_5(OH)_4$), illite $(K,H_3O)(Al,Mg,Fe)\ 2(Si,Al)_4O_{10}\ ((OH)_2,(H_2O)))$, quartz ($SiO_2$), pyrite ($FeS_2$), feldspar ($(KAlSi_3O_8$-$NaAlSi_3O_8$ - $CaAl_2Si_2O_8)$) and calcite ($CaCO_3$)(Vliegasunie, 2011). During the combustion of pulverized coal minerals undergo conversion processes such as melting and oxidation.

It is already proven that fly ash can replace a part of the cement in concrete. Key benefits include: The spherical shape of the fly ash particles have a positive influence on the process ability, resulting in a water - cement factor, which in many cases can slightly be reduced during constant process ability. The sensitivity of concrete products for alkali silica reactivates clearly decreases as a consequence of the binding of calcium hydroxide during the glass-like phases. This is demonstrated in many scientific articles and recognized in legislation (e.g. CUR Recommendation 89).

OXIDE COMPOSITION

In Fig. 2 the ternary phase diagram of SiO_2, Al_2O_3 and CaO is displayed. Fig. 2 illustrates that bottom ash and the fly ashes have a high SiO_2 content and therefore are more favorable for replacing quartz compared to the other additives. Next, paper sludge ash has the most potential to replace Portland cement due to almost same SiO_2, Al_2O_3 and CaO composition. Finally, cyclone ash and bio ash have no similar SiO_2, Al_2O_3 and CaO compared to either quartz or Portland cement, and are therefore less suitable for replacement.

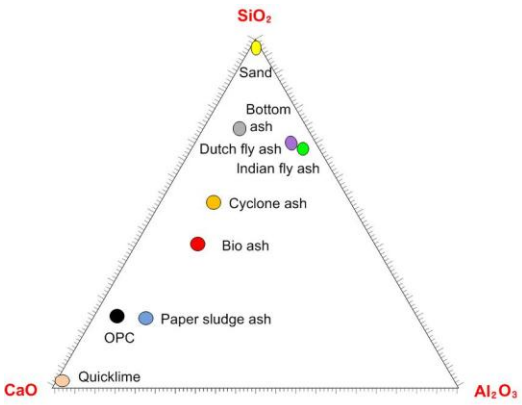

Figure 2: Ternary phase diagram of binders and additives

The oxide compositions of the additives were analyzed by X-ray fluorescence technique (XRF) see Tab. 3.

Table 3: Oxide composition obtained (Canadian laboratory Actlabs)

Additives		SiO_2	CaO	Al_2O_3	Fe_2O_3	MgO	Na_2O	TiO_2	P_2O_5	K_2O	LIO	total
Cyclone ash	[%]	35.96	23.37	7.91	4.46	2.38	1.57	3.56	2.78	2.26	9.32	93.83
Paper sludge ash	[%]	15.13	52.29	9.55	0.86	1.83	0.11	0.37	0.42	0.14	17.61	98.42
Bio ash	[%]	20.42	21.80	7.63	16.31	2.43	0.88	0.64	19.43	1.19	7.00	97.92
Bottom ash	[%]	52.12	11.31	6.84	11.58	1.34	1.48	0.89	0.97	1.18	10.01	97.92
Dutch fly ash	[%]	56.18	4.35	18.91	8.72	1.94	1.25	0.85	0.37	2.23	3.70	98.63
Indian fly ash	[%]	61.52	3.62	24.32	4.95	0.94	0.09	1.60	0.26	1.16	0.36	98.93

As shown in Tab. 3 the sum of SiO_2, Al_2O_3, and Fe_2O_3 of the bottom ash reached 70 %, indicating that it could be classified as F type ash as prescribed by ASTM C 618. Thus, bottom ash could also have pozzolanic properties just like fly ash.

Mineral phases analyses

Fig. 3 shows the quartz, anhydrite, lime and calcite intensity of all additives identified by XRD. These mineral phases were also measured later on by XRD in AAC substitution samples. It can be seen that bottom ash, fly ashes and cyclone ash contain quartz. Lime is present in paper sludge ash and bio ash. Details of XRD results can be found in Appendix A.1.1.

Physical properties and particle size distribution

Key parameters, for substitution are the density (Fig. 4) and the PSD, which were shown in Fig. 5-6 and Tab. 4. The size range of the particles was between 0.02 and 2000 µm. (See Appendix A.1.2 for details of density).

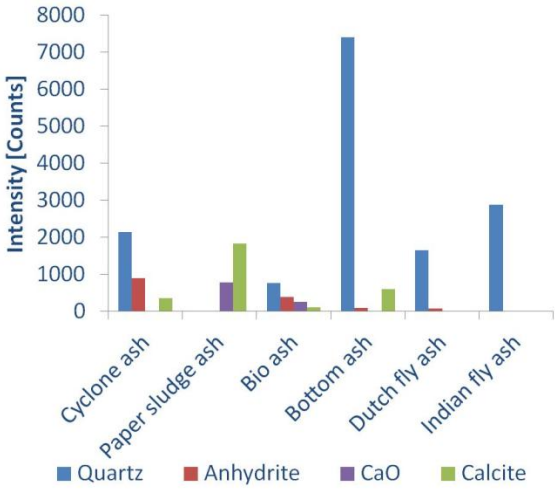

Figure 3: XRD measured mineral phases of additives compositions

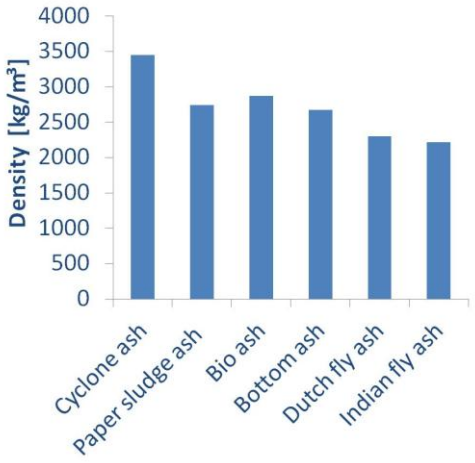

Figure 4: Dry density of additives

Table 4: Physical properties and PSD

Additives	D(0.1) [µm]	D(0.5) [µm]	D(0.9) [µm]
Ground quartz	4.81	43.52	132.42
Portland cement	4.36	22.91	79.43
Cyclone ash	8.62	36.48	126.49
Paper sludge ash	5.43	46.13	230.72
Ground bottom ash	5.70	31.97	104.40
Bio ash	11.02	79.05	464.86
Dutch fly ash	2.57	19.90	108.32
Indian fly ash	2.91	33.62	170.86

Fig. 5 presents the total percentage of all sizes of particles passed by sieve given for a range of sizes, for all additives, ground quartz and Portland cement. The normal PSD is also given for these materials, as illustrated in Fig. 6 and measured with a Mastersizer 2000. A smaller cumulative PSD is observed for Dutch fly ash and paper sludge ash compared to Portland cement. The cumulative PSD of ground quartz is consistent with ground bottom ash and Dutch fly ash, unlike bio ash.

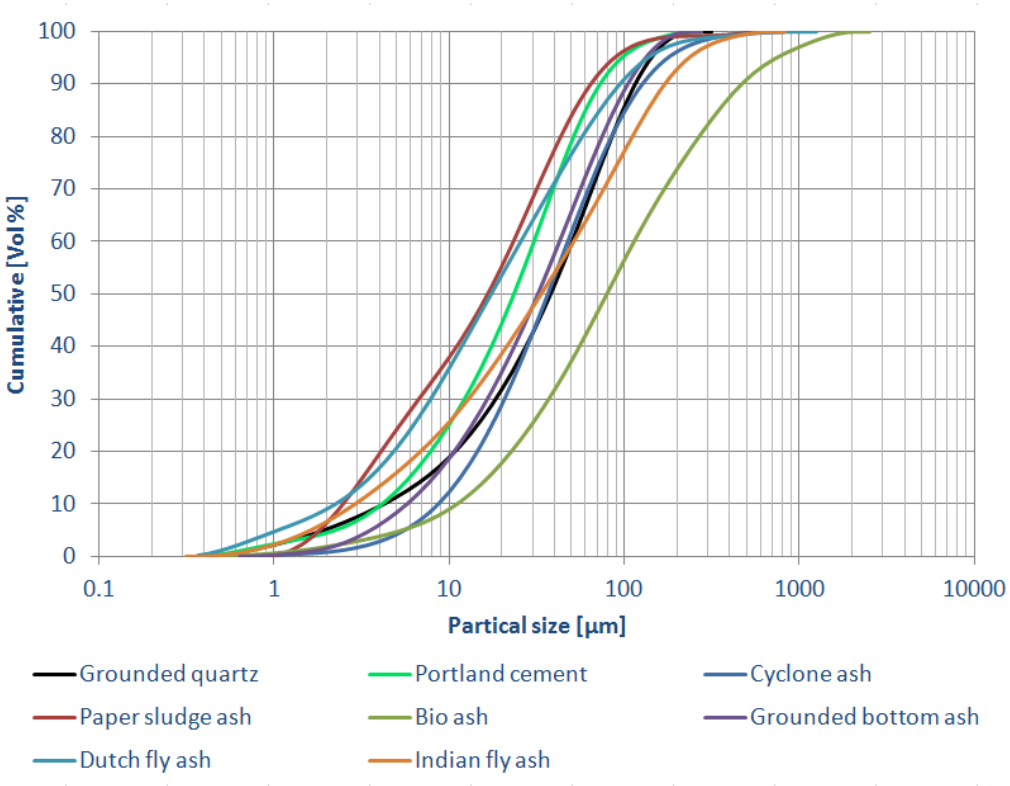

Figure 5: Cumulative PSD of six additives

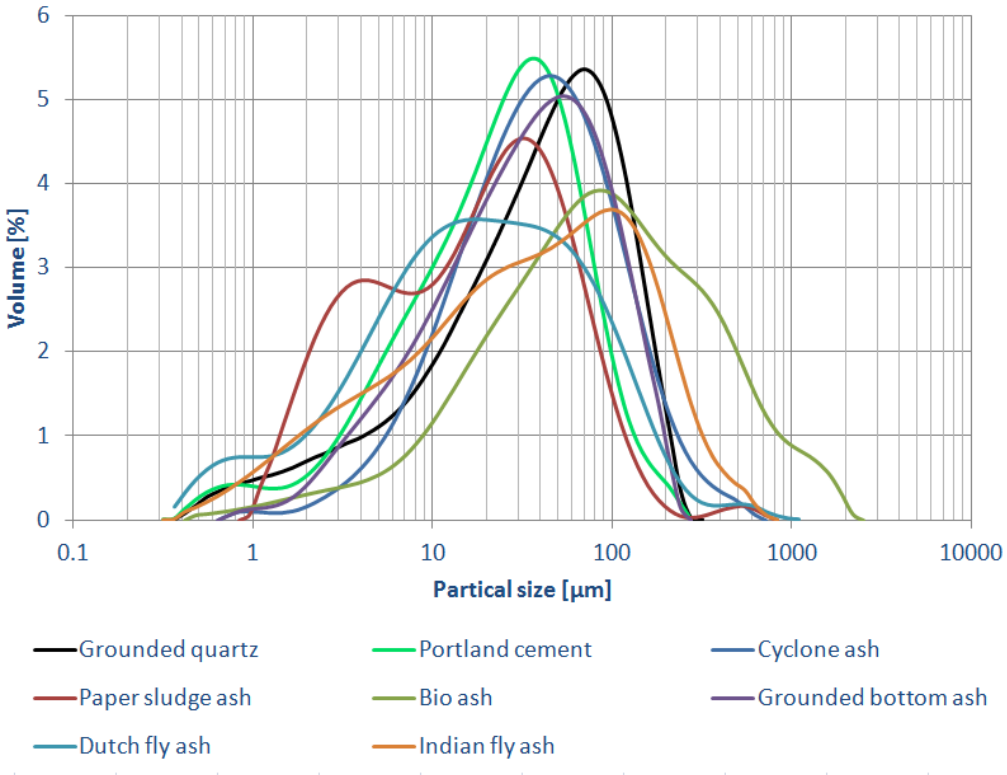

Figure 6: Normal PSD of six additives

FIELD EMISSION SCANNING ELECTRON MICROSCOPY

The FESEM was used to analyze the morphology of the six additives (Fig. 7). During the FESEM testing an electron beam excitation was used. Cyclone ash consisted of very fine glassy amorphous phase particles (Fig. 7a). The average particle size based on Fig. 7d was ranging from approximately 4 µm up to 1 µm. Paper sludge ash consisted of small particles (< 1.7 µm, based on Fig. 7b-e) which perhaps could be filler from paper. Due to these small particles large amounts of agglomerate were formed (Fig. 7e). Bio ash consists of a varied mixture of small and large particles (Fig. 7c). The particle sizes vary between 1 µm to 10 µm. A large amount of small particles (< 1 µm) formed agglomerates (Fig. f).

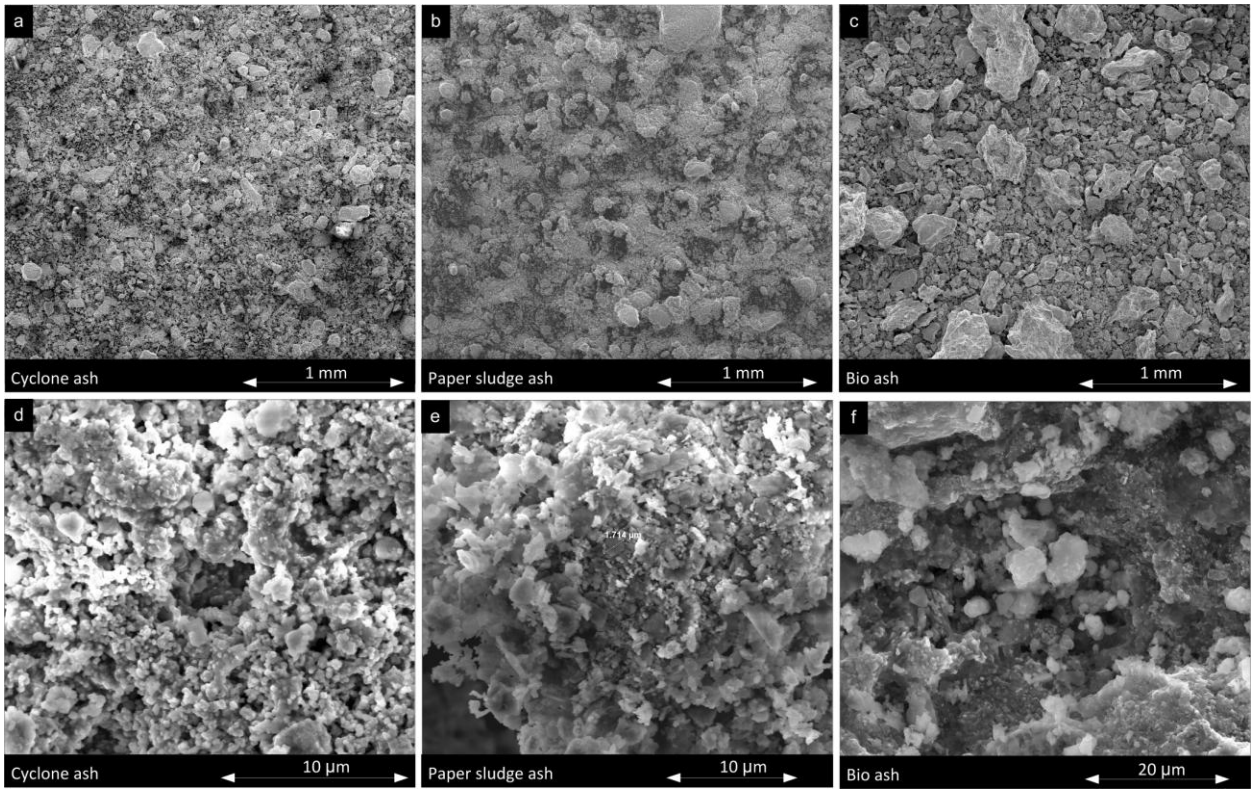

Figure 7: FESEM images of cyclone ash, paper sludge ash and bio ash

Bottom ash consisted of a mixture of small and large angular particles with also glassy phase particles (Fig. 8a). It contained a high quantity of iron and carbon residue which is responsible for the dark color. Simultaneously, glass particles and agglomerates of small particles were found (Fig. 8d). The Dutch and Indian fly ashes had a typical spherical shape however some rectangular particles were detected which in fact is carbon residue (Fig. 8e-f). The Indian fly ash showed overall bigger particles (Fig. 8f) compared to the Dutch fly ash (Fig. 8e).

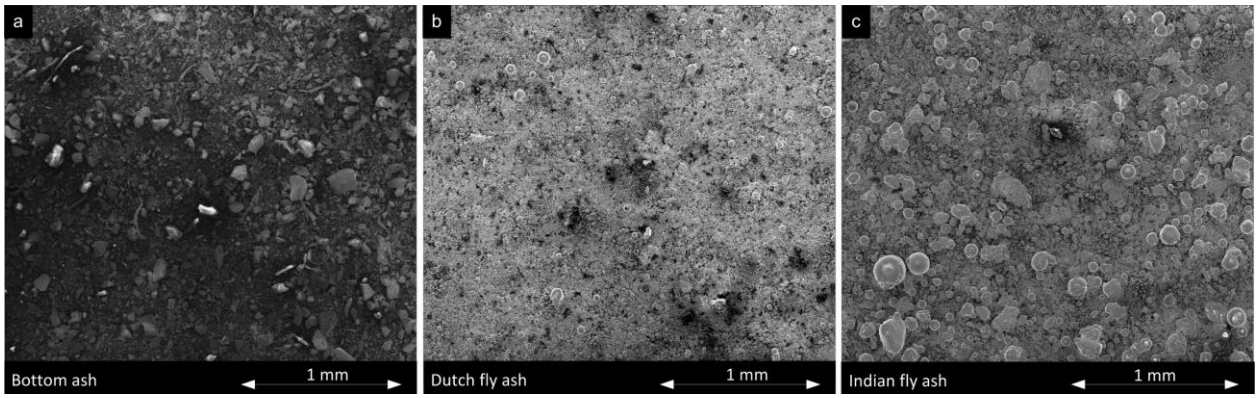

Figure 8: FESEM images of bottom ash, Dutch fly ash and Indian fly ash

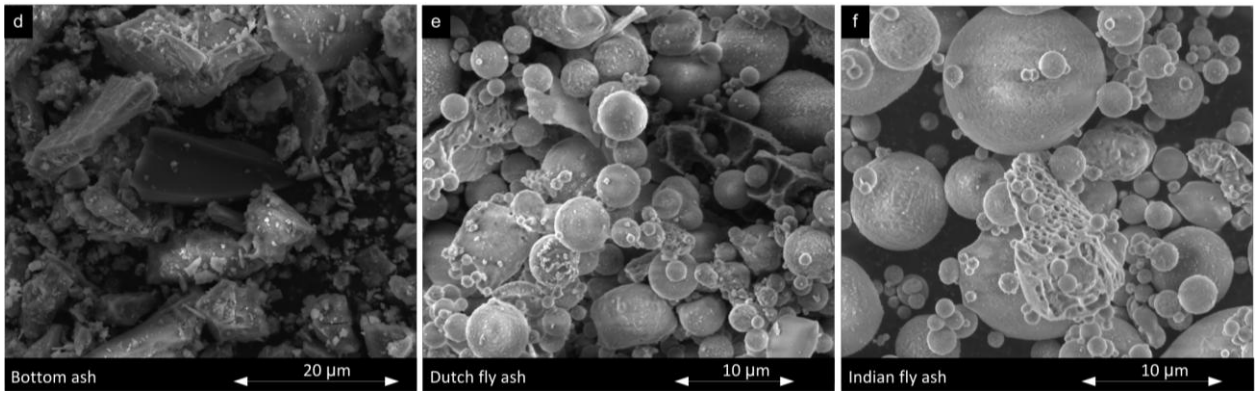

Figure 8: FESEM images of bottom ash, Dutch fly ash and Indian fly ash, cont.

4. EXPERIMENTAL PROGRAM

The main objective for this chapter is to elucidate the experimental program including (I) the AAC laboratory recipe, (II) the manufacturing method, (III) the substitution method of quartz and, (IV) the substitution method of Portland cement. In this report are all percentages (%), which concern the weight of a material are mass based. Firstly, the substitution method is replacing quartz by six different additives, in two or three substitution levels (5, 10 and 15 %). Portland cement and paper sludge ash primarily have a similar oxide composition, which makes paper sludge ash a suitable substitution material. The following five substitution levels (10, 20, 30, 40 and 50 %) are selected.

4.1 RECIPE

RAW MATERIALS

The raw materials used in this research originate from The Netherlands. The raw material used for the AAC recipe in the laboratory consisted of quartz, lime, cement, lime hydrate, gypsum and a small quantity of aluminum powder. The expanding agent, metallic aluminum, is specially fabricated for AAC manufacturing. The aluminum is ground and protected with grease to covers it from air so spontaneous combustion is prevented. The quartz was the only raw material that needed treatment. The other raw materials were delivered in the correct fineness, expect for bottom ash. The quartz was ground with a mechanical mill, till the desired size range was reached (Tab. 5).

Table 5: PSD of ground quartz

Additives	D(0.1) [µm]	D(0.5) [µm]	D(0.9) [µm]
Ground quartz	4.81	43.52	132.42

The reference mixture has a total weight of 12 kg. Additionally, 7 kg of water were added resulting in a w/s ratio of 0.58. The exact substitution quantities are displayed in Tab. 6.

Table 6: Reference mixture

	Mass	Percentage
Raw materials	[kg]	[%]
Lime	1.0	8.33
Cement	2.4	20.00
Gypsum	0.3	2.50
Ground quartz	8.0	66.67
Lime hydrated	0.3	2.50
Aluminum powder	0.014	-
Total	12.0	100

4.2 SUBSTITUTION METHOD

4.2.1 IMPORTANCE OF CURING CONTROLLING

For both the procedures the mixing, curing and autoclaving conditions in all cases were constant. The aim of this research is to study the influence of the different additives on the final product of AAC. The overall product condition for this purpose should be most efficient. It is essential to produce an optimal matrix (the solid structure). Obtaining an optimal product is highly dependent on the development of the mixture during the curing period. The development of the mixture is in turn influenced by the balance of the rising and stiffening development during hydration, both processes occurring approximately at the same time (Fig. 9). It is essential to control the balance between these two processes. In the following section the method is describes and special attention is paid to the importance to control, adapt, optimize and observe the mixture.

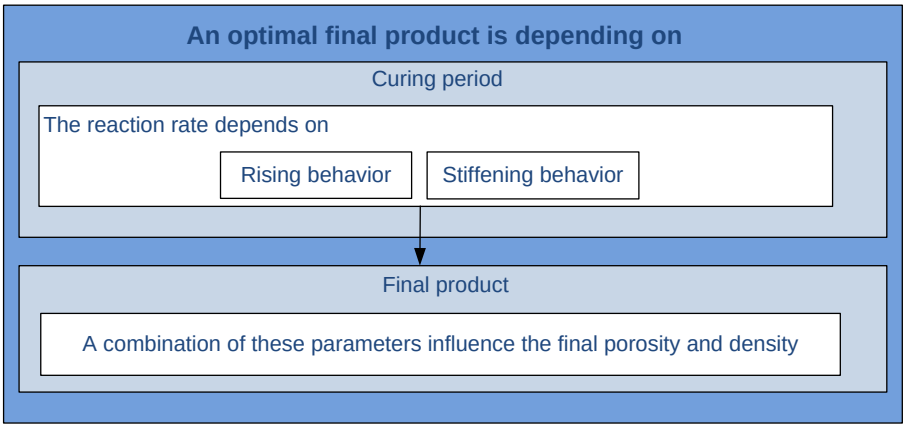

Figure 9: Influencing parameters to obtain an optimal product

ADAPT MIXTURE DUE TO ADDITIVE SUBSTITUTION

The substitution of an additive can influence the balance of the mixture development. The additive can influence the composition mixture (and final sample composition of the matrix). The following behaviors during curing period could occur:

1. Too quick or too slow rising of the mixture.
2. Too fast or too slow stiffening of the mixture.

The aim is to avoid these two negative consequences, which result from the substitution of additives. A measure to control the two important parameters of rising and stiffening are (Heinz, 2012):

1. Aluminum powder correction.
2. Water correction.

Holt and Raivio (2005) confirmed that controlling the reaction rate and duration of the aluminum reactions is important. Therefore, it is necessary to ensure that the hydrogen formed pores (also called macropores) formation is completed at approximately the same time as the AAC initial stiffening starts. Therefore, the controlling of the aluminum powder and water amount should ensure proper sized and distributed macropores.

TEST REACTION RATE

The reaction rate is tested by the following test (Fig. 10): (I) the slump flow test, (II) the rising development measurement, (III) the temperature development measurement and maximum temperature, (IV) the penetration depth test and, (V) final height measurement.

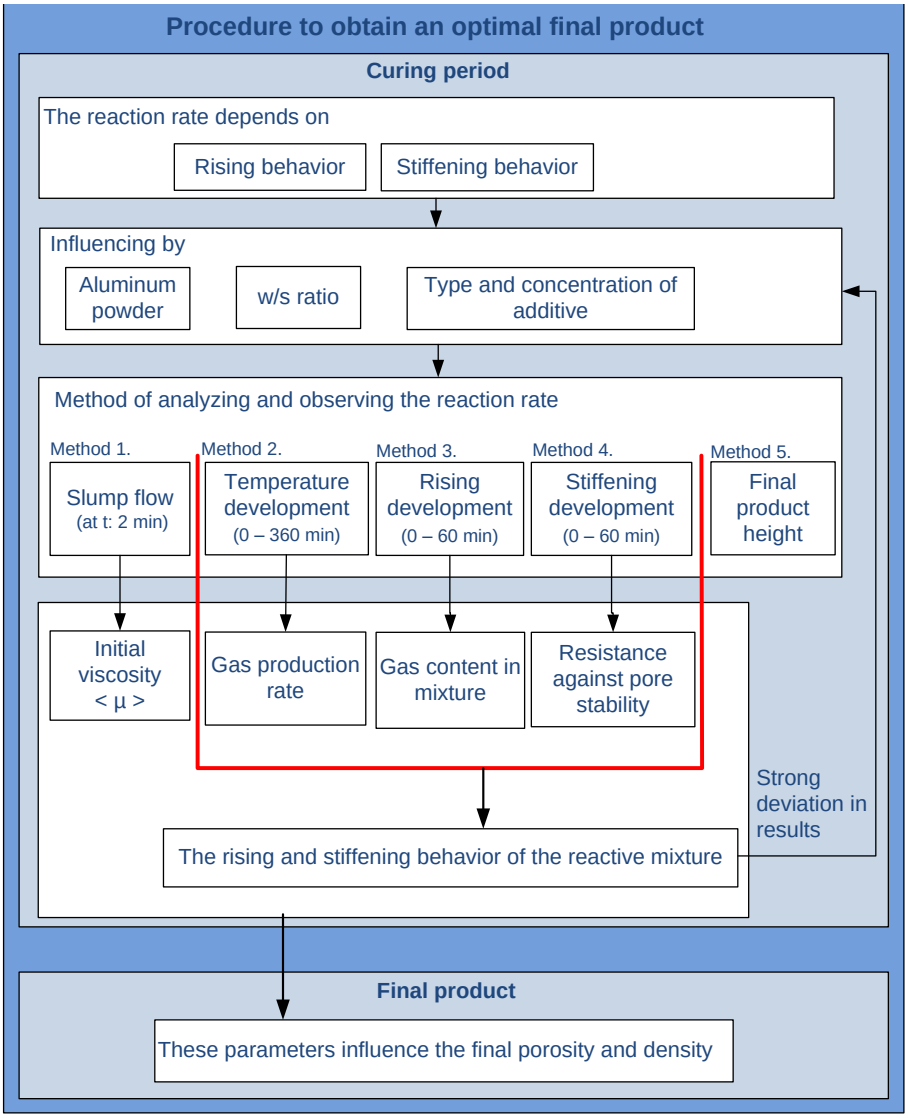

Figure 10: Procedure to obtain an optimal product

As can be seen in Fig. 10, test method gives an indication of one or multiple developments during the period of curing. It is possible that the mixture will slightly sink due to hydrogen gas release, calling the sinking effect (Fig. 11). The sinking effect indicates that the stiffening of the mixture is too stiff to resist the pressure of hydrogen gas produced by aluminum powder. The rising development gives an indication of the rising and sinking.

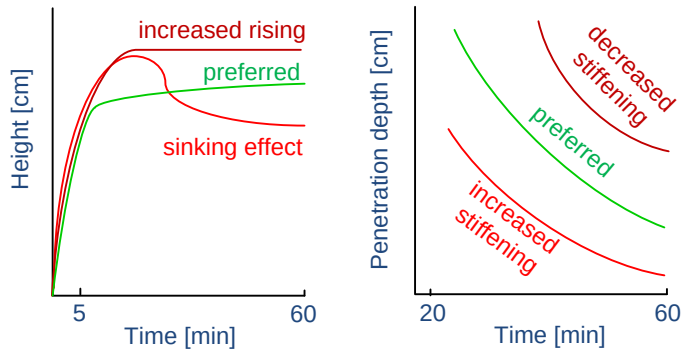

Figure 11: Possible changes in rising and stiffening development

More aluminum powder will postpone the sinking effect and as a consequence prolong the time period for the stiffening development. However not only the aluminum amount, but also the water amount has influence on the sinking effect. Less water will accelerate the sinking effect and as a consequence retards the stiffening development. So, quicker sinking is a prove of an accelerated reaction.

Due to less water and more aluminum powder the mixture will get more quickly stiffened, at the same time more hydrogen bubbles are produced which rise to the surface causing the sinking effect. It is suggested by Heinz (2012) that due to these effects deformed pores (or even cracks in the matrix can be produced), since the hydrogen gas wants to expand while the mass is already stiff.

ADAPT AND OPTIMIZE THE REACTION RATE

Substituting a raw material in the original recipe can influence the reaction rate. The difference in substituting materials can be distinguished by chemical or physical properties namely: (I) oxide composition, (II) calcium/silica ratio, (III) density and, (IV) PSD. These can have a possibly negative effect on the reaction rate, which require in turn adaption of the reaction rate.

The optimal reaction rate can be obtained by increasing the aluminum powder, which results in rising of the mixture, while simultaneously, reducing the water amount, which raises the hydration temperature, resulting in an accelerating stiffening development.

WHEN TO ADAPT THE REACTION RATE?

The question remains when to adapt the reaction rate? Firstly, a mixture including additives needs to be produced. The decision to the change the reaction rate (w/s ratio and aluminum powder amount) for a new sample (higher substitution of additive) is based on integral results (method 1-5) during curing. So, one or more strongly deviated results concerning: rising development, stiffening development or temperature development.

4.3.2 SUBSTITUTION METHOD OF QUARTZ

The low substitution levels were particularly selected, so negative or positive influences on the final product (AAC samples), caused by the mineralogical composition of the additive could be identified more quickly.

In total, 16 test samples were produced, in which all six additives were used for producing samples with a substitution of 5 % and 10 % (Tab. 7). The three best performing additives selected to use for 15 % substitution, based on, the slump flow test and rising development measurements of the 5 % and 10 % substitution results.

Table 7: 5 %, 10 % and 15 % substitution levels of quartz

Substitution levels	5 %	10 %	15 %
	[kg]	[kg]	[kg]
Ground quartz	7.6	7.2	6.8
Additive	0.4	0.8	1.2

4.3.3 SUBSTITUTION METHOD OF PORTLAND CEMENT

Paper sludge ash is selected as a substitution for Portland cement because of their similarity in oxide composition. Five substitution quantities of 0, 10, 20, 30, 40 and 50 % were selected. These substitutions are displayed in Tab. 8. The aluminum powder amount was kept constant for all mixtures. The 40 % and 50 % substitution levels were adjusted. Measurement results of the slump flow test and rising development measurements of the 10-30 % substitution, oxide composition and PSD were used to improve the reaction rate. The w/s ratio was increased for the 40 % mixture to 0.60 and for the 50 % mixture to 0.61.

Table 8: 0 % till 50 % paper sludge ash substitution levels

Substitution levels	0 %	10 %	20 %	30 %	40 %	50 %
	[kg]	[kg]	[kg]	[kg]	[kg]	[kg]
Portland cement	2.40	2.16	1.92	1.68	1.44	1.20
Paper sludge ash	0.00	0.24	0.48	0.72	0.96	1.20

4.3 MANUFACTURING METHOD

The reference mixture in this research was a mixture specially designed by the company HESS AAC Systems B.V. to produce AAC in a laboratory (Heinz, 2012). The procedure of the set-up is divided in the following operations: preparing materials and equipment, producing the mixture, autoclaving the mixture.

Firstly, the oxide composition, physical properties and PSD of the raw materials and additives were analyzed. The PSD of quartz and bottom ash was too coarse, therefore they were ground. The PSD was measured with a laser light scattering device Malvern 2000S.

The AAC test sample production is divided in four stages, (I) the curing period, (II) the autoclave period and (III) the drying period and, (IV) finally the dry test sample. Fig. 12 shows the stages including conditions and final result.

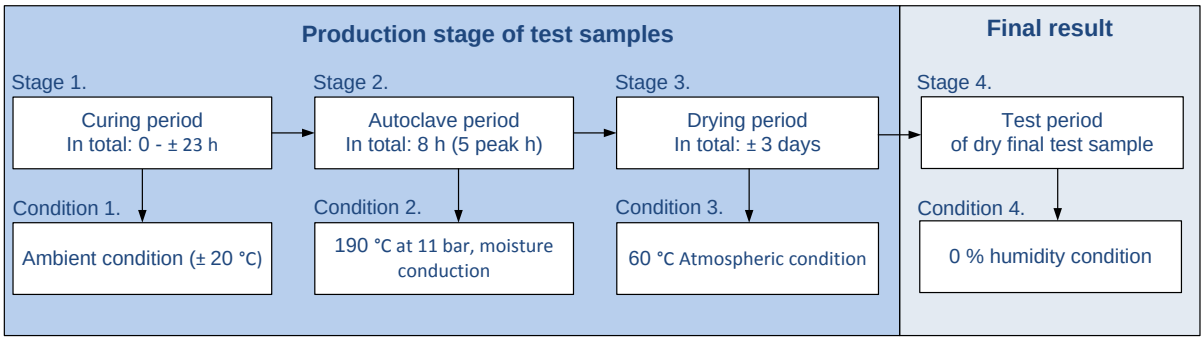

Figure 12: Stages of AAC test sample production

At the beginning the initial condition of the mixture was kept constant with a water temperature of 45 ± 3 °C. All ingredients were mixed in a specific order and within the same time period. A laboratory mixer with agitator was used for mixing. Firstly, lime hydrate and quartz was added to the mixture. Secondly, lime, cement, gypsum and the additive were added after 30 seconds. Next, aluminum powder was added, after 20 seconds. And finally the mixture was poured in an insulated mould with an insulated lid. The curing period starts after mixing, up to 21-23 h, at ambient conditions.

After the curing period the AAC blocks were autoclaved at a temperature of 190 °C for 8 hours (including 5 peak hours), at a pressure of 11 bar. After autoclaving, samples were cut in different dimensions and dried for 2-3 days till 0 % humidity was attained. For testing is it essential to dry the samples after autoclaving, for ± 3 days at 60 °C giving the condition for the final test samples.

4.4 TEST METHODS

During the curing period (Stage 1) and final dry test sample (Stage 4) are tests performed, as displayed in Fig. 13.

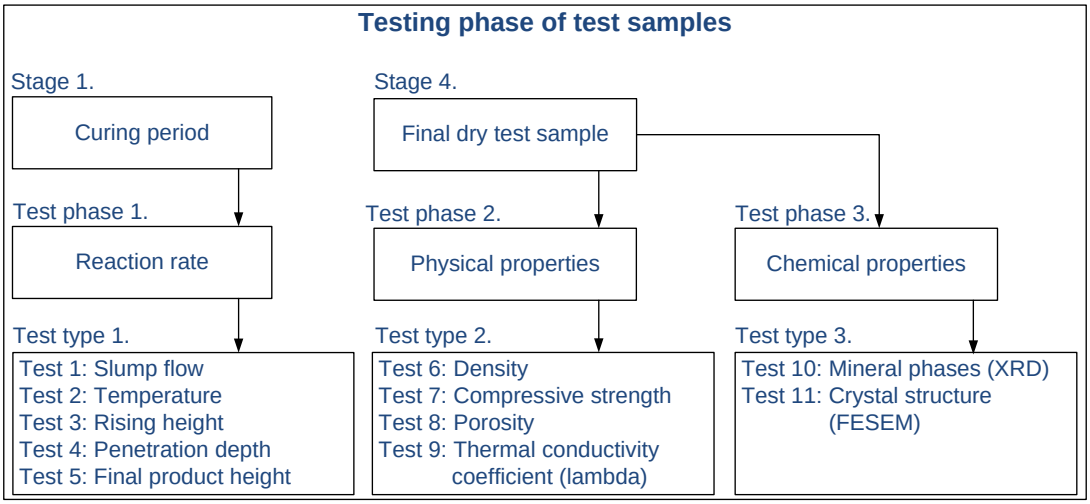

Figure 13: Test phases of samples

4.4.1 TEST METHODS DURING CURING PERIOD

During the curing period the reaction rate is an important parameter. The reaction rate can be observed by the results coming of the following test: (I) the slump flow test, (II) the temperature development measurement and maximum temperature, (III) the rising height (rising development), (IV) the penetration depth (stiffening development) and, (V) the final product height. Fig. 14 illustrates all performed tests, the time window and the frequencies of test performance during curing period. These results give overall information on the reaction rate.

Curing period	
Type of performed tests: (To observe the reaction rate) Test 1-5: Test the reaction rate Test 1: Slump flow test Test 2: Temperature measurements Test 3: Rising height test Test 4: Penetration depth test Test 5: Final product height	**These results give overall information on the reaction rate:** (All test are needed to get an integral overview on rising and stiffening development) Test 1-5: Rising and stiffening behavior of the reactive mixture Test 1: Initial viscosity and reactivity of the mixture Test 2: Reaction rate (gives information on gas production rate) Test 3: Gas content (development) in mixture Test 4: Resistance against coalescence and homogeneity of the porosity Test 5: Final gas content
Time window and frequencies of test performance: (All tests start direct after mixing) Test 1: Performed once after 2 min of mixing Test 2: Performed once after 3 min of mixing for 360 min, at ▵5 min Test 3: Performed once after 3 min of mixing till 60 min, at ▵5 min Test 4: Performed once after ± 25 min of mixing till 60 min, at ▵5 min Test 5: Performed once after ± 22 h of mixing	

Figure 14: Test types, results analysis and time window of test performing during curing period

Slump flow test

Each additive has its one characteristic properties like high pozzolanic properties, lower PSD and lower density. These properties can affect the binder. This effect either can reduce or increase the w/s ratio which can be visible in the slump flow results. The slump flow test is a tool to assess the reactivity and the water demand of the mixture.

After mixing, the slump flow test was performed. A steel cylinder (h: 60 mm, d: 72 mm) was filled up to the top and was lifted, so the mixture could flow. The diameter of the slump flow was only measured once. The slump flows were obtained using tape measure. This test is only used to have a rough indication of the bonding qualities of the mixture therefore it was only measured once.

Rising development measurement

After casting the mixture will rise till approximately twice its original height, within approximately the first hour. A special measurement device produced by HESS AAC Systems B.V. was used for measuring the rise height during the first 60 min. The measurements will give an indication of the sinking effect influenced by the rising and stiffening development.

Hydration temperature measurement

The reaction rate is analyzed by measuring the hydration temperature with thermocouples. For all substitution samples the temperature of hydration was monitored, form the moment the mixture entered the mould, each 30 sec. for 360 min.

The maximum temperature and corresponding time was determined based on the first measured maximum value for each mixture. Based on this approach all mixture should have the same initial temperature, to limit the uncertainty. However, the temperature of the water varied ± 4 °C which indicates that the uncertainty could slightly change the outcome. This is important because a higher temperature accelerate the reactions. After 240 min curing the temperature is measured and is assumed to be a measure for the reactivity.

Penetration depth test

The stiffness of the mixture was measured by the penetration depth method. The mixture was casted in the mould and after 25 min the first measurement was performed followed by further measurements an interval of 5 min till 60 min after casting. The penetration depth was performed by dropping an aluminum cone in the mixture. The tip of the cone was only several millimeters above the mixture, before the cone was dropped and afterwards measured with a tape measure, with an uncertainty of ± 5 mm. The location of the measurement was the same for all samples. After 55 min of curing the penetration test is executed and is assumed to be a measure for the stiffening development.

Final product height

After approximately 21-23 hours of curing (at ambient temperature) the height of the final product was measured once again with a measuring tape. This measurement gives a rough (± 15 cm) indication if a sample experienced an extensive or retard rising.

4.4.2 TEST METHODS ON FINAL PRODUCT

The test methods including type of tests and frequency of testing on the final product (dry test sample) are illustrated in Fig. 15.

Dry final test sample: Physical properties	
Type of performed tests: Test 6: Density Test 7: Compressive strength Test 8: Porosity Test 9: Thermal conductivity coefficient (lambda)	**Frequencies of test performing:** Test 6: Performed 4 times Test 7: Performed 4 times Test 8: Performed 30 times Test 9: Performed 2 times

Dry final test sample: Chemical properties	
Type of performed tests: Test 10: Mineral phases (XRD) Test 11: Crystal structure (FESEM)	**Frequencies of test performing:** Test 6: Performed once Test 7: Performed once

Figure 15: Test on dry final test samples

COMPRESSIVE STRENGTH

The test is performed on cubes. The humidity of the test cubes should be 6 %, according to the NEN-EN 771-4. A humidity of 6 % though is difficult to attain and is likely to cause errors in the case of a low number of test samples (and tests). For this research a humidity of 0 % was selected, since this is precisely measurable. It is taken into account that the CS will be 20 % higher in dry stage than with 6 % humidity (Heinz, 2012).

Two samples (U1 and U2) located in the lower part and two samples (O1 and O2) located in the upper part of the total sample were analyzed (See Fig. 16). The variance of the four samples is displayed with error bars. The error bars give 2 standard deviation (SDV) in each sample based on 4 samples.

All 16 samples were tested on CS. The dimensions of the test samples need to be exactly 100 x 100 x 100 mm, according to the NEN-EN 771-4 (Specification for masonry units - Part 4: Autoclaved aerated concrete masonry units). CS measurements were performed with 'Form+test Prüfsysteme DigiMaxx C-22', according to the NEN-EN 771-4 (Specification for masonry units - Part 4: Autoclaved aerated concrete masonry units). The loading speed of the CS device was 0.05 (N/mm^2)/s. The average CS and average dry density for each sample was based on four measurements. The compensated compressive strength (CCS) was used in order to take into account the influence of the dry density on the CS. CCS was calculated as follows:

$$CCS = \frac{\text{average CS} \times 450}{\text{average } \rho} \quad [1]$$

After cutting, the samples were mechanically polished to the correct dimensions. Fig. 16a-b shows how the cubes were cut. The load during testing was applied perpendicularly to the rising direction.

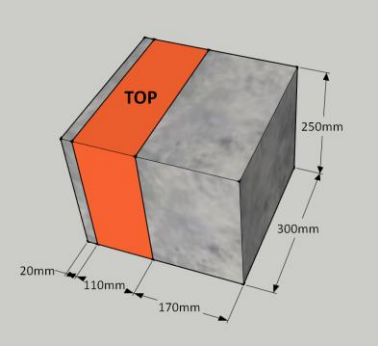

a) One AAC mixture

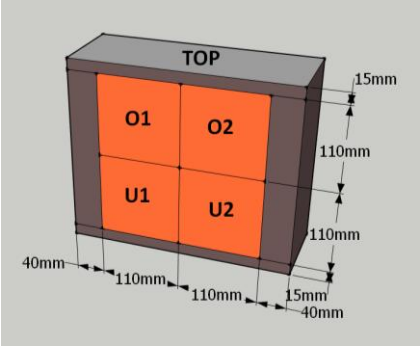

b) Four CS samples

Figure 16: Cutting procedure for CS sample

Dry density

The dry density was calculated by weighing the cubes. The dry density measurements were performed with same cubes which were used for the CS measurements (100 x 100 x 100 mm).

Porosity

The method used includes a sample with the same size (volume), which were measured with a Micromeritics helium pycnometer (AccuPyc II 1340). The porosity can be calculated from the difference of dry density and specific density obtained with the pycnometer. (The porosity is calculated as follows: 1-(dry density/ specific density).

The specific density was analyzed with three dried cylinders (h: 40 mm, D: 38 mm) for each sample. All cylinders were extracted of each sample. Each cylinder was measured 10 times to determine the standard deviation. Three cylinders are extracted from each sample and measured 10 times. The average porosity is based on these 30 measurements. However, the results of series of 10 measurements are not linear. The results fluctuate largely in some cases. There is no optimum after a number of measurements. It is suggested that the helium can difficulty reach every macropore, due to the dens matrix. The accuracy /reliability of the test could be better. The results only give an indication of the porosity.

Thermal conductivity

The thermal conductivity, called lambda (W/m.K) gives an indication of the quantity of heat which can be transported through a material. The differential thermal analyzer measurements were carried out on all samples. Thermal conductivity measurements were performed on dry samples (100 x 100 x 20 mm), according to EN 1745 (2002): Metselwerk en producten: Methode voor bepaling van de thermische rekenwaarden. According to the standard, the maximum value is 0.11 W/m.K. Every sample was measured once on each side (100 x 100 mm). The method of measuring is displayed in Fig. 17.

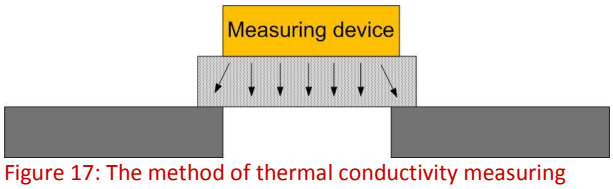

Figure 17: The method of thermal conductivity measuring

Mineral phase analysis

In this investigation, we sought to establish a methodology for explaining the CS results with XRD findings. Therefore, a semi-quantitative study was performed. Two methods to calibration the AAC samples were tested.

Firstly, aluminum oxide 90, (PSD 0.063-0.20 mm, art. 1097, 70-230 mesh ASTM) was selected to calibrate. It is known that aluminum oxide is well visible in a XRD diffraction pattern. So, 10 mass% of aluminum oxide of the ground AAC sample was added to Portland cement replacement samples. Unfortunately, the 10 mass% aluminum oxide was not visible during the identification of the diffraction pattern with the program DIFFRACplus BASIC. Finally, no aluminum oxide based diffraction pattern peak(s) were displayed. This method of calibration was disregarded.

It should be noted that another calibration medium was selected, namely the original ground quartz. It is known that quartz is a reliable material for calibration since the highest diffraction pattern peak of the original quartz can be used to calibrate the highest diffraction pattern peak of quartz in the AAC samples. The difference gives an indication of the dissolved quartz amount. This method was applied for all samples.

It should be noted that two different batches of quartz were ground. The batches were ground separately. It can be assumed that both batches have similar PSD, however this is not analyzed with the Mastersizer 2000. One batch of ground quartz is used for the production of 5 %, 10 % and 15 % substitution of quartz. The ground quartz used for 10-50 % substitution of Portland cement contained the ground quartz which was left from the first batch and included the ground quartz of the second batch. In this way, it is likely that the PSD's are almost similar for both batches. Finally, the batch including the ground quartz of the two batches combined was analyzed with XRD.

The XRD results were analyzed with the software DIFFRACplus EVA. The peak identification of the diffraction pattern was analyzed with the 'DIFFRACplus BASIC Evaluation Package PDFMaint 12, Bruker axs'. All the samples were subjected to XRD to detect the mineral phases. XRD analyses were performed using an automated diffractometer (Rigaku) at a step size of 0.02°, a scan rate of 3° per min and a scan range from 3° to 99° 2θ. A Ni-filtered Cu Kα radiation was used while operating with a voltage of 30 kV and an emission current of 15 mA.

Field emission scanning electron microscopy

FESEM was performed using a FEI FEGSEM Gatan 600 instrument. This FESEM was equipped with a secondary detector and energy dispersive X-ray (EDS) analyse system. The performance of a microscope, and therefore, the quality of an examination, depends on the resolution of the microscope and its ability to provide an image which has sufficient contrast to distinguish the observed phases against the background. The resolution or the resolving power of a microscope to reproduce the object is defined as the smallest separation of two points in the object that can be distinctly shown by the image.

All samples were examined by FESEM, to identify the reaction products in the AAC samples. The measurements were performed on 10 x 10 x 10 mm samples. The measured side was fractured while the other sides where straightly cut with a metal saw. The following parameters are determent: Pore formation, matrix, reaction of the additive in de matrix, crystal size distribution in a big pore and crystal size.

Color

Firstly, to give an indication of the color a picture is taken of all samples. Secondly, measurements with a spectrophotometer were performed on the quartz substitution samples.

5. MEASUREMENTS DURING CURING PERIOD OF QUARTZ SUBSTITUTION

5.1 INTRODUCTION

This chapter elucidates important influencing parameters and results obtained by test during the curing period of 5 %, 10 % and 15 % substitution of quartz with six different additives. The main purpose of this chapter is to determine the reaction rate of all quartz substitutions. No reviewed scientific article reports the observation of the mixture or any tests that has been done during the curing period. The following tests were conducted for all samples: (I) the slump flow test, (II) rising development (of the mixture) test, (III) the temperature development measurement and maximum temperature, (IV) the penetration depth test and, (V) the final product height measurement. In the next section a limited section of literature regarding the influence of the properties of additives on the rising and stiffening development is elucidated. Furthermore, a brief explanation of the used test methods is given.

SLUMP FLOW TEST

As mentioned before, the additives can be distinguished by their chemical or physical properties namely: (I) oxide composition, (II) calcium/silica ratio, (III) density and, (IV) PSD. In the early stage of the AAC hydration phases are two main reactions occurring which can be influenced by the properties of the additives. Firstly, the reaction of water with alite (and belite) in Portland cement generating C-S-H gel and portlandite ($Ca(OH)_2$). Secondly, water which reacts with quicklime producing portlandite. It is known from the literature that additives can amplify the binder effect due to their pozzolanic properties, varying PSD and decreased density. These properties can reduce w/s ratio which can be visible in the slump flow results. The slump flow test is a tool to confirm the enhanced or reduced reactivity and water demand of the additives in an early stage and of the mixture.

RISING DEVELOPMENT

The measurements will give an indication of the reaction rate which is influenced by the rising and stiffening development. If these developments are not occurring simultaneously a collapse of the mixture will be visible, also called the sinking effect. This is controlled by aluminum powder amount and w/s ratio. The rising development was measured once, during the first 60 min at frequency of 5 min.

TEMPERATURE MEASUREMENT DURING HYDRATION PERIOD

Siddique (2003) states that a low calcium Class F fly ash normally acts as a fine aggregate of spherical form in early stages of hydration, whereas a high calcium Class C fly ash may contribute to the early cementing reactions in addition to its presence as a fine particulate in the AAC mixture. Hydration of AAC mixture is an exothermic reaction and the released heat causes a rise of temperature of mixture. In this investigation, the reaction rate is analyzed by measuring the hydration temperature with thermocouples. For all substitution samples the temperature of hydration was monitored, from the moment the mixture entered the mould, each 30 sec. for 360 min. Generally, the maximum temperature occurred during the first 360 min.

PENETRATION DEPTH TEST

The interacting effects of fly ash with other chemical and mineral admixtures used in concrete may also influence the setting of concrete defined by Siddique (2003). It has been observed that all class F fly ashes, especially low calcium fly ashes with high carbon content or LOI, increase the setting time.

An indication of the setting also called stiffening can be measured globally with the penetration depth method. A low penetration depth would indicate a more solid or more stiffened mixture. A low penetration depth could be an indication a higher binder content. A higher binder content is the result of portlandite reacting with quartz forming C-S-H gel. Portlandite alone does not contribute to the strength. The C-S-H gel is a cementitious compound, the material responsible for holding AAC together. Less portlandite and more cementing compounds means stronger AAC. The penetration depth method was obtained by dropping an aluminum cone in the mixture. Firstly, the mixture was casted in the mould, 35 min later, the first measurement was performed each 5 min, till first hour of the curing period.

FINAL PRODUCT HEIGHT

Finally, there is the product height measurement to give a rough (± 15 mm) indication if a sample experienced an extensive or retarded rising of the mixture. The accuracy of the preformed tests discussed above can be doubtful, since all tests were only performed once. But, it should be noted that this method provides insight in general differences between the additives.

CONTROLLED REACTION RATE

As mentioned previously, the aim is to try to create an optimal reaction rate which can control by adjusting the aluminum powder and water amount. In total, 16 test samples were produced, in which all six additives were used for producing samples with a substitution of 5 % and 10 %. Based on, oxide composition, PSD, slump flow test and rising development measurements results of the 5 % and 10 % substitution, were the three best performing additives selected to use for 15 % substitution. Tab. 9 gives all substitution levels with quartz.

Table 9: All substitution levels with quartz

Substitution levels	5 %	10 %	15 %
	[kg]	[kg]	[kg]
Ground quartz	7.6	7.2	6.8
Cyclone ash	0.4	0.8	-
Paper sludge ash	0.4	0.8	1.2
Bio ash	0.4	0.8	-
Bottom ash	0.4	0.8	1.2
Dutch fly ash	0.4	0.8	-
Indian fly ash	0.4	0.8	1.2

5 % SUBSTITUTION

In critical cases, it was necessary to adjust the aluminum powder amount and/or w/s ratio, depending on the substitution level and water requirement of the additive. For 5 % substitution, only the aluminum powder amount for the cyclone ash sample was increased (by 1 g). Based on, chemical composition it was assumed that cyclone ash would have a low reactivity in an early stage. However, limited information made it difficult to predict the reaction rate. The w/s ratio was kept constant at 0.58, for all mixtures.

10 % SUBSTITUTION

Since the optimum reaction rate is critical, the effect of the 10 % substitution of additives was investigated experimentally. It is known from previous results of the 5 % replacement of quartz which mixture does not have an efficient balance, namely cyclone ash, bio ash and the Indian mixture. The aluminum powder amount was increased (by 1 g) for the 10 % substitution mixtures with bio ash, bottom ash and Indian fly ash. Simultaneously, the w/s ratio was decreased for bio ash to 0.54 and for bottom ash and Indian fly ash to 0.55. Less water was added since insufficient curing was reached in 10 % substitution.

15 % SUBSTITUTION

The aluminum powder amount was increased with 2 g for 15 % bottom ash and Indian fly ash samples and the w/s ratio was simultaneously decreased to 0.56. The w/s ratio was only increased for paper sludge ash mixture to 0.59, because of its high water absorption properties.

5.2 RESULTS AND DISCUSSIONS

In the next section, each graph displays all substitution results of one test to give a general overview. The following tests are shown: Slump flow, temperature of hydration, rising development and stiffening development results. Details of these results can be found in Appendix A.2.1.1. The results of each additive substitution is separately elucidated and discussed, followed by, a detailed presentation. Differences in the aluminum powder amount and w/s ratio influence the performance of the tests. Therefore, no statement can

be made based on direct comparison of all mixtures. However, the performance of each additive substitution is comparable.

5.2.1 GENERAL OVERVIEW OF RESULTS

A general overview of the slump test is visible in Fig. 18. An increased substitution of paper sludge ash, bottom ash and Indian fly ash illustrates a reduction of slump flow compared to the reference. But cyclone ash substitution demonstrates the contrary.

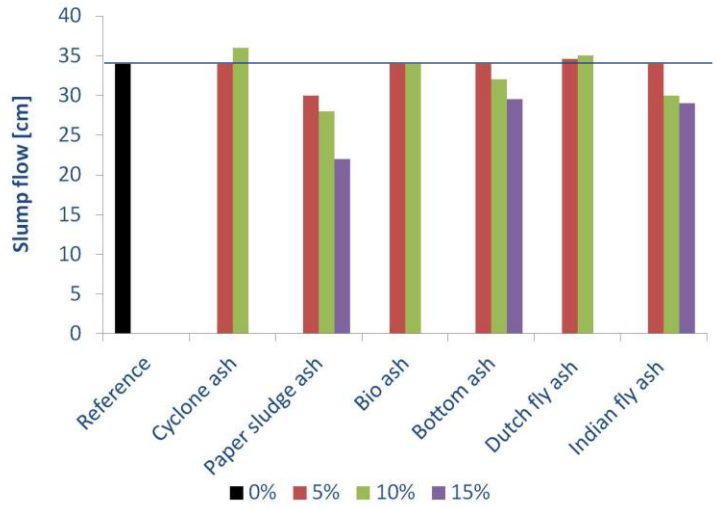

Figure 18: Slump flow results of all quartz substitutions with six different additives, measured after 2 min of mixing

The temperature of the mixture is measured during the first 6 h (Fig. 19). The temperature rapidly increases in the first 5 min, except for the 10 % bio ash. A significantly disturbed temperature development is detected for 10 % bio ash compared to the other samples, from the start till the end (360 min). For all mixtures, except for 10 % bio ash, a slightly higher temperature (from 0-360 min) was observed compared to reference. For all other samples show, a slightly retarded temperature during 5-15 min was spotted. Afterwards, a gradual increase of temperature till approximately 190 min is visible for all mixtures.

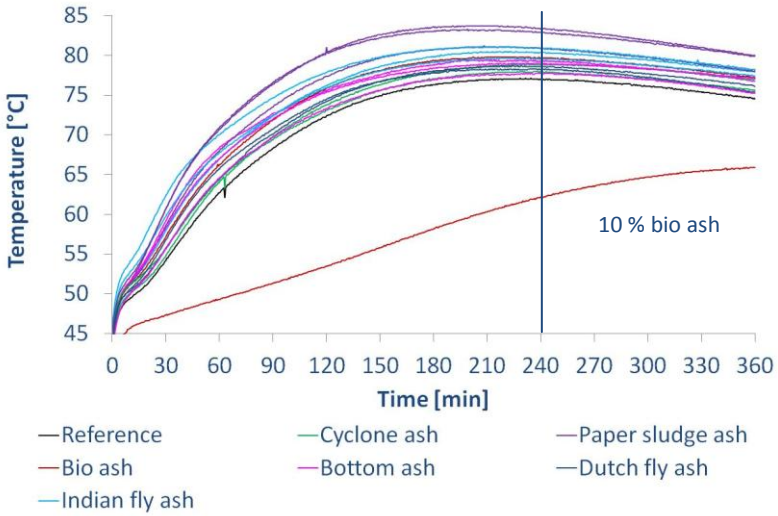

Figure 19: Results of temperature of hydration of all quartz substitutions with six different additives

The rising development in relation to the temperature increase was observed to obtain an indication of the reaction rate (Fig. 19-20). A higher rising height for the majority of the mixtures was demonstrated in comparison with reference. Only, a significant different rising height development is revealed for 10 % cyclone ash mixture. It should be noted that the rising height of 5% cyclone ash mixture could not be measured after 35 min since the mixture lifted the lid of the mould.

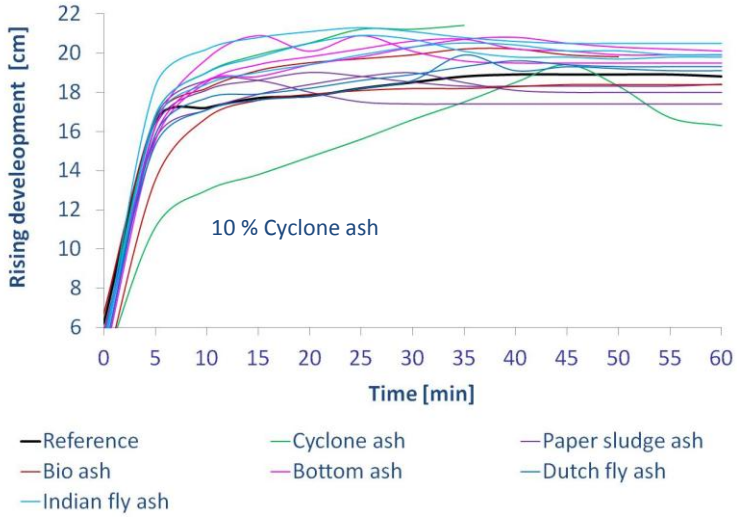

Figure 20: Results of rising development during of all quartz substitutions with six different additives

The penetration depth of the mixture was measured after ± 25 min till 60 min (Fig. 21). A prolonged stiffening period for Dutch fly ash, cyclone ash and bio ash substitution were demonstrated compared to reference. This could be due to a lower reactivity, too low w/s ratio or too high aluminum powder amount resulting in a retarded temperature development. In contrast, a significantly enhanced stiffening time is illustrated for paper sludge ash, bottom ash and Indian fly ash substitutions. It is assumed that these additives are more reactive, producing more heat and therefore react more quickly, giving a low penetration value.

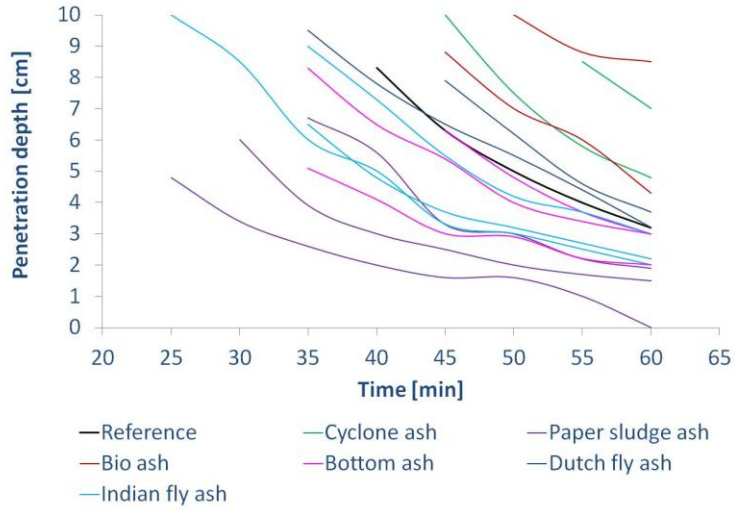

Figure 21: Results of penetration depth measurement of all quartz substitutions with six different additives

5.2.2 CYCLONE ASH SUBSTITUTION

DISCUSSION OF 5 % SUBSTITUTION

It should be noted that the aluminum powder amount is increased with 1 g (and the w/s ratio remained standard). Fig. 22 illustrates similar slump flow results for 0 % and 5% cyclone ash substitution. Next, a slightly higher temperature is observed for 5 % compared to the 0 % substitution, during the first 360 min of curing (Fig. 23). Tab. 10-11 show that a higher maximum temperature and higher T_{240} was found for 5 % than 0 % substitution. An elevated rising height and noticeably higher penetration depth are displayed in Fig. 24-25 and Tab. 12. Eventually, an increased final product height was obtained (Fig. 26). It seems that cyclone ash is not highly reactive after 2 min of mixing. Also, no increase or decrease of water demand is detected. It is seen that the increased temperature, penetration depth and final product height and an enhanced rising height of 5 % mixture, were due to extra aluminum powder. Based on, the increased rising, it can be concluded that the reaction rate is not in balance.

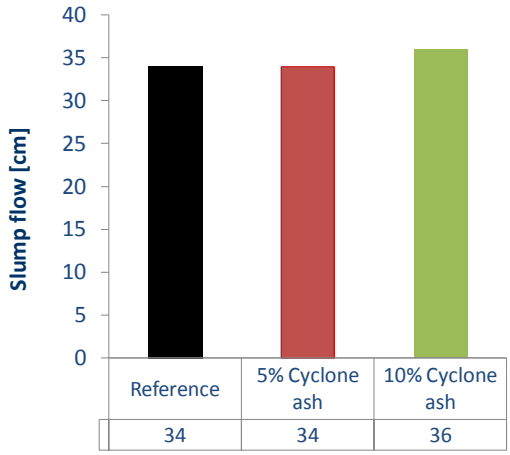

Figure 22: Results slump flow of cyclone ash substitution

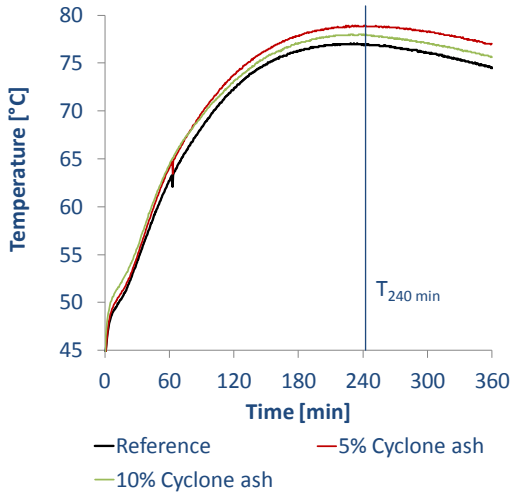

Figure 23: Results temperature of cyclone ash substitution, during first 360 min of curing period

Table 10: The maximum temperature for cyclone ash

Cyclone ash substitution	Max. Temp. [°C]	Time [min]
0 %	77.0	228
5 %	78.9	227
10 %	78.0	227

Table 11: Temperature at $T_{240\ min}$ cyclone ash

Cyclone ash substitution	Temperature [°C]
0 %	77.0
5 %	78.8
10 %	77.9

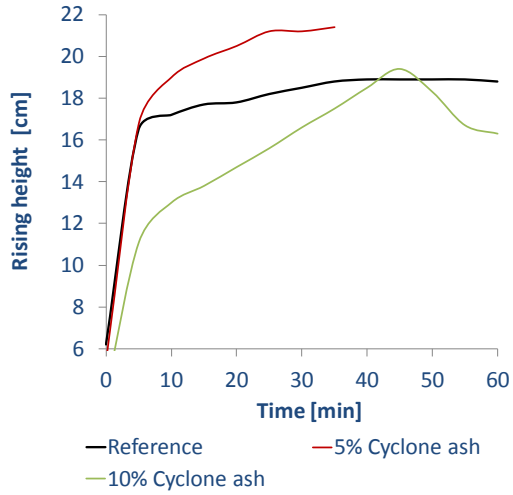

Figure 24: Results rising development cyclone ash substitution, during first 60 min of curing period

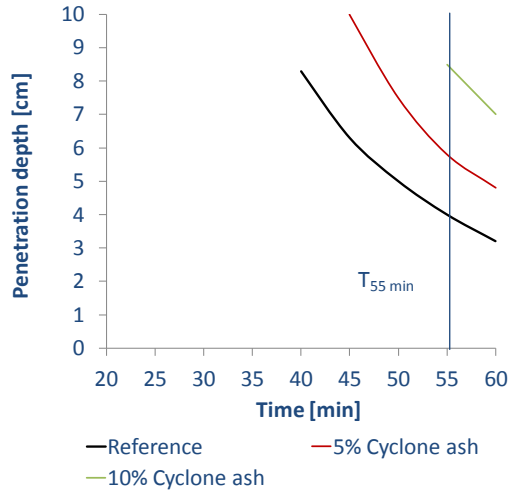

Figure 25: Results penetration depth of cyclone ash substitution, during first 60 min of curing period

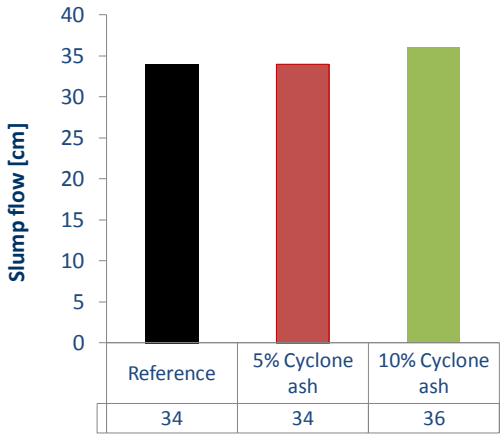

Figure 26: Results final product height of cyclone ash substitution

Table 12: Results penetration depth at $T_{55\,min}$ for cyclone ash

Cyclone ash substitution	Penetration [cm]
0 %	4.0
5 %	5.8
10 %	8.5

DISCUSSION OF HIGHER SUBSTITUTION

The aluminum powder amount and w/s ratio were kept standard for 10 % cyclone ash substitution. A wider slump flow for 10 % compared 0 % substitution is seen in Fig. 22. A retarded rising development and noticeably sinking effect after 45 min for 10 % is displayed in Fig. 24. At the same time, a slightly high temperature (Fig. 23) and delayed stiffening development (Fig. 25) is measured. A lower final product height for 10 % in comparison with the 0 % is seen in Fig. 26.

It can be seen that the hydrogen reaction is retarded due to components in cyclone ash, covering aluminum particles causing less dissolving and retarding of the rising development. After the retarded rising of the mixture a noticeable sinking effect was detected. The major sinking indicates a large amount of hydrogen gasses being released in combination with the retarded stiffening development. It seems that the wider slump flow, the rising and the stiffening development stagnated due to unknown components in cyclone ash. It is assumed that the slightly reduction in temperature is caused by the reduction in the aluminum powder amount and due to the retarding properties of cyclone ash (however this is not demonstrable). To conclude, the reaction rate was far from optimal.

5.2.3 PAPER SLUDGE ASH SUBSTITUTION

DISCUSSION OF 5 % SUBSTITUTION

All results are compared to the reference. A significantly lower slump flow (Fig. 27) and significantly high temperature (Fig. 28, Fig. 30 and Tab. 13-14) resulted in fairly low penetration depth (Fig. 30 and Tab. 15). Next, Fig. 29 displays an increased rising development and increased sinking effect which results in a lower final product height (Fig. 31).

Paper sludge ash contains the following calcium-rich minerals: 41 % calcium carbonate (also called calcite, $CaCO_3$), 23% calcium oxide (also called quicklime, CaO) and 2.5 % calcium hydroxide (also called portlandite, $Ca(OH)_2$). Quicklime reacts with water producing heat by the formation of the hydrate, portlandite [1] while producing heat. As it hydrates, an exothermic reaction results and the mixture will bind.

Additional to this, metakaolin ($Al_2Si_2O_7$) reacts with cement, lime [7] and consumes portlandite [8]. Because metakaolin consumes portlandite, it takes away the alkali and the reaction does not occur. The reaction of metakaolin produces C-S-H or C-S-A-H phases. In addition, metakaolin has a fine particle size producing a seeding of the cement reaction and therefore accelerates reaction. As a consequence, the pozzolanic reaction will form more C-S-H leading to an earlier strength development. The adding of metakaolin will increase the cement content. This will affect the w/s ratio, a critical factor in mixture design. This binder content enhances the stiffening development of the mixture, resulting in an accelerated stiffening effect.

Based on the slump flow test, it is seen that a paper sludge ash mixture consumes more water as a result of increased binder content indicating a high reactivity in an early stage.

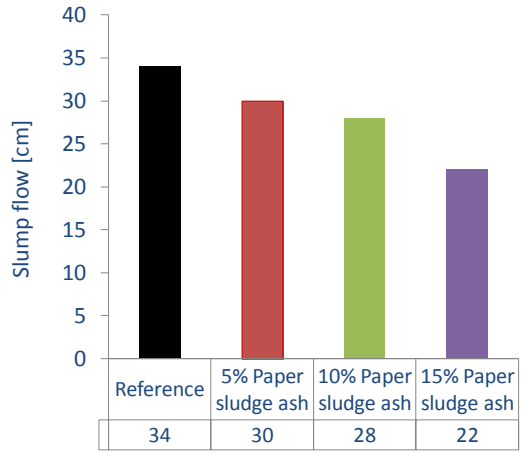

Figure 27: Results slump flow of paper sludge ash substitution

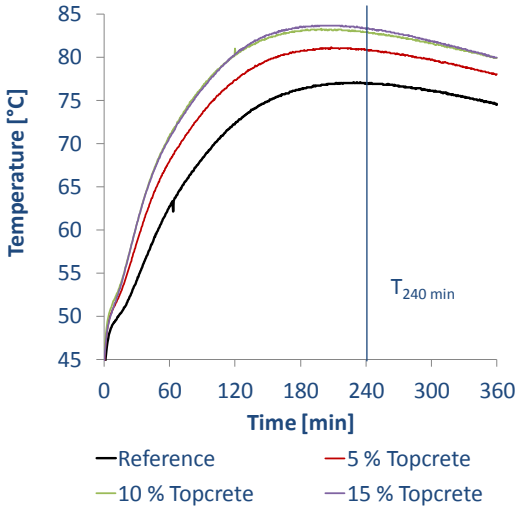

Figure 28: Results temperature of paper sludge ash substitution, during first 360 min of curing period

Table 13: The maximum temperature for paper sludge ash

Paper sludge ash substitution	Max. Temp. [°C]	Time [min]
0 %	77.0	228
5 %	83.3	199
10 %	83.3	199
15 %	83.7	191

Table 14: Temperature at $T_{240\ min}$ for paper sludge ash

Paper sludge ash substitution	Temperature [°C]
0 %	77.0
5 %	80.9
10 %	82.9
15 %	83.3

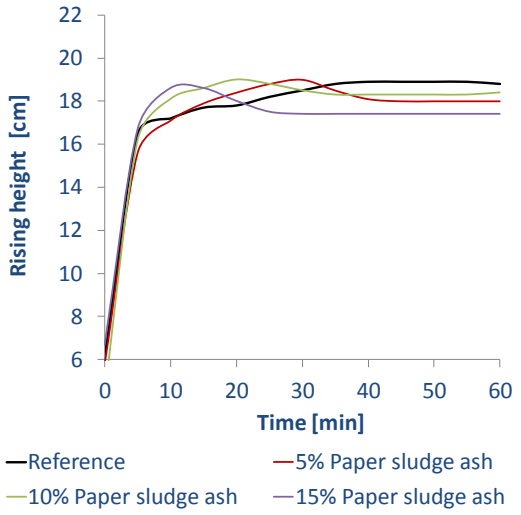

Figure 29: Results rising development of paper sludge ash substitution

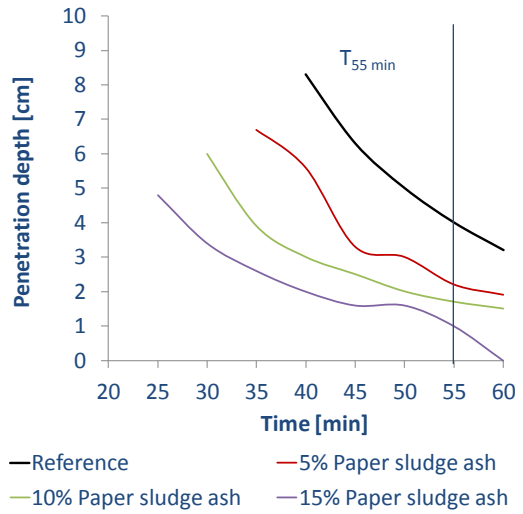

Figure 30: Results penetration depth of paper sludge ash substitution

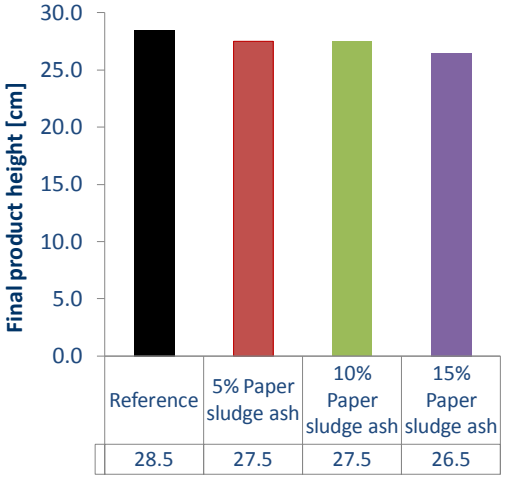

Figure 31: Results final product height of paper sludge ash substitution

Table 15: Results penetration depth at $T_{55\ min}$ for paper sludge ash

Paper sludge ash substitution	Penetration [cm]
0 %	4.0
5 %	2.3
10 %	1.7
15 %	1.0

DISCUSSION OF HIGHER SUBSTITUTION

It should be noted that to improve the slump flow a higher w/s ratio for 15 % substitution of paper sludge ash is selected. It is known beforehand that more water retards stiffening time and reduces the sinking effect. A higher paper sludge ash substitution increases the binder content by lime, metakaolin and portlandite resulting in increased water consumption. This results in a reduced slump flow (Fig. 27), an accelerated temperature development (Fig. 28), a slightly prolonged rising development (Fig. 29), an accelerated sinking effect, an accelerated stiffening development (Fig. 30) and a reduced final product height (Fig. 31).

Normally, the w/s ratio is reduced to correct for the slump flow and the sinking effect. Although, the 10 % and 15 % substitution had an already increased w/s ratio, an early sinking effect occurred, due to the necessity of an even higher w/s ratio. To conclude, the reaction rate for higher substitutions was not optimal.

5.2.4 BIO ASH SUBSTITUTION

DISCUSSION OF 5 % SUBSTITUTION

The w/s ratio and aluminum powder amount was kept in standard condition. The 5 % bio ash mixture shows a slightly increased temperature (Fig. 33 and Tab. 16-17) causing a similar slump flow (Fig. 32), a prolonged rising (Fig. 34), an enhanced stiffening development (Fig. 35 and Tab. 18) and finally an marginally increased final product height (Fig. 36) compared to 0 % substitution.

The differences in results are directly related to 5 % bio ash substitution. The presence of phosphates probably retarded the stiffening development. As results the stiffening and rising development do not occur simultaneously. However, no sinking effect was detected during the period of hydrogen gas release because of a sufficient stiffened mixture.

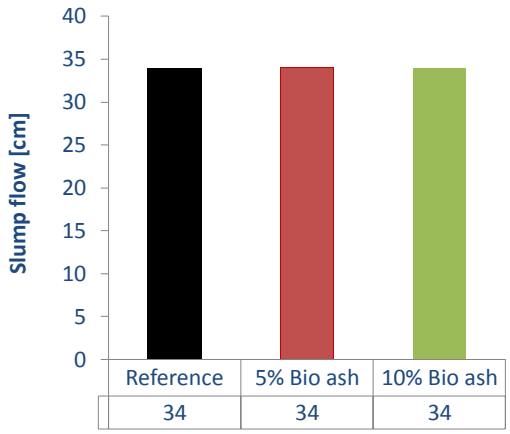

Figure 32: Results slump flow of bio ash substitution

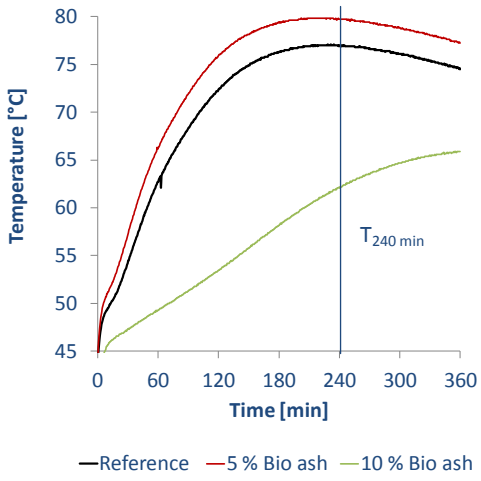

Figure 33: Results temperature of bio ash substitution, during first 360 min of curing period

Table 16: The maximum temperature for bio ash

Bio ash substitution	Max. Temp. [°C]	Time [min]
0 %	77.0	228
5 %	79.8	199
10 %	66.0	360

Table 17: Temperature at $T_{240\ min}$ for bio ash

Bio ash substitution	Temperature [°C]
0 %	77.0
5 %	79.7
10 %	62.2

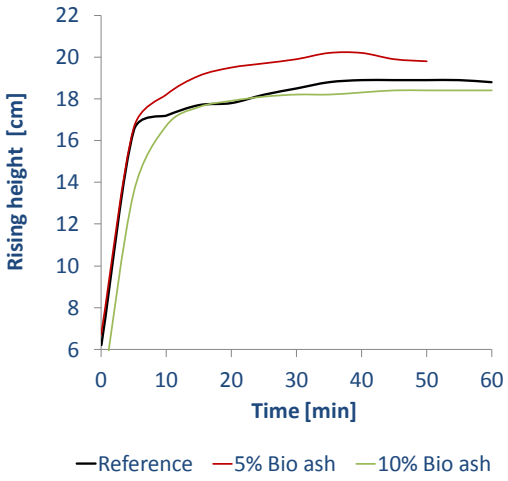

Figure 34: Results rising development of bio ash substitution, during first 60 min of curing period

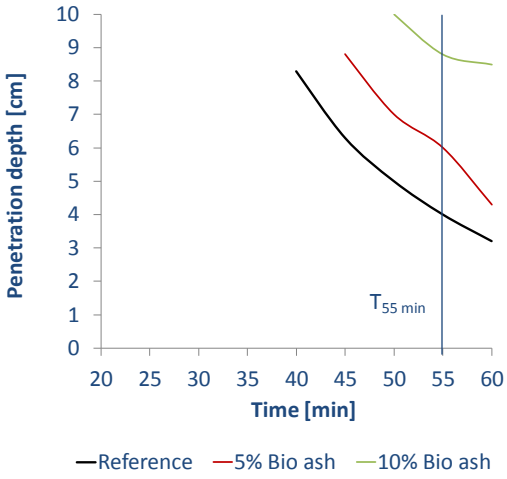

Figure 35: Results penetration depth of bio ash substitution, during first 60 min of curing period

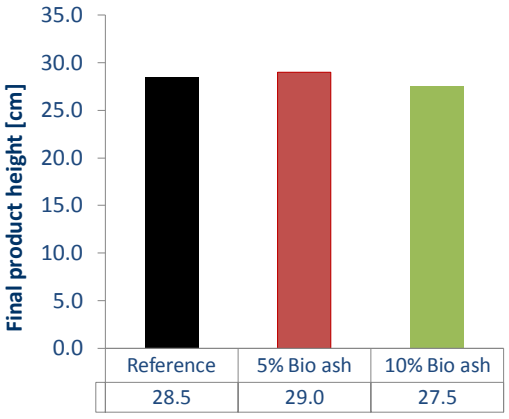

Figure 36: Results final product height of bio ash substitution

Table 18: Results penetration depth at $T_{55\ min}$ for bio ash

Bio ash substitution	Penetration [cm]
0 %	4.0
5 %	6.0
10 %	8.8

Discussion of higher substitution

To improve the slump flow the w/s ratio was reduced and consequently the aluminum powder amount was increased for the 10 % bio ash. These changes in parameters and the higher substitution of bio ash resulted in: similar slump flow (Fig. 32) and similar rising development (Fig. 34). But a noticeably retarded temperature development (Fig. 33 and Tab. 16-17) was observed resulting in a slightly reduced final product height (Fig. 36). However, strangely also a significantly enhanced stiffening development is demonstrated in Tab. 18 and Fig. 35.

It is suggested that a higher amount of phosphates in bio ash retarded the aluminum and cement reactions, thereby reducing the production of hydrogen gas. The rising development shows that although the mixture was less stiffened it was sufficient enough to resist the reduced hydrogen gas release. However, the rising development of higher substitution is comparable to the reference.

5.2.5 BOTTOM ASH SUBSTITUTION

DISCUSSION OF 5 % SUBSTITUTION

The w/s ratio and aluminum powder amount was kept as the standard. The 5 % bottom ash substitution has led to: an identical slump flow (Fig. 37), a slightly increased temperature (Fig. 38 and Tab. 19-20), a noticeably enhanced rising development (Fig. 39), an identical stiffening development (Fig. 40 and Tab. 21) and a slightly higher final product height (Fig. 41). All results were compared to the reference.

5 % bottom ash substitution caused an increased rising development suggesting that the mixture is not sufficiently stiffened when the hydrogen is produced. However, an increased temperature suggests an increase in binder content due to pozzolanic properties of bottom ash. It is assumed that this prevented the sinking effect. Based on this, no optimum reaction rate is obtained.

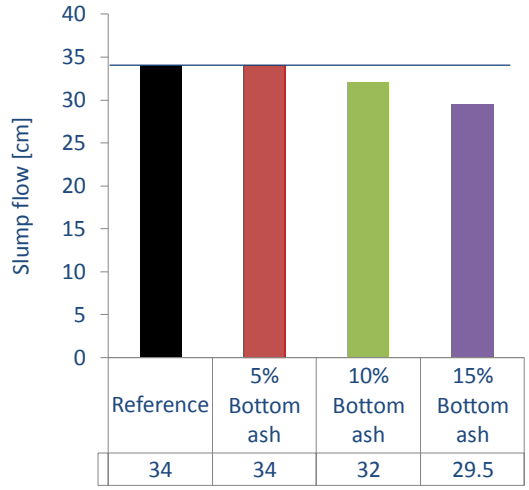

Figure 37: Results slump flow of bottom ash substitution

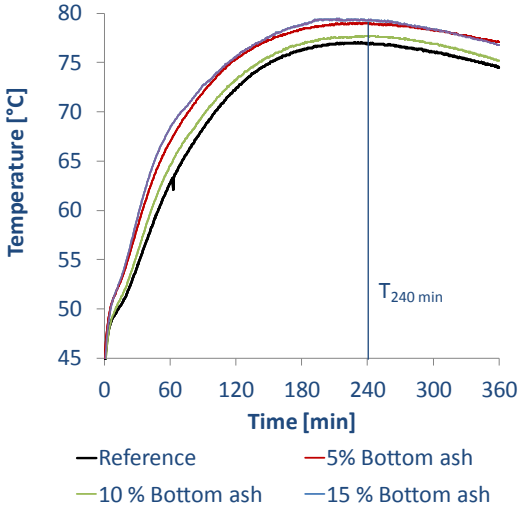

Figure 38: Results temperature of bottom ash substitution, during first 360 min of curing period

Table 19: The maximum temperature bottom ash

Bottom ash substitution	Max. Temp. [°C]	Time [min]
0 %	77.0	228
5 %	79.0	211
10 %	77.7	229
15 %	80.5	207

Table 20: Temperature at $T_{240\ min}$ bottom ash

Bottom ash substitution	Temperature [°C]
0 %	77.0
5 %	79.0
10 %	77.7
15 %	79.3

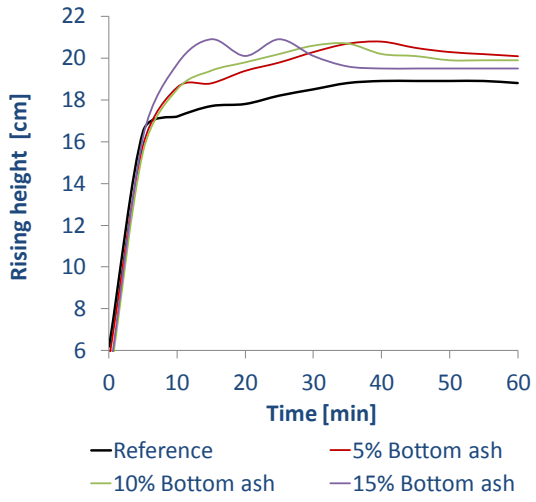

Figure 39: Results rising development of bottom ash substitution, during first 60 min of curing period

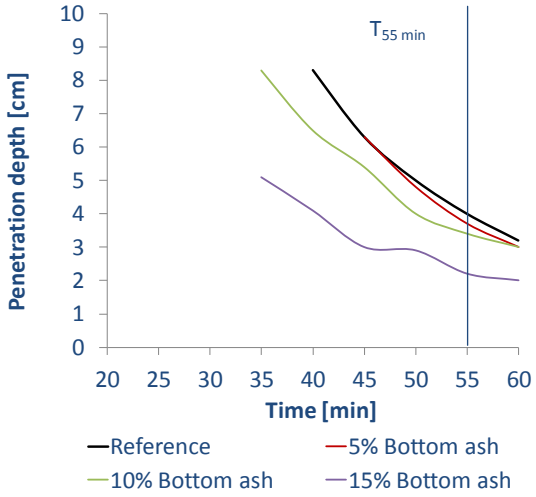

Figure 40: Results penetration depth of bottom ash substitution

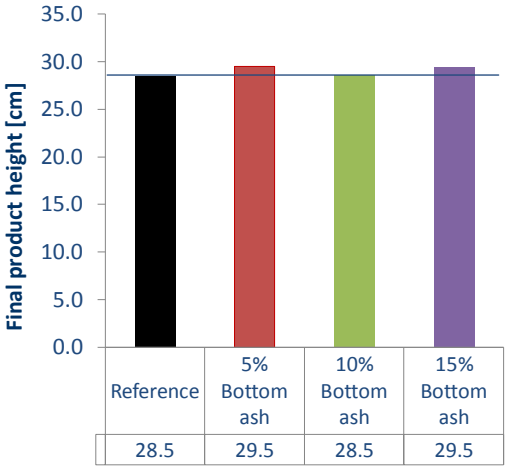

Figure 41: Results final product height of bottom ash substitution

Table 21: Results penetration depth at $T_{55\ min}$ for bottom ash

Bottom ash substitution	Penetration [cm]
0 %	4.0
5 %	3.8
10 %	3.4
15 %	2.3

DISCUSSION HIGHER SUBSTITUTION

To improve the slump flow the w/s ratio was decreased (0.55 and 0.53) and consequently the aluminum powder had to be increased (15 g and 16 g) for the 10 % and 15 % substitution. The results are compared to the 5 % substitution. The 10 % substitution showed a slightly lower temperature (Fig. 38 and Tab. 19-20) which resulted in a gradual decrease in slump flow (Fig. 37) and an increased stiffening development (Fig. 40 and Tab. 21), an identical rising development (Fig. 39) and a slightly decreased final product height (Fig. 41).

The decreased penetration depth and increased rising development are evidence of the pozzolanic properties of bottom ash (in combination with the lower w/s ratio and the additional aluminum powder) causing an increased binder effect. The increased rising development and the minor sinking effect show no optimal reaction rate, since the rising and stiffening do not occur simultaneously.

Only, a strange rising development is illustrated. It is assumed that the first drop in height (at 20 min) was a measurement error. However, the sinking effect is clearly present, suggesting a disturbed reaction rate.

5.2.6 DUTCH FLY ASH SUBSTITUTION

DISCUSSION OF 5 % DUTCH SUBSTITUTION

The w/s ratio and aluminum powder amount was kept as the standard. The 5 % Dutch fly ash mixture shows a slightly increased temperature (Fig. 43 and Tab. 22-23) causing a similar slump flow (Fig. 42), an identical rising (Fig. 44), a slightly retarded stiffening development (Fig. 45 and Tab. 24) and finally a marginally increased final product height (Fig. 46) compared to 0 % substitution. When the rising development is at 35 min a small increase in height is visible, but this is assumed to be a measurement error.

The slightly higher temperature suggests that Dutch fly ash has less pozzolanic properties. Also, the results of the penetration test, seems to indicate a minor increase in binder content. Both confirm low cementitious activity during the first 6 hours of curing. However, the reaction rate is optimal for the 5 % Dutch fly ash mixture with the standard aluminum powder amount and w/s ratio.

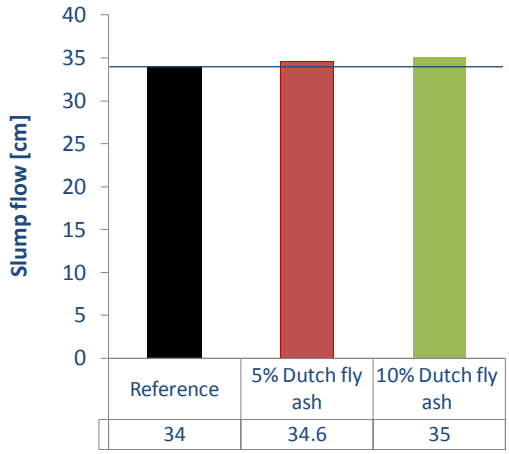

Figure 42: Results slump flow Dutch fly ash substitution

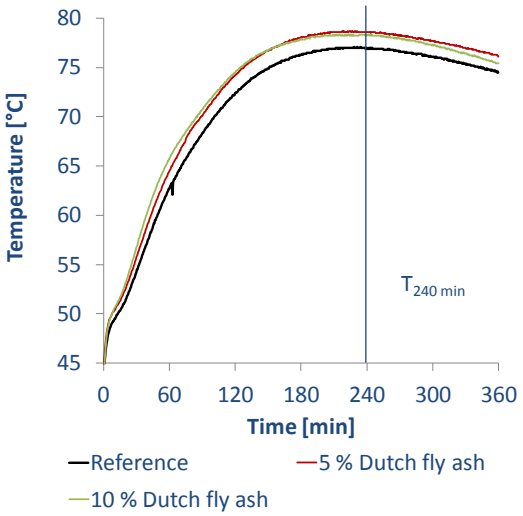

Figure 43: Results temperature of Dutch fly ash substitution

Table 22: The maximum temperature for Dutch fly ash

Dutch fly ash substitution	Max. Temp. [°C]	Time [min]
0 %	77.0	228
5 %	78.8	217
10 %	78.3	206

Table 23: Temperature at $T_{240\ min}$ Dutch fly ash

Dutch fly ash substitution	Temperature [°C]
0 %	77.0
5 %	78.6
10 %	78.2

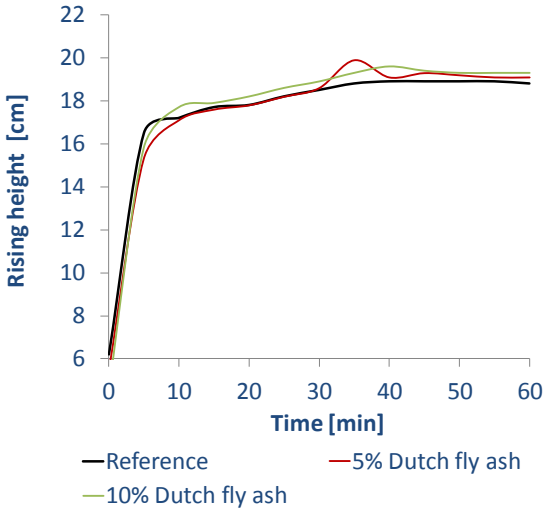

Figure 44: Results rising development Dutch fly ash substitution

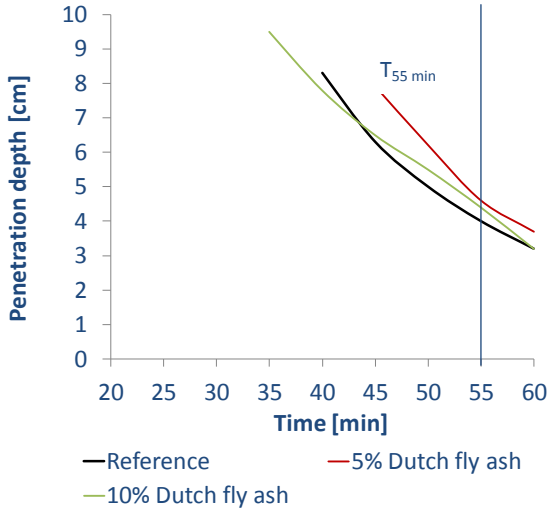

Figure 45: Results penetration depth of Dutch fly ash substitution, during first 60 min of curing period

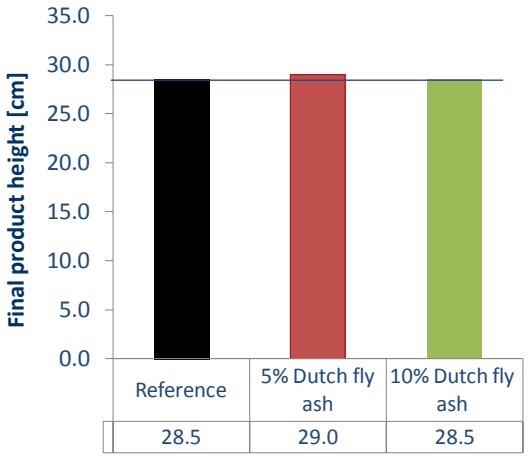

Figure 46: Results final product height of Dutch fly ash substitution

Table 24: Results penetration depth at $T_{55\ min}$ for Dutch fly ash

Dutch fly ash substitution	Penetration [cm]
0 %	4.0
5 %	4.5
10 %	4.8

DISCUSSION OF HIGHER SUBSTITUTION

For the 10 % Dutch fly ash the w/s ratio and the aluminum powder amount were kept standard, since the slump flow was sufficient for the 5 % substitution. The combination of these parameters resulted in almost the same results as the 5 % Dutch fly ash substitution. Only, the stiffening development of the 10 % substitution was more similar to the reference. So, also here it can be assumed that an optimal reaction rate is obtained.

5.2.7 INDIAN FLY ASH SUBSTITUTION

DISCUSSION OF 5 % SUBSTITUTION

The w/s ratio and aluminum powder amount was kept as the standard for the 5 % Indian fly ash. Comparing all result with the reference, the following conclusions can be made: Fig. 47 illustrates the same slump flow as the reference. Next, a slightly higher temperature (Fig. 48 and Tab. 25-26) resulted in a lower penetration depth (Tab. 27 and Fig. 50). Next, an increased rising development results in an increased final product height (Fig. 51).

It is assumed that the presence of several components in Indian fly ash increased the stiffening development. However, the accelerated stiffening occurred after 25 min and the rising development increased after 10 min. Because the stiffening and rising development did not occur simultaneously, it is possible that the increased rising caused a disturbed reaction rate.

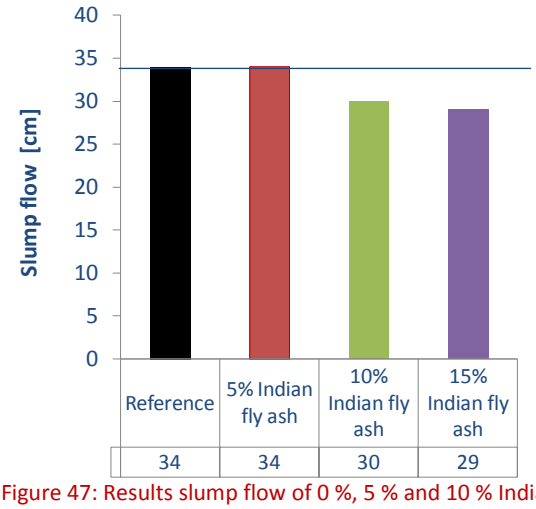

Figure 47: Results slump flow of 0 %, 5 % and 10 % Indian fly ash substitution

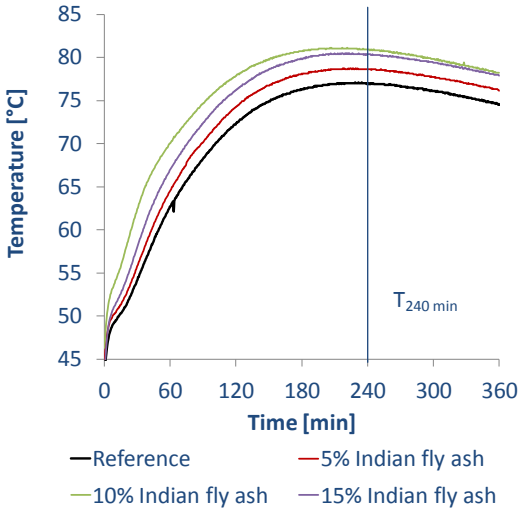

Figure 48: Results temperature of Indian fly ash substitution

Table 25: The maximum temperature for Indian fly ash

Indian fly ash substitution	Max. Temp. [°C]	Time [min]
0 %	77.0	228
5 %	78.7	218
10 %	81.1	206
15 %	79.5	212

Table 26: Temperature at $T_{240\ min}$ for Indian fly ash

Indian fly ash substitution	Temperature [°C]
0 %	77.0
5 %	79.5
10 %	80.9
15 %	80.4

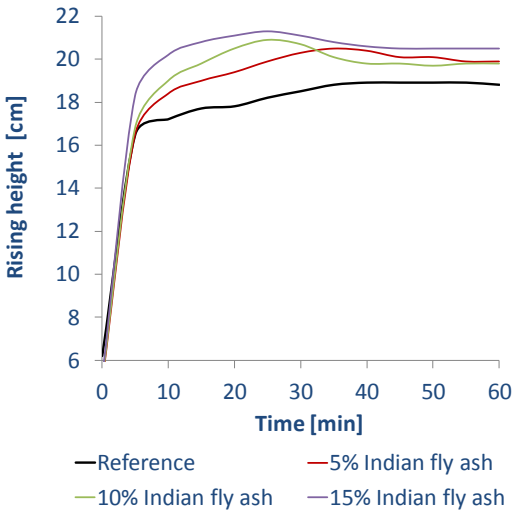

Figure 49: Results rising development of Indian fly ash substitution

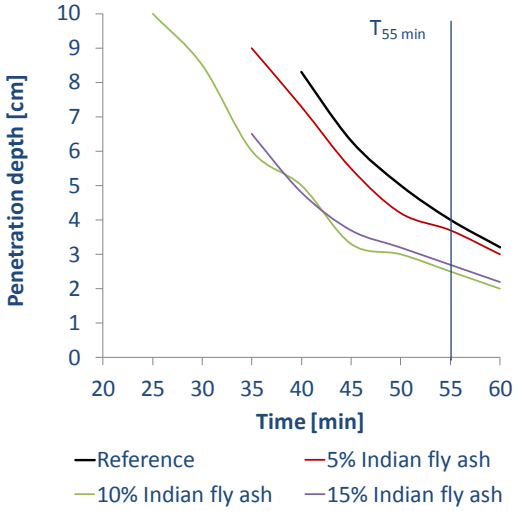

Figure 50: Results penetration depth of Indian fly ash substitution

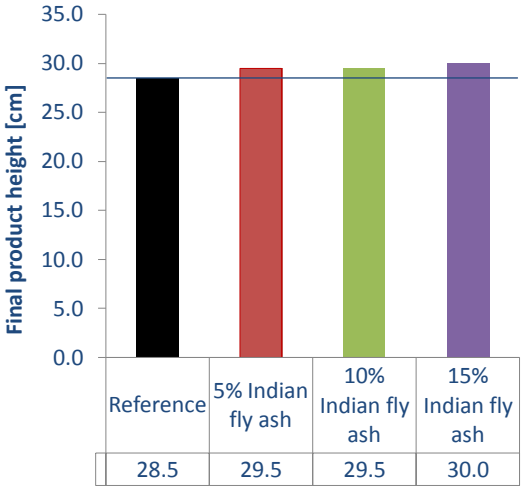

Figure 51: Results final product height of Indian fly ash substitution

Table 27: Results penetration depth at $T_{55\ min}$ for Indian fly ash substitution

Indian fly ash substitution	Penetration [cm]
0 %	4.0
5 %	3.8
10 %	2.6
15 %	2.8

Discussion of higher substitution

To improve the slump flow the w/s ratio was decreased (0.55 and 0.52) and consequently the aluminum powder was increased (15 g and 16 g) for the 10 % and 15 % substitution. The results are compared to the 5 % substitution. The 10 % substitution showed an increase in temperature (Fig. 48 and Tab. 25-26) resulting in a decrease in slump flow (Fig. 47) and a noticeable increased stiffening development (Fig. 50 and Tab 27), increased rising development with noticeably sinking effect (Fig. 49) and a similar final product height (Fig. 51). The presence of the sinking effect is clearly visible suggesting a disturbed reaction rate.

To prevent the sinking effect, significantly less water was added to the 15 % substitution. The 15 % substitution is compared to the 10 % substitution gives the following data: a reduced slump flow, an increased rising development and increased final product height. But, also a decrease in temperature was observed since less could react with lime producing heat and a similar stiffening development.

5.3 CONCLUSION

Tab. 28 illustrates all results of quartz substitution during the curing period in order to compare the reaction rate results of all additive substitutions with the reference.

Table 28: All test results during curing period

				Reaction rate			
		Slump test	Maximum temperature	Stiffening development	Rising development		
[%]		[cm]	[°C]	at $T_{55\ min}$ [min]	Comparable	Small deviation	Large deviation
0	Reference	34.0	77.0	4.0	x		
5	Cyclone ash	34.0	78.8	5.8			x
10	Cyclone ash	36.0	77.9	8.5			x
5	Paper sludge ash	30.0	83.3	2.3		x	
10	Paper sludge ash	28.0	83.3	1.7		x	
15	Paper sludge ash	22.0	83.7	1.0			x
5	Bio ash	34.0	79.8	6.0		x	
10	Bio ash	34.0	66.0	8.8	x		
5	Bottom ash	34.0	79.0	3.8		x	
10	Bottom ash	32.0	77.7	3.4		x	
15	Bottom ash	29.5	80.5	2.3			x
5	Dutch fly ash	34.6	78.8	4.5	x		
10	Dutch fly ash	35.0	78.3	4.8	x		
5	Indian fly ash	34.0	78.7	3.8		x	
10	Indian fly ash	30.0	81.1	2.6			x
15	Indian fly ash	29.0	79.5	2.8			x

General conclusions:

1. It is proven that the slump flow test is an efficient tool to define if the mixture is successful based on the viscosity. The viscosity of the mixture is influenced by the reactivity of the mixture.
2. All substitutions, except for the 10 % bio ash substitution, generate more heat than the reference, indicating more reaction is taking place.
3. The 10 % bio ash, 5 % and 10 % Dutch fly ash show a comparable reaction compared to the reference. This would suggest that an optimal final product can be obtained.

The following conclusions based on the slump test can be drawn:

1. All paper sludge ash substitutions have a decreased slump flow, compared to the reference.
2. All 5 % substitutions have a similar slump flow, compared to the reference, indicating that the substitution has no influence on the slump test.
3. The 10 % cyclone ash has an increased slump flow, compared to the reference.
4. All 10 % and 15 % substitution result in smaller slump flow, indicating that the substitution has a noticeable influence on the slump test.

Based on the assumption that the rising development should be comparable to the reference the following conclusions can be drawn: A similar rising development is obtained for 10 % bio ash and 5 % and 10 % Dutch fly ash substitutions, suggesting comparable porosity and density.

6. PHYSICAL PROPERTIES OF QUARTZ SUBSTITUTION

6.1 INTRODUCTION

The main purpose of this work was to test the performance of the physical properties and to determine the possibilities and restrictions of the additives incorporated into AAC. The different analyzed physical properties are: dry density, CS, porosity and thermal conductivity.

In earlier studies attempts were performed to study a substitute of quartz in AAC with at the same time retaining or increasing the CS. It was suggested that the CS is (highly) depending on the density, influenced by porosity. The porosity is based on the macropores produced by hydrogen gas and the micropores both open space in the matrix. After, the curing period the macropores have reach their final size. However, the micropores will change in the autoclave (humid) environment which stimulates the crystal grow, thereby decreasing the micropores in the matrix.

Jing et al. (2008) confirms that the CS is:

1. Closely related to the filling degree of tobermorite crystals in the matrix.
2. And depends on the tobermorite formation.
3. And is closely related to the filling degree of the formed tobermorite in the spaces between additives particles.

Crennan et al. (1977) states if much unreacted quartz remains, strength is controlled by its particle size distribution and the porosity. But if the material is largely C-S-H, the distribution of particle types within the C-S-H has a major effect; increasing crystallinity in C-S-H can either raises or lowers strength depending on the amount of unreacted quartz.

It is known that met kaolin combined with the portlandite produces additional cementing compounds, the material responsible for holding all materials together. Portlandite accounts for up to 25% of the hydrated Portland cement, and portlandite does not contribute to the strength. So, less portlandite and more cementing compounds means a stronger product. Metakaolin is present in paper sludge ash. It is expected that an increased CS will be obtained for the paper sludge ash substitution.

METHODOLOGY COMPRESSIVE STRENGTH AND DENSITY

The CS and corresponding density are critical parameters which determine the performance of the samples. As outlined in the introduction the samples should be within the density range of 350-500 kg/m³ and meet the standard (NEN-EN 772-1:2000) as is illustrated in Tab. 29. It should be noted that according to the standard the humidity of the test samples should be 6 % during the CS test. However, a humidity of 6 % though is difficult to attain and is likely to cause errors in the case of a low number of test samples (and tests). For this research a humidity of 0 % was selected, since this is precisely measurable. It was taken into account that the CS will be reduced with approximately 20 % (Heinz, 2012).

Table 29: Dry density and CS requirements according to NEN-EN 772-1:2000

	Name of density range	Density range	Minimum CS
	[kg/m³]	[kg/m³]	[N/mm²]
ρ 4.0	400	350 ≤ ρ 4.0 ≤ 400	2
ρ 4.5	450	400 ≤ ρ 4.5 ≤ 450	3
ρ 5.0	500	450 ≤ ρ 5.0 ≤ 500	4

METHODOLOGY POROSITY AND THERMAL CONDUCTIVITY

The porosity is not specified in the standard. The results of the porosity and thermal conductivity are divides in several ranges, shown in Tab. 30-31. This makes comparison of the results more suitable.

Table 30: Tolerated variance range of porosity

	Porosity [%]				
Range	79-80	81-80	81-82	82-83	83-84
Increase/decrease value	- 1.5	± 0.5	+ 1.5	+ 2.5	+ 3.5

Table 31: Tolerated variance range of thermal conductivity

	Thermal conductivity [W/m.k]			
Range	0.092 - < 0.092	0.095 - 0.092	0.095 - 0.099	0.099 - 0.102
Increase/decrease value	< - 0.010	- 0.005	± 0.002	+ 0.005

It is known that a minor change (± 1 %) in porosity gives a large variation in CS and density.

The porosity is analyzed based on difference of the dry density and the specific density obtained by the pycnometer. Three identical dry cylinders (h: 40 mm, D: 38 mm) for each sample were measured. Each cylinder was measured 10 times to guarantee a SDV of less than 5 %. In some cases a higher SDV was obtained, however this method is less sufficient to measure porous material.

The standard EN-1745 (2002) gives only a maximum thermal conductivity value of 1.1 W/m.K. The porosity is measured twice for each sample. These two measurements give an indication, however the accuracy is questionable.

COMPENSATED COMPRESSIVE STRENGTH

The CCS in N/mm² is now mass based which makes comparison on mass possible.

6.2 RESULTS AND DISCUSSION

This section contains the physical properties results and discussion. Firstly, a general overview is given by showing all substitution results of each test are incorporate and displayed in one figure. Fig. 52 illustrates the dry density, Fig. 53 the CS, Fig. 54 the porosity, Fig. 55 the thermal conductivity and Fig. 56 the CCS. Each additive substitution is separately discussed in one section. Appendix A.2.2 illustrates physical properties measurement in detail.

In the following section all results are compared to the reference.

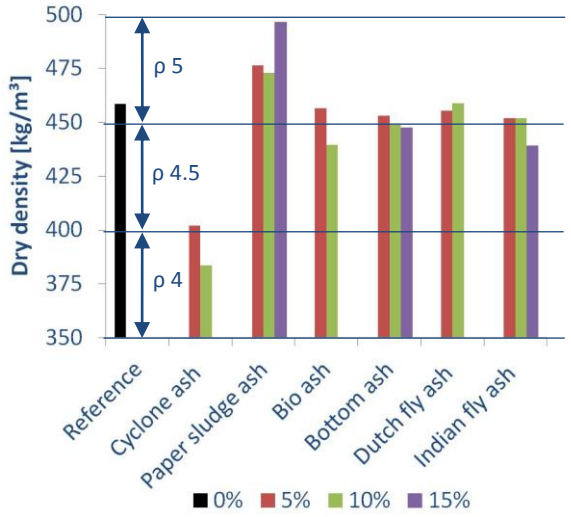

Figure 52: Dry density results versus substitution levels

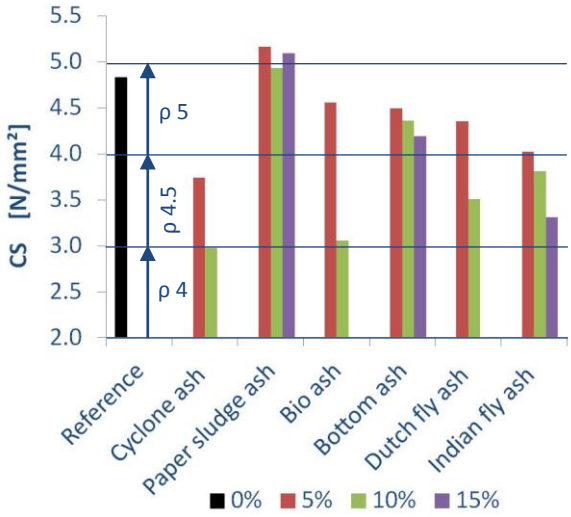

Figure 53: CS results versus substitution levels

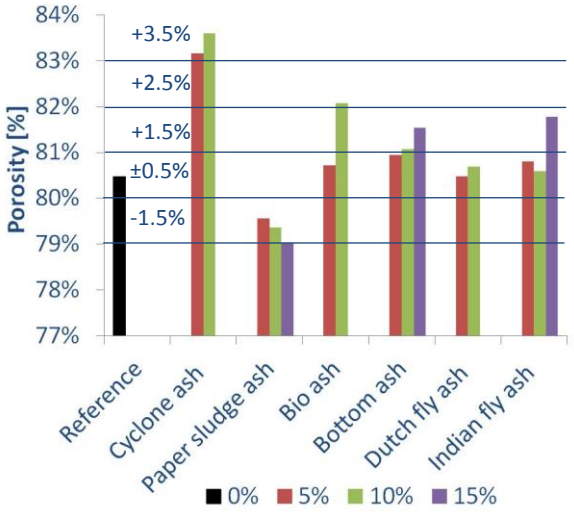

Figure 54: Porosity versus substitution levels

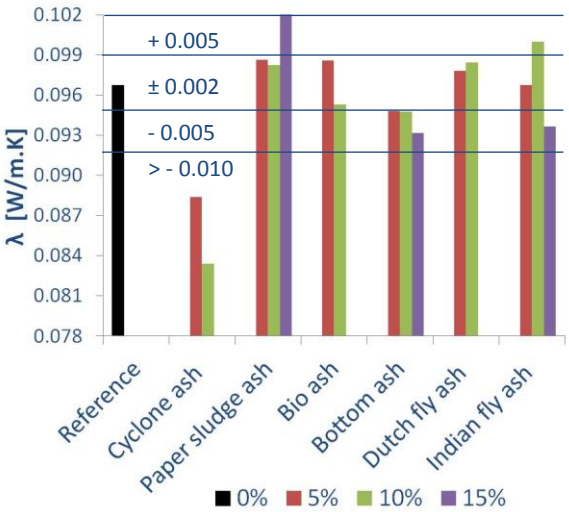

Figure 55: Thermal conductivity versus substitution levels

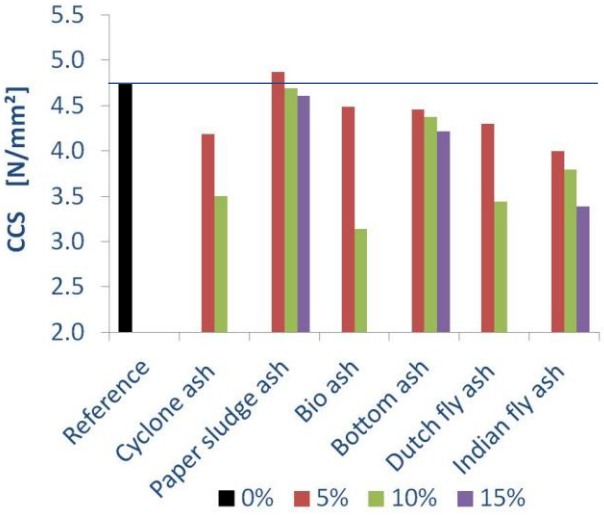

Figure 56: CCS versus substitution levels

6.2.1 CYCLONE ASH SUBSTITUTION

DISCUSSION OF 5 % SUBSTITUTION

It should be noted that the aluminum powder amount is increased with 1 g (and the w/s ratio remained standard). All results are compared to the reference. A significantly reduced dry density (Fig. 52) and relatively high porosity (Fig. 54) is observed for the 5 % cyclone ash substitution. Consequently, as was assumed, a fairly reduced CS (Fig. 53) and noticeably low thermal conductivity (Fig. 55) were reported.

These properties are in line with the higher final product height, which suggests a higher porosity. Empirically, it seems that the sample is most sensitive to density and porosity. The 5 % cyclone ash substitution is not in line with the reference. It should be noted that the porosity method is not optimal. The reaction rate was not optimal therefore it can be concluded that no additional aluminum powder was necessary.

It is suggested that the combination of the additional aluminum powder amount with 5 % cyclone ash substitution caused the increased and decreased physical properties. Unfortunately, based on the results it cannot be inferred which of the additional added materials caused the accelerated change in physical properties.

The 5 % substitution meets the minimum CS requirement of 3 N/mm² and 400 kg/m³ of ρ 4.5. Finally, based on the low CS a fairly reduced CCS is illustrated in Fig. 56. This shows that the lower density and lower CS cannot be compensated up till 450 kg/m³.

Discussion of higher substitution

10 % cyclone ash substitution contained a standard aluminum powder level and w/s ratio. A markedly decreased density for 10 % cyclone ash substitution is visible in Fig. 52. It is likely that this is due to the increased porosity (Fig. 54). As a result of the decreased density and increased porosity, an extensively reduced thermal conductivity (Fig. 55) and a significant decreased CS is illustrated in Fig. 53.

The negative drastic changes in physical properties are directly related to the cyclone ash substitution. To conclude, a higher substitution of cyclone ash is not in line with the reference and not favorable to AAC. The 10 % substitution only meets requirements of ρ 4 (ranging from 350 ≤ ρ 3 ≤ 400 kg/m³ with a minimum CS of 2 N/mm²) and showed an accelerated reduction in the CCS (Fig. 56).

6.2.2 Paper sludge ash substitution

Discussion of 5 % substitution

It can be observed in Fig. 52 and Fig. 54 that the elevated dry density and declined porosity resulted in a significantly increased CS (Fig. 53) and a substantially lower isolation value (Fig. 55), due to 5 % paper sludge ash substitution. The 5 % substitution meets the standard for ρ 5 and a slightly increased CCS is visible in Fig. 56, as result of higher density and higher CS.

The presence of portlandite, quicklime and metakaolin in paper sludge ash substitution, increases the binder content. It is assumed that the presence of metakaolin formed additional C-S-H gel and C-A-S-H gel resulting in an increased filling degree of micropores in AAC causing a higher CS. This confirms the statements of Jing et al. (2008) and The Countertop Institute (2012).

Discussion of higher substitution

The 10 % substitution results are compared to 5 % substitution. A slightly decreased dry density and porosity are illustrated in Fig. 52 and Fig. 54. Fig. 53 and Fig. 55 display, a slightly reduced CS and a slightly reduced thermal conductivity.

The 15 % substitution contains a higher w/s ratio in order to improve the reaction rate. All substitution physical properties accelerate due to a higher substitution and additional water. These results are in line with the results during the curing period. Both, the 10 % and 15 % substitution showed a slightly decreased CCS (Fig. 56). Finally, the higher substitution fulfills the requirement for ρ 5.

6.2.3 Bio ash substitution

Discussion of 5 % substitution

All results are compared to the reference. Almost the same dry density and porosity are visible in Fig. 52 and Fig. 54. The CS is slightly reduced and the thermal conductivity is slightly higher as can be seen in Fig. 53 and Fig. 55. Finally, a slightly decreased CCS is visible in Fig. 56.

The results during the curing period were more or less in line with the reference. The physical properties show the same trend. The 5 % substitution meets the requirement for ρ 5.

Discussion of higher substitution

The 10 % bio ash has a reduced w/s ratio and an increased aluminum powder. As mentioned previously, the bio ash mixture resulted in a disturbed temperature of hydration and stiffening development. Data in Fig. 52 and Fig. 54 suggest a noticeable lower dry density and fairly increased porosity for the 10 % bio ash substitution compared to the reference. A significantly declined CS, a relatively decreased thermal conductivity and extremely declined CCS are spotted in Fig. 53 and Fig.55-56.

However, it seems highly unlikely that the low CS is caused by the slightly lower density. It is suggested that the low CS is caused by phosphates in the bio ash resulting in a disrupted temperature and stiffening development (Fig. 33 and Fig. 35). The 10 % bio ash substitution meets the requirement for ρ 4.5.

6.2.4 Bottom ash substitution

Discussion of 5 % substitution

The following results are obtained for 5 % bottom ash substitution compared to the reference. A similar density (Fig. 52) and a slightly increased porosity (Fig. 54) resulted in noticeably decreased CS (Fig. 53) and a decreased thermal conductivity (Fig. 55). The slightly reduced CS resulted in a slightly reduced CCS (Fig. 56)

It seems that a similar stiffing development (Fig. 40) causes almost similar density as the reference. Nevertheless, it is suggested that the increased rising development (Fig. 39), resulting in a slightly increased final product (Fig. 41). It could have caused the slightly increased porosity. The 5 % substitution meets the ρ 5 requirements.

Discussion of higher substitution

The 10 % and 15 % substitution contained a lower w/s ratio (0.55 and 0.53) and consequently a higher aluminum powder level (15 g and 16 g). The results are compared to the 5 % substitution. As is displayed in Fig. 52 and Fig. 54 a higher substitution gave a marginally decrease in density and marginally increase in porosity. As a result a slightly decrease in CS and thermal conductivity were seen in Fig. 53 and Fig. 55. Finally, a slightly reduced CCS is visible Fig. 56 compared to 0 % and 5 % substitution.

It is thought that the decreased CS indicates that bottom ash has little pozzolanic properties. The filler to binder content balance is not optimal. However, it is possible that pozzolanic reaction of reactive silica in bottom ash reacted with lime forming a stable calcium silicate and aluminate hydrates (Kurama and Kaya, 2007). This reaction improves the CS. The question remains if the bottom ash reacted well or if a lower density caused the lower CS. Nevertheless, the higher substitution of bottom ash meets the ρ 4.5 requirements.

6.2.5 Dutch fly ash substitution

Discussion of 5 % substitution

The w/s ratio and aluminum powder amount was kept as the standard. As can be seen in Fig. 52 and Fig. 54, a slightly increased density and almost similar porosity for 5 % substitution compared to the reference were observed. Due to this, a fairly decreased CS and a slightly increased thermal conductivity were demonstrated in Fig. 53 and Fig. 55. Finally, a noticeably reduced CCS is given in Fig. 56.

The results during curing were almost similar to the reference indicating that the binder/filler ratio is optimal. No strange developments were detected which could explain the decreased CS. However, it is evident that the decrease in CS is not due to the density, since the density is almost similar to the reference. It should be noted that it is difficult to state what is the reason for this behavior. But, the evidence points to the probability that this sudden change is related to the mineral phase development. Nevertheless, the ρ 5 requirement is fulfills.

Discussion of higher substitution

For the 10 % Dutch fly ash the w/s ratio and aluminum powder amount is kept standard, since the reaction rate was sufficient for the 5 % substitution. The higher substitution gave almost the same results for the density, porosity and thermal conductivity as the 0 % and 5 % substitution (Fig. 52, Fig. 45-55). Only, the CS showed a significant decrease (Fig. 53).

The same curing results were found for the 0 %, 5 % and 10 %. This decrease is directly related to the higher substitution of Dutch fly ash and not to the density. It is assumed that the filler to binder ratio is optimal, but the final reaction products were retarded due to the adding of Dutch fly ash. This will be analyzed in the next chapter. Finally, based on the decreased CS a lower requirement (ρ 4.5) was obtained and an extremely reduced CCS (Fig. 56).

6.2.6 INDIAN FLY ASH SUBSTITUTION

DISCUSSION OF 5 % SUBSTITUTION

It should be noted that the w/s ratio and aluminum powder amount were standard. The 5 % Indian fly ash substitution illustrated that all physical properties were almost similar to the reference, except for the CS result (Fig. 52-55). The reduction in CS caused the decrease in CCS (Fig. 56).

The increased rising development (Fig. 49) and increased final product height (Fig. 51) confirms the slightly lower density. However, it is suggested that the CS has decreased so extremely that this cannot only be due to the marginally lower porosity, since the CS has decreased too extreme. It is thought that Indian fly ash has less pozzolanic properties, based on the reduced CS, but this will be investigated in the next chapter. Finally, the 5 % substitution fulfills the ρ 5 requirement.

DISCUSSION OF HIGHER SUBSTITUTION

The 10 % and 15 % substitution possess an increased aluminum powder (15 g and 16 g) and decrease w/s ratio (0.55 and 0.52) thereby improving the reaction rate. The 10 % substitution showed an almost similar density and a marginally lower porosity compared to the 5 % substitution (Fig. 52 and Fig. 54). As a result, declined CS and increased thermal conductivity are seen in Fig. 53 and Fig. 55. The 15 % substitution shows accelerated results for all properties.

Firstly, it seems that dry density and porosity were only marginally different due to the changed in w/s ratio, aluminum amount and higher substitution level. Secondly, it is plausible that the significantly lower CS of the Indian fly ash sample was not only due to the lower porosity.

It is appears that the minor difference in thermal conductivity was not due to the porosity. However, for both the thermal conductivity and the porosity, it is difficult to state what the reason is for this behavior. The evidence points to the probability that this sudden change is related to the mineral phase development. This will be analyzed in the next chapter. Finally, both additives have fulfilled the ρ 4.5 requirement (Fig. 56).

6.3 CONCLUSION

The conclusions regarding physical properties are elucidated for positive and negative performance. Tab. 32 allows comparison the physical properties (dry density, CS, porosity and thermal conductivity) of all additive substitutions with the reference.

Table 32: Comparison of relation density-CS, porosity and thermal conductivity for all substitutions

		Density + CS				Porosity				Thermal conductivity				
		[kg/m³] [N/mm²]				[%]				[W/m.K]				
	range	350 - 400	400 - 450	450 - 500	79 - 80	81 - 80	81 - 82	82 - 83	83 - 84	<-0.01	-0.005	±0.002	+0.005	>+0.01
[%]	Min. value	2	3	4	- 1.5	±0.5	+1.5	+2.5	+3.5					
0	Reference			x		x						x		
5	Cyclone ash		x						x	x				
10	Cyclone ash	x							x	x				
5	Paper sludge ash			x	x								x	
10	Paper sludge ash			x	x								x	
15	Paper sludge ash			x	x								x	
5	Bio ash			x				x					x	
10	Bio ash		x			x						x		
5	Bottom ash			x		x					x			
10	Bottom ash		x				x				x			
15	Bottom ash		x				x				x			
5	Dutch fly ash			x		x						x		
10	Dutch fly ash		x			x							x	
5	Indian fly ash			x		x						x		
10	Indian fly ash		x			x					x		x	
15	Indian fly ash		x				x							

COMPRESSIVE STRENGTH

The following conclusions were drawn, based on, CS and density results:

1. The reference sample fulfills the ρ 5 requirements.
2. All 5 % substitution, except for the cyclone ash substitution meets the ρ 5 requirements.
3. All 10 % substitution, except for the cyclone ash substitution meets the ρ 4.5 requirements.
4. All cyclone ash substitutions perform significantly less regarding CS.
5. All paper sludge ash substitutions were comparable to the reference regarding CS.

General conclusions:

1. All substitutions, except for the 10 % cyclone ash substitution meets the ρ 4.5 requirements.
2. All applied substitutions, procedures and conditions are not optimal regarding the combination of CS and density, which leaves room for significant improvement of performance.

The current results are based on operation procedures and conditions as currently standard applied. Only, small deviations regarding procedures and conditions are allowed in the performed experiment. The CS performance can be optimized regarding the following conditions:

1. The homogeneity of the porosity and density of the mixture.
2. The CS of the matrix.
3. The CS of the shield of crystals around the macropores.

The following constant technological parameters influence the properties of the CS:

1. The properties of raw material and additives (PSD and oxide composition).
2. The process parameters (mixing, curing conduction temperature, water content, aluminum amount and residence time).
3. The autoclaving parameters (temperature, pressure, residence time and moisture conditions).

Remark

It should be noted that the CS should be obtained at a relative humidity of 6 %. It is taken into account that the CS will be 20 % higher in dry stage than with 6 % humidity. This suggests that all CS results are even higher if the humidity had been according to the standard.

Porosity and thermal conductivity

Based on the porosity and thermal conductivity results the following conclusions can be drawn:

1. A higher porosity is achieved by an increased rising development during curing period.
2. Porosity depends on reactivity of the mixture, rising development and stiffening development occurred during curing period.
3. The thermal conductivity depends on the porosity. A higher porosity results in a lower thermal conductivity, and vice versa.
4. The used method to determine the porosity resulted in a large variance. No significant quantitative statement can be drawn. Only, a general statement can be given on the large difference in porosity.

7. MINERAL PHASE ANALYSES OF QUARTZ SUBSTITUTION

7.1 INTRODUCTION

The main purpose of this chapter is to report the determined concentration of the different mineral phases measured by XRD. To investigate this, a semi-quantitative study was performed. In order to perform a semi-quantitative study a medium to calibrate the AAC samples was needed. As calibration medium original ground quartz is selected. One XRD measurement is performed for each substitution sample. The sample of ± 1 g used for XRD was assumed to be representative for 12 kg of AAC product. In the autoclaving stage C-S-H gel forms tobermorite at a high pressure (± 11 bar), a high temperature (± 190 °C) and a high humidity.

The reference sample is used to compare the concentration of the different mineral phases of the different substitution samples. The measured main mineral phases present in the AAC samples are quartz, tobermorite (11.30 Å), calcium sulfate (anhydrite) and calcium carbonate (calcite).

In earlier studies attempts were made to link the tobermorite and quartz concentrations to the CS. The determined mineral phases are linked to the type and concentration of additives, the results obtained during curing and ultimate resulting in the physical properties of product. In the next section literature regarding the tobermorite phase and the various applied additives influencing the tobermorite formation are elucidated.

C-S-H gel is considered of significant importance for the AAC production. The C-S-H gel is not only the most abundant reaction product, but it is also responsible for most of the engineering properties (Thomas and Jennings, 2008). This is not because it is an intrinsically strong or stable phase, but because it forms a continuous layer that binds together the original cement particles into a cohesive product. All the other hydration products form discrete crystals that are intrinsically strong but do not form strong connections to the solid phases. They are in contact with and so cannot contribute much to the overall CS. The ability of the C-S-H gel to act as a binding phase arises from its nanometric-level structure.

It is known that tobermorite belongs to the calcium silicate hydrates group. This group can be subdivided into crystalline, semi-crystalline and near amorphous tobermorites, as defined by Alexanderson (1979). The term crystallinity was defined as the percentage of 11.30 Å tobermorite out of the total amount of calcium silicate hydrates. The CS also increased with increasing amounts of hydrates and with decreasing porosity. Other features of the reaction products were indicated by thermal behavior and micropore size distributions and may have been of importance for the mechanical properties of the material.

It is suggested that the tobermorite formation seems to be very sensitive to the additive content. According to Jing et al. (2008) excessive additives, like fly ash, appears to avoid the tobermorite formation. According to Kurama et al. (2009) the replacement of bottom ash with quartz increases the tobermorite formation owing to the pozzolanic activity.

The CS is closely related to its tobermorite content, which depends partly on the silica content of the fly ash and bottom ash, especially the silica in the glass phase as stated by Kurama et al. (2009) and Aroni (1993). According to Jing et al. (2008) the tobermorite formation seemed to be negatively influenced by the fly ash content, so excessive addition of fly ash appeared to avoid the tobermorite formation. It looked that the added fly ash had a higher reactivity compared to quartz (used during the initial hydrothermal processing) due to the higher solubility of the glassy phase in fly ash. Hauser et al. (1999) confirmed that high proportions of fly ash delayed the formation of the C-S-H phases, resulting in the drop in CS. The AAC structure became more and more porous thereby reducing the filler effect.

The replacement of bottom ash with quartz increases the tobermorite formation in the composite matrix owing to the pozzolanic activity, according to Kurama et al. (2009). The reaction of bottom ash with $Ca(OH)_2$, which occurred during the hydration of Portland cement, supports the formation of new C-S-H gels and thus enhancing the CS development of AAC.

As outlined in the literature, paper sludge ash contains metakaolin. Klimesch and Ray (1998) stated that the increase of metakaolin slows the lime-quartz reaction, while enhancing the initial C-S-H formation.

The most important reaction is the reaction of aluminum (foaming agent) with water and calcium hydroxide [2]. This reaction produces hydrogen required for expanding and creating pores in the mixture. The speed at which the hydrogen gases are formed is critical to the final AAC product (Holt and Raivio, 2005).

METHODOLOGY OF CALIBRATION OF XRD

In this work a semi-quantitative study is conducted. In order to perform this semi-quantitative analysis a medium to calibrate the AAC samples was selected. Ground quartz was selected as calibration medium and criteria regarding the selection of the medium can be founded in section Test methods. The program DIFFRACplus BASIC is used to identify the diffraction patterns and measure the peak heights (in counts). Afterwards, the peak heights were plotted. The highest peak of the original quartz is used to calibrate the main peak of quartz in the AAC samples, as shown in Tab. 33. The peak height of quartz in the AAC samples is divided by the peak height of the original quartz to determine the dissolved quartz content, which is an indication of the formed tobermorite in AAC sample. This procedure was used for all samples.

Table 33: Peak height of the XRD pattern of the ground quartz and dissolved quartz

	Result of diffraction pattern peak height	Dissolved quartz
	[Counts]	[%]
Original ground quartz	42323	100
AAC reference (undissolved)	9368	22
Difference (dissolved)	32955	78

METHODOLOGY OF INTERPRETATION OF XRD

With XRD the quantity of dissolved quartz is determined. The two highest quartz peak intensities of a diffraction pattern were observed at 3.34 Å. The tobermorite phase is identified with XRD by the diffracted intensity peaks at 3.08 Å and 11.30 Å. The peak intensity at 3.08 Å refers to the crystalline quantity level and the 11.30 Å to the crystalline quality level (Heinz, 2012). The accuracy was determined ranging ± 100 counts, as defined by Heinz (2012). Furthermore, the calcite 3.04 Å and anhydrite level at 3.53 Å were analyzed.

7.2 RESULTS AND DISCUSSIONS

Fig. 57 displays the quartz, anhydrite, lime and calcite concentration present in the additives. Fig. 58-62 illustrate the concentration of quartz, tobermorite at 3.08 Å and 11.30 Å, anhydrite and calcite present in the AAC substitution samples. The anhydrite and calcite concentration are included since noticeable differences were detected for the different additives substitution. Details of XRD results can be found in Appendix A.2.3.

GENERAL STATEMENT

XRD results give semi-quantitative or qualitative results, which can be used for determining a correlation between the different parameters. It is however not suitable for exclusive explanation of exceptions. The available information allows the following statements to be made:

1. It is not commen that calcite is identified in AAC. This is based on practical experience at HESS AAC Systems B.V. which excludes calcite in AAC. Calcite is inert and if present does not dissolve during the curing phase and the autoclave phase. There is no explanation for the absence of a relation between 0 %, 5 %, 10 % and 15 % additive substitution and the calcite variations.
2. Anhydrite could be formed out of gypsum as a reaction during autoclaving. When gypsum is heated, as high as 170 °C the mineral partly dehydrates [3] and forms calcium sulfate hemi-hydrate or γ-anhydrite. The presence of anhydrite indicates an imbalanced final product, since only low anhydrite levels should be present in a proper AAC final product.
3. Possible errors regarding anhydrite and calcite levels could be introduced as not representative samples and/or dosing deviations. However, it is possible that calcite and anhydrite is coming from the raw material.
4. Taking a representative sample of a solid product is hard to achieve with limited samples.

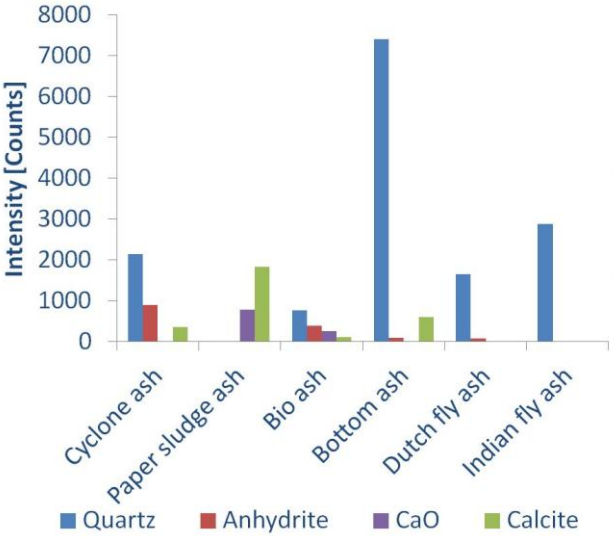

Figure 57: XRD measured mineral phases of additives compositions

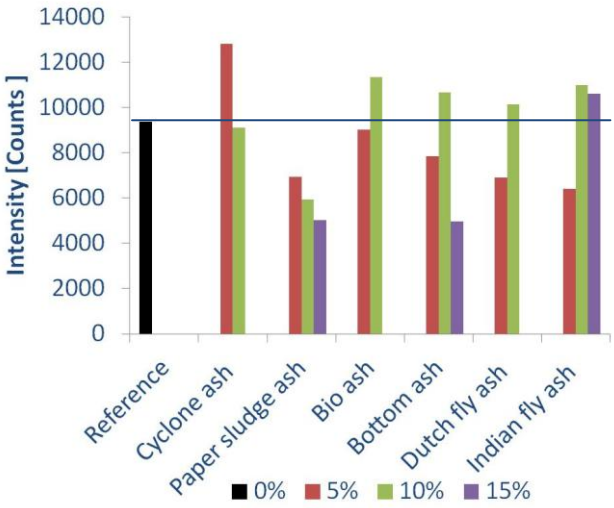

Figure 58: Intensity of quartz at 3.34 Å, for all substitution

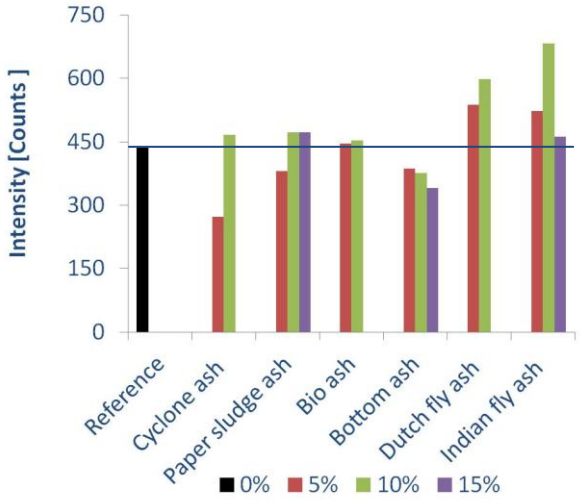

Figure 59: Intensity of tobermorite at 11.30 Å, for all substitution

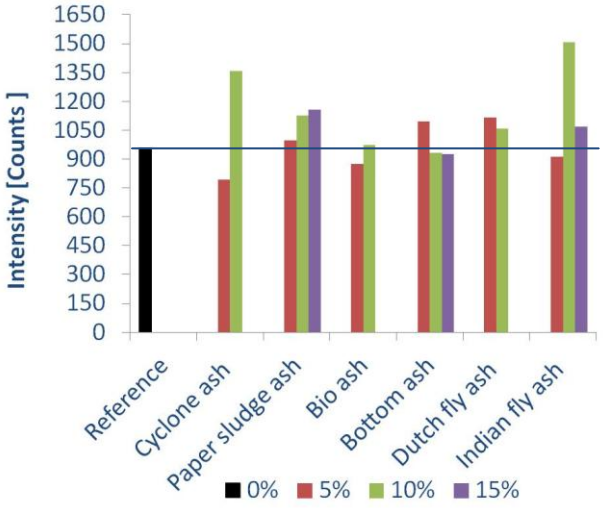

Figure 60: Intensity of tobermorite at 3.08 Å, for all substitution

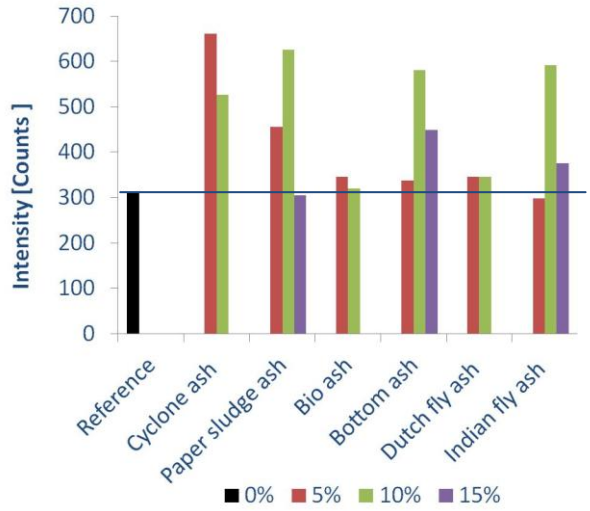

Figure 61: Intensity of calcite at 3.04 Å, for all substitution

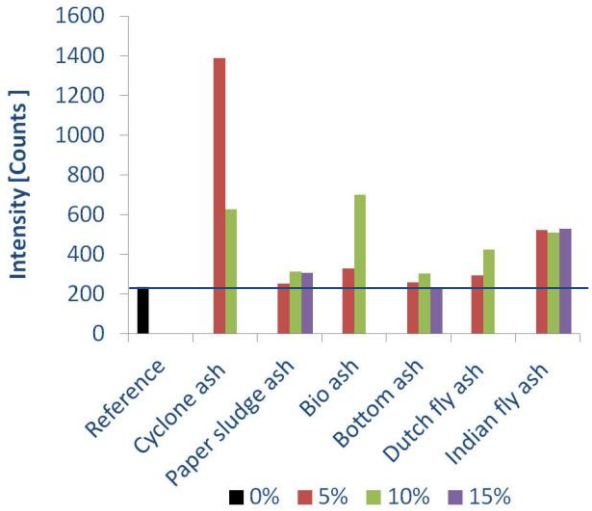

Figure 62: Intensity of anhydrite at 3.53 Å, for all substitution

7.2.1 Cyclone ash substitution

Discussion of 5 % results

It is known that cyclone ash contains mainly the mineral phases: quartz, anhydrite and calcite (Fig. 57). As seen in Fig. 58 the highest amount of undissolved quartz (compared to all tested additives) is present in the 5 % cyclone ash sample. The lowest amount of tobermorite (compared to all tested additives) is observed, at 3.08 Å and 11.30 Å (Fig. 59-60). In Fig. 61-62, a significantly higher level of calcite and anhydrite (compared to all tested additives) is observed. Small traces of Bassanite ($CaSO_4 \cdot 0.5H_2O$) were reported but not shown.

More undissolved quartz is present in the case of 5 % cyclone ash compared to the reference. It is assumed that significantly less tobermorite was formed (Fig. 59-50) due to a high level of undissolved quartz (Fig. 58). It seems that components in the cyclone ash could have retarded the formation of tobermorite. However, with this semi-quantitative method it is not possible to determine the precise components in cyclone ash.

Fig. 57 illustrates that cyclone ash contains a high level of anhydrite compared to the reference. As is seen in Fig. 62, a higher level of anhydrite is visible in the final product. All reactions take place under hydrothermal conditions, so there is plenty of water in the autoclave. However, it seems that there is a tendency to favor the formation of anhydrite. It is recognized that calcium sulfate ($CaSO_4$) is present in the cement. The AAC mixture includes 2.5 % anhydrite, 2.5 % gypsum and 3.3 % added cyclone ash (containing traces of anhydrite). Furthermore, it is assumed that the amount and form of calcium sulfate influences the AAC CS because of interactions with the tricalcium aluminate (C_3S) compound. For the 5 % cyclone ash this would indicate that less anhydrite has reacted to form the tricalcium aluminate (C_3S) compound. It is believed that high anhydrite levels could be formed by gypsum reacting in the autoclave. The cyclone ash itself possessed a high level of calcite (Fig. 57), compared to the reference which explains the higher calcite level (Fig. 61).

Discussion of higher substitution

The undissolved quartz amount in 10 % cyclone ash sample is in line with the reference (Fig. 58). A noticeably higher tobermorite level at 3.08 Å and a similar tobermorite level at 11.30 Å were demonstrated compared to the reference (Fig. 59-60). As illustrated by Fig. 61-62, fairly higher levels of undissolved calcite and calcium sulfate were observed.

Comparing 5 % and 10 % cyclone ash substitution the following differences can be seen for 10 % substitution: (I) a lower undissolved quartz level, (II) a higher tobermorite level, (III) a slightly lower calcite level and, (IV) significantly lower calcium sulfate level. It is suggested that these differences are due to a higher substitution of cyclone ash. It is assumed that the components in cyclone ash are the factors which cause the decreased quartz dissolved resulting in higher tobermorite level (at 11.30 Å and 3.08 Å). Furthermore, the lower levels for calcite (and anhydrite) are an indication of a sampling or dosing error.

7.2.2 Paper sludge ash substitution

Discussion of 5 % results

It is known that paper sludge ash contains mainly the mineral phases: 41% calcite, 23% quicklime, 29 % metakaolin and 2.5 % portlandite. It is known that metakaolin is considered to have twice the reactivity properties of most other pozzolans and therefore reacts more quickly. A disadvantage of portlandite is reducing available water for the hydration of Portland cement.

Less undissolved quartz is found in 5 % paper sludge ash samples compared to the reference (Fig. 58) A slightly higher tobermorite level at 3.08 Å and slightly lower tobermorite levels at 11.30 Å as the reference are visible in Fig. 59-60. In Fig. 61-62 it is illustrated that there is an almost similar anhydrite level and a noticeably higher level of calcite, as in the reference. Paper sludge ash itself contains a large amount of lime (Fig. 57). It is suggested that these will increase the following reactions: More quicklime will react with water [1] increasing the portlandite production and dissolve more quartz to produce C-S-H gel [5]. Furthermore, metakaolin can react with portlandite [8], quicklime [7] and with Portland cement producing C-S-A-H gel and C-S-H gel. The metakaolin, portlandite and quicklime provided by paper sludge ash, increased the production of C-S-A-H gel and C-S-H gel and as a result increased the tobermorite formation.

DISCUSSION OF HIGHER SUBSTITUTION

Less undissolved quartz is present in the 10 % and 15 % paper sludge ash sample compared to the 5 % substitution and the reference (Fig. 58). Both 10 % and 15 % substitution illustrated a noticeably higher tobermorite level at 3.08 Å and a similar tobermorite levels at 11.30 Å (Fig. 59-60). Fig. 61-62 displayed a significantly increased calcite level for the 10 % substitution and a similar anhydrite level compared to the reference for 5 % and 15 % substitution. Next, both 10 % and 15 % substitution have a similar anhydrite level compared to the 5 % substitution and the reference.

Comparing the tobermorite level for 5 %, 10 % and 15 % paper sludge ash substitution, it is suggested that a 10 % substitution gives the optimum tobermorite level. The 15 % substitution does not reveal significant higher levels. The retarded lime-quartz reaction by the metakaolin, as was stated by Klimesch and Ray (1998) is not empirically confirmed by the resulted experiment.

7.2.3 BIO ASH SUBSTITUTION

DISCUSSION OF 5 % RESULTS

The mainly mineral phases present in bio ash are: quartz, anhydrite, calcite, quicklime, hematite (Fig. 57). Fig. 58 illustrates slightly more undissolved quartz for the 5 % bio ash sample. This is slightly lower compared to the reference. Fig. 59-60 show that an almost similar tobermorite level as the reference were found for paper sludge ash and Indian fly ash sample. Fig. 61-62 display a comparable level of calcite and anhydrite to the reference. Almost similar quantities of quartz, tobermorite, calcite and anhydrite were observed for 5 % bio ash as to the reference.

DISCUSSION OF HIGHER SUBSTITUTION

Two mineral phases changed while increasing the substitution: (I) more undissolved quartz was detected (Fig. 58) (II) an increased level of anhydrite is demonstrated (Fig. 62). (III) almost similar tobermorite levels (at 3.08 Å and 11.30 Å) and, (IV) almost similar calcite levels as in the reference were observed in the 5 % substitution (Fig. 59-61).

The 10 % substitution sample shows the same intensity levels as the 5 % cyclone ash sample. To conclude a higher substitution of bio ash, reduces the dissolving of quartz and strangely slightly increases the tobermorite formation. Finally, bio ash itself contains anhydrite so, a higher substitution results in a high anhydrite level.

7.2.4 BOTTOM ASH SUBSTITUTION

DISCUSSION OF 5 % RESULTS

Bottom ash contains the mainly mineral phases: quartz, calcite, mullite and anhydrite (Fig. 57). In general, less undissolved quartz remained in the 5 % bottom ash sample (19 %) (Fig. 58). Increased tobermorite levels at 3.08 Å and an almost similar tobermorite level 11.30 Å is seen in Fig. 59-60. Fig. 61-62 show similar calcite levels for bottom ash and the reference.

Bottom ash contains mainly quartz (compared all other additives). As a result of this, more quartz can react with portlandite to form C-S-H gel [5]. It is assumed that the increased quartz led to the increased tobermorite formation at 3.08 Å causing a relatively high CS (of 4.5 N/mm²).

DISCUSSION OF HIGHER BOTTOM ASH SUBSTITUTION

Comparing the 10 % and 15 % substitution shows, that in the 10 % noticeably more undissolved quartz and in the 15 % significantly less undissolved quartz remained (Fig. 58). Almost similar anhydrite and tobermorite amounts (3.08 Å and 11.30 Å) compared to the 5 % and the reference are illustrated for both 10 % and 15 % substitution (Fig. 59-60 and Fig. 62). As being visualized in Fig. 61, the 10 % substitution reveals a considerably increased calcite level compared to the reference. The 15 % substitution contains less increased calcite levels.

Bottom ash itself possesses some higher calcite levels (Fig. 57). However, the calcite level varies for the 5 %, 10 % and 15 % substitution this indicates a sampling or dosing error. It is assumed that components in bottom ash slight reduce the tobermorite formation (3.08 Å and 11.30 Å). The contrary is found for the 15 % substitution. More quartz was dissolved than in the 5 % and 10 % [1] and only a slightly reduced tobermorite level was observed. It seems that for the 15 % substitution not enough quartz dissolved to produce a higher tobermorite formation.

7.2.5 Dutch fly ash substitution

Discussion of 5 % results

The Dutch fly ash possesses mainly lower amounts of quartz (compared to bottom ash) and small amounts of anhydrite, hematite and mullite (Fig. 57). Less undissolved quartz remained in 5 % Dutch fly ash (16 %) in comparison to the reference (22 %) (Fig. 58). An increased tobermorite levels at 3.08 Å and 11.30 Å were demonstrated (Fig. 60). Fig. 61-62 show similar calcite and anhydrite levels for 5 % bottom ash and the reference.

It is known that the fly ashes have pozzolanic properties (siliceous and aluminous material), but they possess little or no cementitious value. However, in the presence of water the fly ash will chemically react with portlandite (at ambient temperatures) to form compounds possessing cementitious properties [5 and 2]. The amorphous silica in fly ash will react faster than ordinary quartz. In the 5 % substitution noticeably more quartz reacts [5] compared to the reference, since Dutch fly ash possess quartz and cementitious properties (Fig. 57). As a result slightly higher tobermorite levels at 11.30 Å and 3.08 Å are obtained.

Discussion of higher substitution

In the 10 % Dutch fly ash sample more undissolved quartz was present, compared to the 5 % substitution Dutch fly ash and the reference (Fig. 58). A slightly higher tobermorite quantity (at 3.08 Å) and almost similar quality of tobermorite (at 11.30 Å) compared to the 5 % substitution are visible in fig. 59-60. Only, higher calcite levels and an almost similar anhydrite level are visible for both the reference and 5 % Dutch fly ash substitution (Fig. 61-62).

Dutch fly ash itself does not contain anhydrite. It is suggested that some gypsum has reacted in the autoclave to form anhydrite. It is evident that a higher substitution of Dutch fly ash retards the quartz dissolving [5] and results in tobermorite quantity (3.08 Å) reduction and slightly increases of tobermorite quality (11.30 Å). The evidence points to the likelihood that less tobermorite was produced caused by components in the Dutch fly ash disturbing the C-S-H gel reaction.

7.2.6 Indian fly ash substitution

Discussion of 5 % results

The Indian fly ash possesses mainly quartz, hematite and mullite. The 5 % Indian fly ash contains less undissolved quartz (15 %) compared to the reference (22 %) (Fig. 58). At 3.08 Å, similar tobermorite levels and at 11.30 Å slightly higher tobermorite levels were demonstrated for 5 % Dutch fly ash and reference (Fig. 59-60). Fig. 62 show similar calcite levels and Fig. 61 illustrates an increase of the anhydrite level in comparison with the reference. Indian fly ash does not contain anhydrite but possesses 24 % aluminum oxide. It is possible that this retard the dissolving of anhydrite.

Discussion of higher substitution

Significantly more undissolved quartz was displayed for the 10 % substitution compared to the 5 % substitution (Fig. 58). The 10 % substitution illustrates a significant increase in tobermorite. The 15 % substitution shows similar tobermorite levels, at both 3.08 Å and 11.30 Å. Similar increased levels of anhydrite were demonstrated for the 5, 10 and 15 % substitution (Fig. 62). Fig. 61 displays significantly increased calcite levels for the 10 % substitution and a slightly increased calcite level for the 15 % substitution, compared to the 5 % substitution and the reference. However, the calcite level varies for the 5 %, 10 % and 15 % substitution indicating a sampling or dosing error.

Strangely, a far higher tobermorite was observed for the 10 % substitution although less quartz dissolved. Only less quartz dissolved for the 15 % substitution compared to the 5 % substitution, but a higher tobermorite level was detected (3.08 Å). There is reason to belief that the pozzolanic properties of Indian fly ash are caused by the high tobermorite levels.

7.3 CONCLUSION

As stated by Heinz (2012), the peak at 3.08 Å gives an indication of the present quantity of tobermorite and the peak at 11.30 Å resembles the crystalline quality level. Tab. 34 illustrates the relation of undissolved quartz (in percentages) to the highest tobermorite levels (in counts) and the corresponding CS (in N/mm²).

Table 34: Relation between undissolved quartz, tobermorite intensity and CS

	Undissolved quartz [%]	Tobermorite intensity [counts]	Highest peak of tobermorite [Å]	CS [N/mm²]
Dutch fly ash	15	1120	3.08 (quantity)	4.4
Paper sludge ash	16	1000	3.08 (quantity)	5.2
Bottom ash	19	1100	3.08 (quantity)	4.5
Reference	22	950	3.08 (quantity)	4.8

In general:

1. Based on, the results of the semi-quantitative analysis no linear relation between the undissolved quartz, the tobermorite intensity and CS was obtained.
2. The XRD results can give information about the composition but cannot given information on the CS, based on tobermorite concentration at 11.3 Å and 3.08 Å.
3. The XRD results show significant amounts of not hydrolyzed products, as can be concluded by the presence of calcium sulfate (anhydrite) and calcite. This indicates that no optimal mixture (insufficient water presence) and/or process conditions during curing period and autoclaving were achieved.
4. It is seen that the amount of phosphates in bio ash consumes water, resulting in a high anhydrite concentration in the sample.
5. It should be noted that the pH effect is not measured and the hardening of concrete by reaction with CO_2 is not included. It is assumed that the hardening is a slow process and is not interfering with the short-term measurements. The difference regarding the reaction of cyclone ash or bio ash is not understood but the pH difference might have an impact.

The following conclusions can be drawn:

1. The quantity and of quality tobermorite concentration are not the only parameters influencing the CS when using additives.
2. The higher quicklime, portlandite and metakaolin level in paper sludge ash may be increased binder content and thereby causing a higher CS.
3. The reduction in quartz content is a measure for the increased tobermorite formation, except for bottom ash and both fly ashes, (due to the presence of different reactions).
4. The assumed increase in CS based on the increased presence of tobermorite at 11.3 Å and 3.08 Å is not always valid.

8. FIELD EMISSION SCANNING ELECTRON MICROSCOPY OF QUARTZ SUBSTITUTION

8.1 INTRODUCTION

In this report, all substitution samples are examined by FESEM, to discover the crystal morphology. All samples are compared to the reference and to the other samples with the same substitution ratio. FESEM images give qualitative information based on one representative picture of each sample. No conclusive comparison can be made, based on one picture, although in the results and discussion it is assume that the picture shows a representative situation.

FESEM gives a 2D picture displaying the shape of the pores or crystals. However, since it is a 2D picture it is possible that it gives an optical illusion. This is depending on the angle of the fractured surface of the sample. FESEM gives additional information which is not exclusive if compared to other methods determining crystal formation. Based on these pictures some remarks are given.

LITERATURE

The size of macropores is depending on the amount of aluminum (which produces hydrogen gas) and properties of the solid mass (also called matrix). The reaction rate, binder effect and filler effect are the main parameters which influence the viscosity of the mixture and control the properties of the matrix. According to Jing et al. (2008) micropores are depending on the (tobermorite) crystal filling degree. Hauser et al. (1999) observed that, with a high proportion of fly ash, the formation of C-S-H gel was delayed with a corresponding drop in strength and increase in shrinkage.

THEORY MODEL

In this section an attempt is made to link the CS of the final product to the (tobermorite) crystal structure. The CS is depending on a lot of factors. A number of factors which influence the crystal grow or formations are being discussed.

Crystals are formed in the matrix and at the surface of the macropores. The overall strength is determined by the sum of the - **weakest strengths -** of adjacent local crystal volumes. It is assumed that the crystal formation in the matrix (Fig. 63a) and the crystals shielding around the macropores or growing into macropore (Fig. 63b), contribute to the CS of to final product. Fig. 63-64 illustrate the theoretical model.

Fig. 64. shows the negative local impact of different factors on the matrix. All factors have an influence during the curing phase, where the matrix is formed.

1. The homogeneity of the mixture: A no homogeneous mixture contains weak-spots which influences the total AAC sample negatively. This is especially the case when a lot of weak-spots are percent.
    - 1a. The PSD of the entire mixture: A coarser additive could weaken the matrix since the solubility of the additive is less therefore reducing the homogeneity of the mixture.
    - 1b. The oxide composition of the additive: A different oxide composition can change the calcium to silicate ratio and the binder to filler ratio, which lead to a less optimal mixture.
    - 1c. The macropore shape and size influences the overall CS of the matrix: It is suggested that a smaller size macropores distribution can give the highest strength, due to the constant (maximum) distance between macropores. The CS is determined by the minimum solid volume of the matrix between the adjacent macropores.

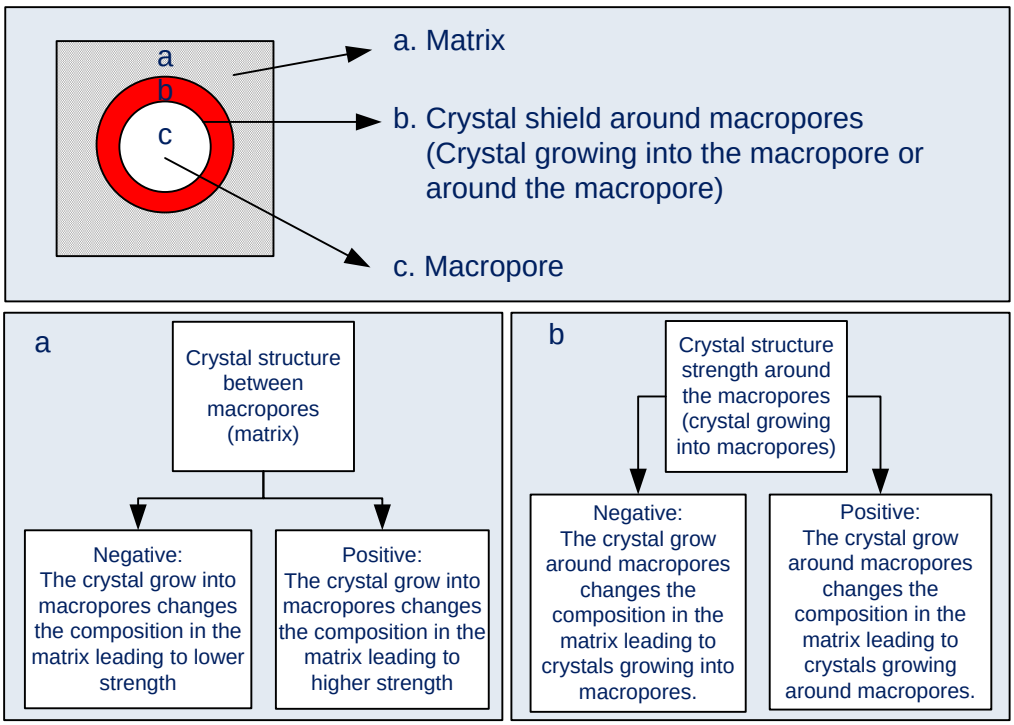

Figure 63: Model CS influence of crystals type and grow

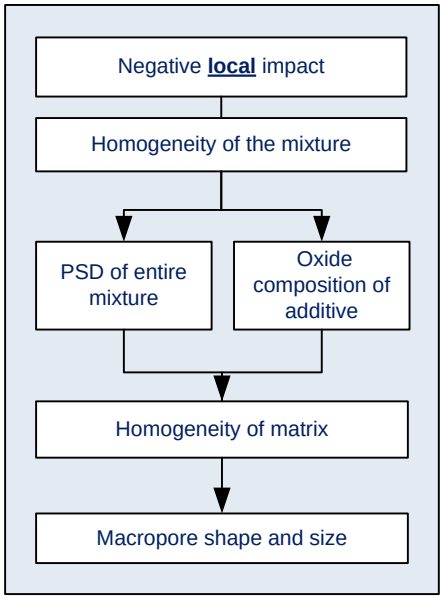

Figure 64: Model CS influence of pores and porosity

A. Matrix

Different crystal types are visible in the matrix compared to those at the surface of the macropore. The crystals in the matrix have less space to develop compared to the crystals in the macropores. It is suggested that the matrix strength thereby is determined by the strength of the crystals and their connections with adjacent crystals. It is assumed that the formation of the crystals in the matrix are influenced by the extracted material from the matrix to form the shield (of crystals around the macropores). It is likely that this may result in different crystal structures in the matrix compared to the shield, which eventually results in a different local strength.

B. Crystal shield around macropores

The crystal materials (e.g. tobermorite) and their structure (e.g. crystalline or amorphous) determine the crystal strength. It is assumed that a compact combined crystal structure has a higher strength than a loose crystal structure. This also applies to the matrix. Furthermore, it thought that a crystal structure growing into the macropores delivers no (structural) strength.

c. Macropores

The macropore itself has no strength. However, the crystals at the surface of the macropore form a shield which influences the strength of the matrix around the macropore. It is assumed that the shield around the macropore gives the following two effects:

1. The shield around the macropore can be stronger compared to the matrix, which may allow bigger macropores, with constant strength.
2. The shield around the macropore can be weaker compared to the matrix, which allows only smaller macropores, with constant strength.

Methodology

A fractured surface was used to analyze the morphology of the matrix, because this is more representative. For each substitution material a comparison was made. The following FESEM images were made: (I) pore formation, (II) matrix of the fractured surface, (III) overview crystal structure inside pore and, (IV) detail of crystals located at the edge of the fracture surface and inside pore. The discussed characteristics are the difference and/or similarity in: (I) amount of pores and pore distribution, (II) crystal size, shape and clustering and, (III) composition of the fractured surface (matrix).

8.2 Results and discussion

It should be noted that the statements in this chapter only refer to the samples seen in the picture. It might be possible that the difference or similarities observed in the pictures are based on coincidence. The samples might look identical however this is based on one picture which is assumed to be representative for the entire sample.

8.2.1 Macropore formation

Discussion 5 % substitution

Fig. 65a-g illustrates the distribution of macropores. Firstly, increased macropores for 5 % cyclone ash are spotted in Fig. 65b. These findings confirm both the high porosity and low density caused by an out of balance mixture. Secondly, comparing Fig. 65a and Fig. 65d, it seem that an almost identical macropore distribution is presented for 5 % bio ash and reference samples. In general, slightly smaller macropores are demonstrated for the 5 % paper sludge ash sample (Fig. 65c). This is consistent with the higher density and lower porosity. Next, it is suggested that, in the 5 % bottom ash sample slightly more and smaller macropores are present compared to the 5 % paper sludge ash sample (Fig. 65a and Fig. 65e). It is believed that these trends are in line with the previously discussed results of the penetration test. Finally, it is evident that overall larger macropores and larger matrix volume for the fly ash samples are revealed.

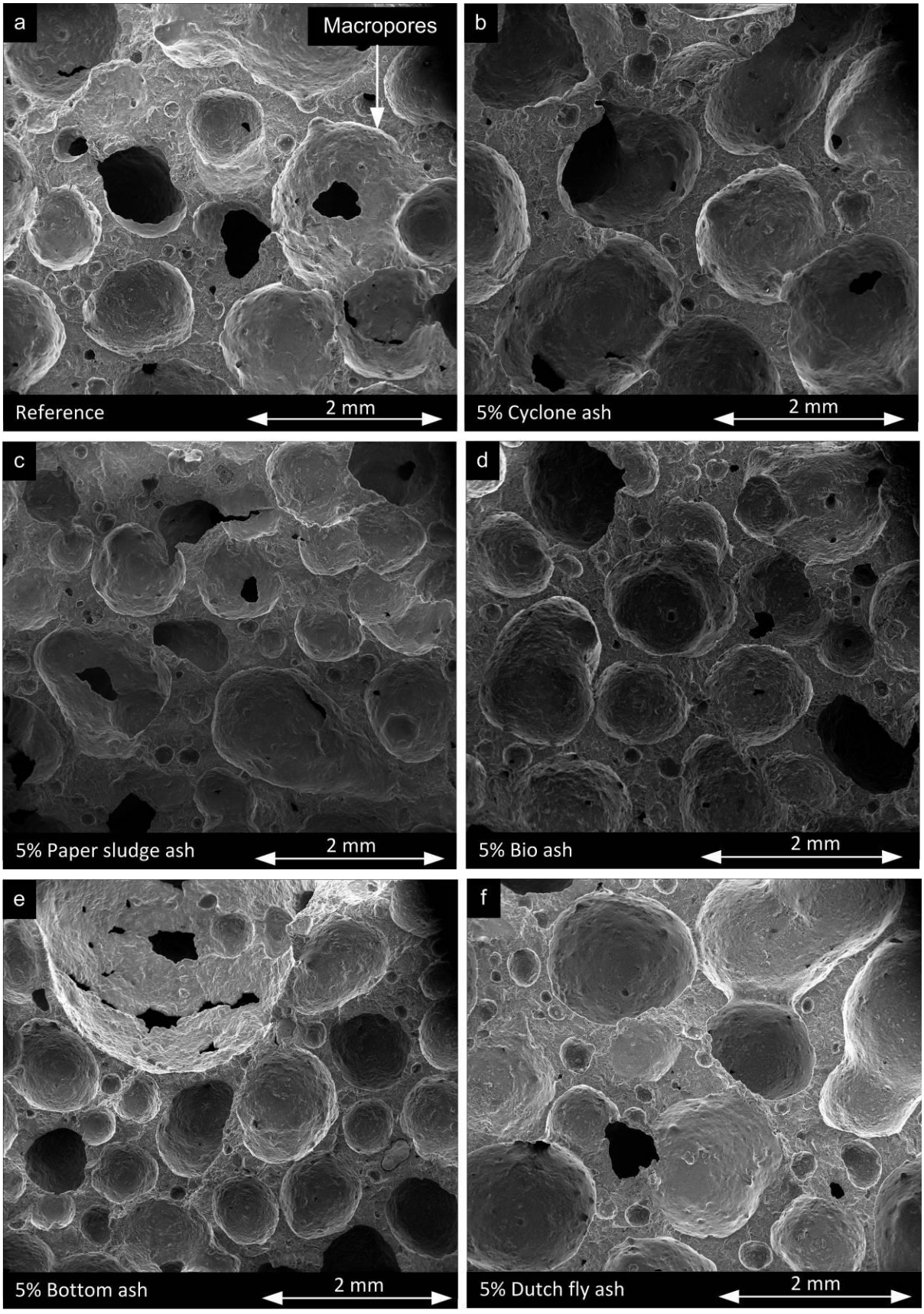

Figure 65: Pore formation of 5 % substitution

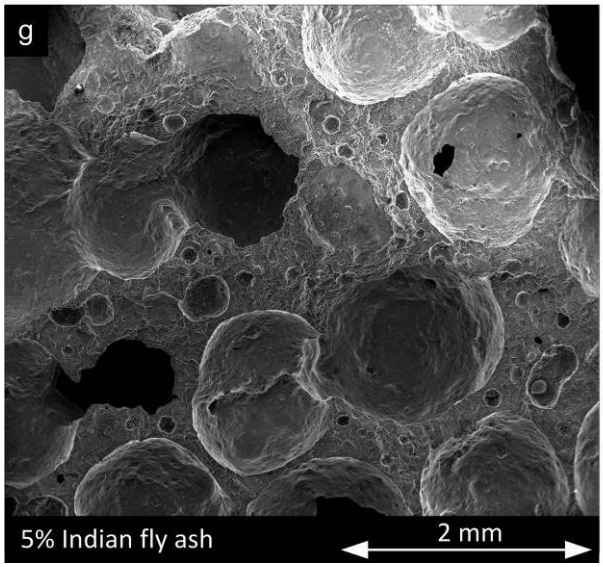

Figure 65: Pore formation of 5 % substitution, cont.

Discussion 10 % substitution

All substitutions are compared to the reference. The pore distribution of the 10 % substitution is detailed in Fig. 66a-g. The 10 % cyclone ash sample has significantly increased macropores (Fig. 66a-b). Initially, the macropore of the 10 % cyclone ash are bigger compared to the macropores of the 5 % cyclone ash (Fig. 65b and Fig. 66b). Next, is appears that the 10 % paper sludge ash sample has smaller macropores (Fig. 66c). The rising development of the paper sludge ash sample was different causing a different macropore formation.

Furthermore, inspection of Fig. 66d indicates that 10 % bio ash has more or less similar macropores as the reference. This result is in good agreement with results of the 5 % substitution, although the 10 % bio ash had a lower w/s ratio and a higher aluminum powder amount. Next, a larger number of decreased macropores are revealed in the bottom ash sample as displayed in Fig. 66e. It seems that the pore formation of the Indian fly ash is comparable to the reference. Finally, it is suggested that Dutch fly ash and the Indian fly ash samples display enlarged macropores (Fig. 66a and Fig. 66f-g). Eventually, it is appears that the slightly larger macropores in the Dutch fly ash confirm the slightly higher porosity compared to the Indian fly ash.

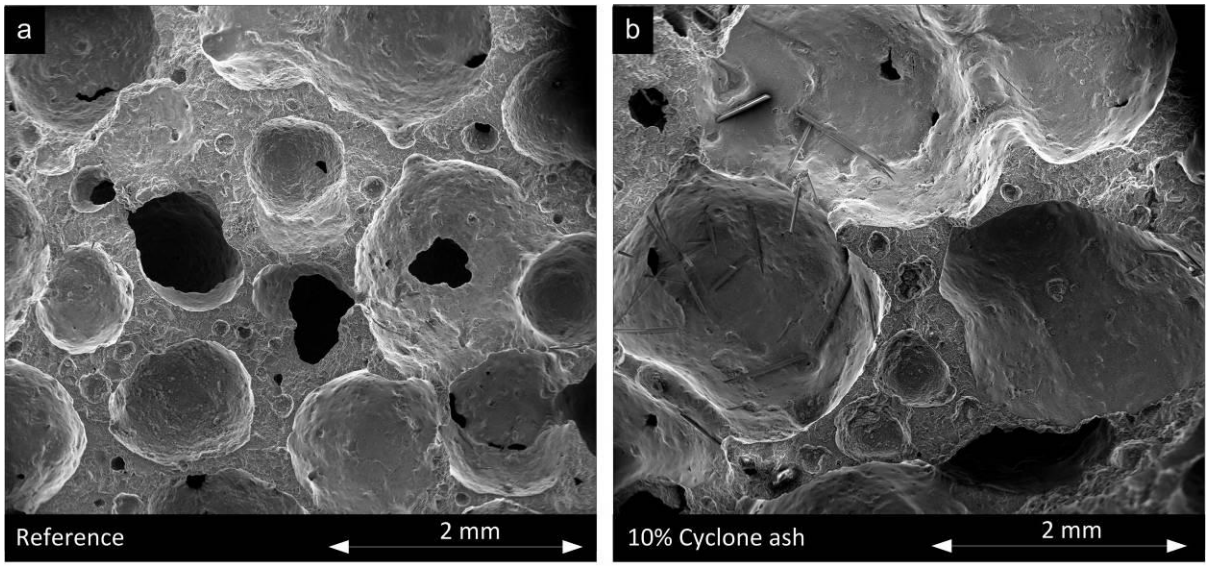

Figure 66: The pore distribution on micro level of 10 % substitution

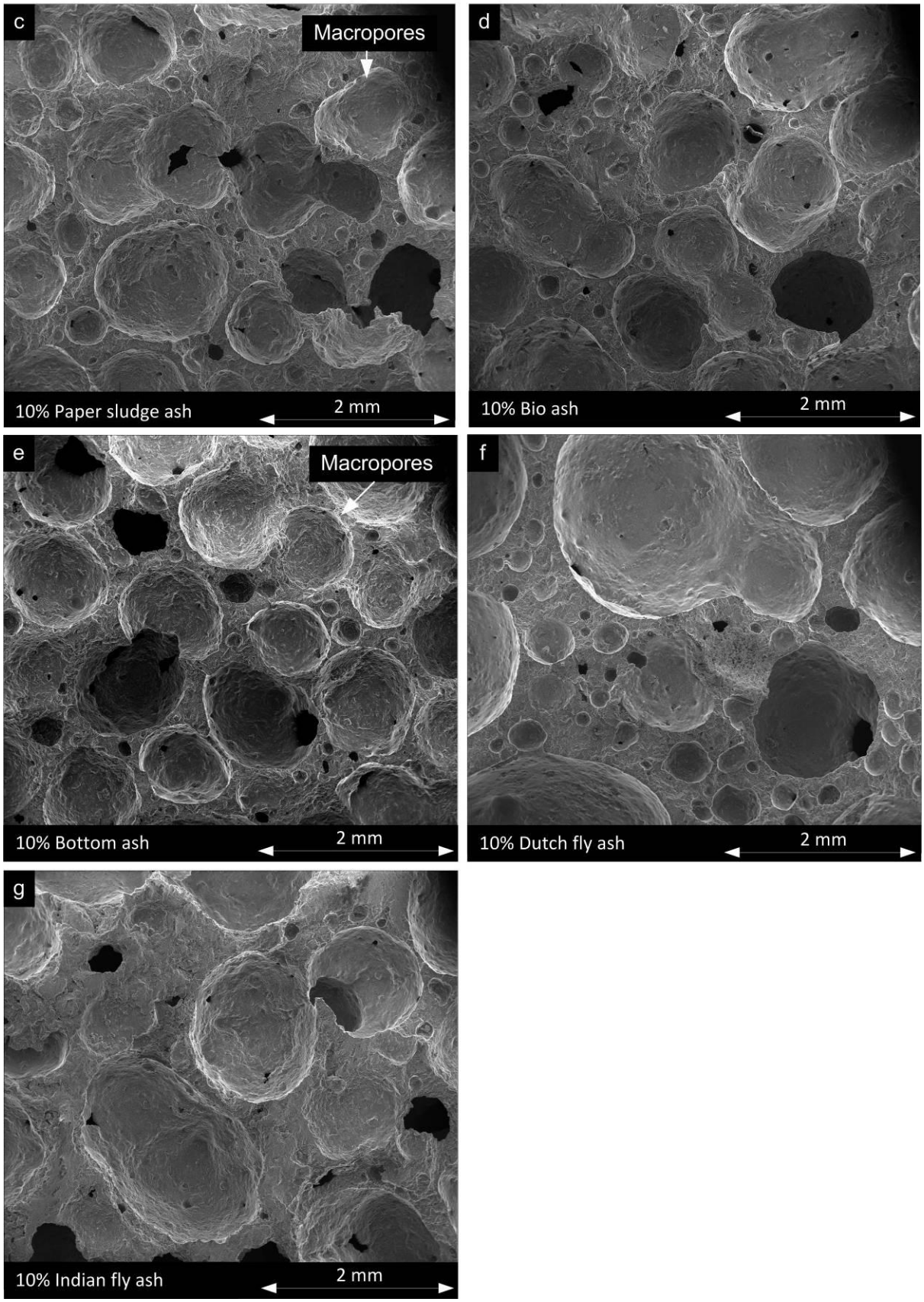

Figure 66: The pore distribution on micro level of 10 % substitution, cont.

DISCUSSION 15 % SUBSTITUTION

The FESEM micro pictures for the 15 % substitution samples are represented in Fig. 67a-d. Firstly, it can be indentified from Fig. 67a-b that the 15 % paper sludge ash has a slightly slimmer matrix as compared to the reference. It is reasonable to suppose that these results are coherent with the obtained porosity and density results of 15 % paper sludge ash sample. Secondly, noticeable larger macropores are shown for 15 % bottom ash and 15 % Indian fly ash due to increased rising development (Fig. 67a and Fig. 67c-d). Therefore, it is likely that no similar results are found in the 5 % and 10 % substitution (Fig. 65e and g, Fig. 66e and g, Fig. 67 c and d). Finally, it can be seen in Fig. 67d that the Indian fly ash has a fairly wider matrix in contrary to the Dutch fly ash. It may be inferred that these results confirm the higher porosity, the lower density, the higher lambda and the lower CS.

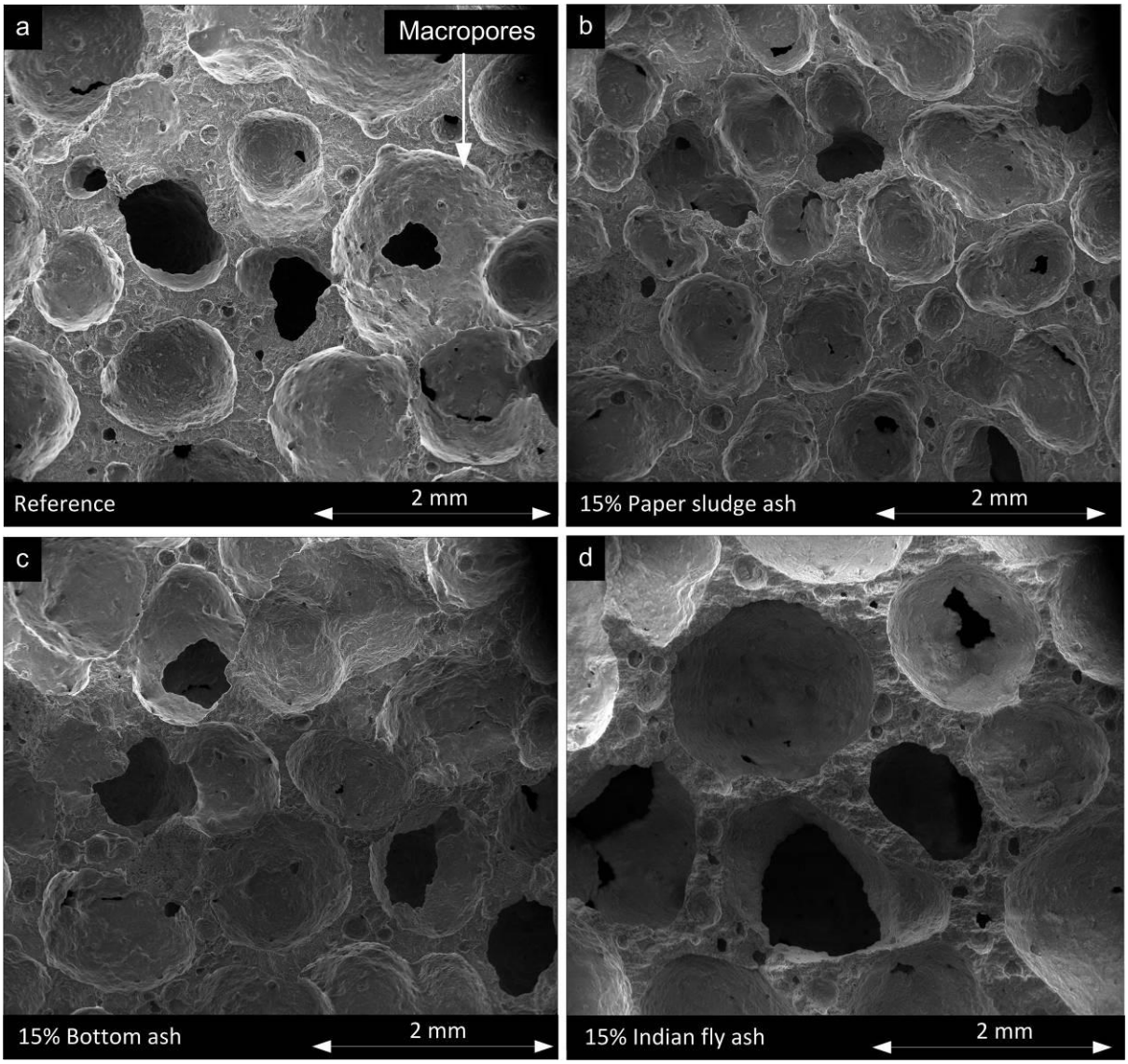

Figure 67: Pore formation of 15 % substitution

8.2.2 FRACTURED MATRIX

The main purpose of this work was to examine the bonding degree of the additives and the tobermorite filling degree. A high filling degree will reduce the micropores, and visa versa.

As mentioned in literature, according to Mitsuda et al. (1992) it was observed by FESEM technique, that the filling degree starts at 1 h and 2 h of autoclaving. C-S-H gel has to be dominant in the samples, thus replacing the 6 µm micropores in the green body with 100 nm micropores. With increasing autoclave time, the C-S-H gel reacts with quartz and gives platy tobermorite crystals, resulting in micropore sizes of 50 to 100 nm.

According to Mostafa (2005) the effect of Al substitution on the stability field and the rate of crystallization of tobermorite has been studied by many investigators. Jing et al. (2008) states that a lot of crystals (tobermorite) were formed and that the formed crystals have filled in the space between particles with increasing fly ash content. This reveals that the strength enhancement depends mainly on both of tobermorite formation and the filling degree of tobermorite. Furthermore, this also indicates that the excessive addition of fly ash affects the formation of tobermorite, and in turn exerts a minus influence on the strength development.

According to Mostafa (2005) the high reactivity of the added fly ash modifies this system by introducing Al and increasing the Ca/Si ratio. In this investigation does found the formation of new Al-containing phases, such as hydrogarnetes. It seems that all the aluminum can be accommodated in either the C-S-H gel or the tobermorite. This is in line with Jing et al. (2003). Isu et al. (1995) states that the addition of slag to AAC produces tobermorite with a higher Al substitution and lower Ca/ (Al+Si) ratio and increased the crystallinity.

The variation of the crystal structures in the matrix and in the macropore detected is extremely large, which makes comparison with literature information very discussible. The procedure of the preparation of the mixture is not specified and therefore the pictures of the final product not comparable.

Discussion 5 % substitution

The microstructure of the fractured matrix is visible in Fig. 68a-g. In all samples a different amorphous (C-S-H) gel phase is mainly surrounded by spotted quartz particles mixed with (tobermorite) crystals. These crystals bond particles together and fill in the space between particles. Furthermore, the degree of hydration is important in forming tobermorite crystals. In general, it seems that almost all additives have reacted and crystallized. The small white needles indicating tobermorite crystals are seen in Fig. 68a-g. Fig. 68a reveals an unreacted particle and needle-like and gel-like phases in the matrix in the reference.

Fig. 68b indicates the presence of some unreacted cyclone ash in combination with gel-like and fiber-like phases. It appears that the 5 % paper sludge ash sample has a more dense structure and smaller crystals (Fig. 68c). Next, 5 % bio ash has gel located in between the crystal, as can be seen in Fig. 68d. Some gels are very small and fiber-like and are produced in an early stage of the hydration. It is observed in Fig. 68f a more homogeneous crystal structure. Finally, as illustrated in Fig. 68g more C-S-H gel was detected.

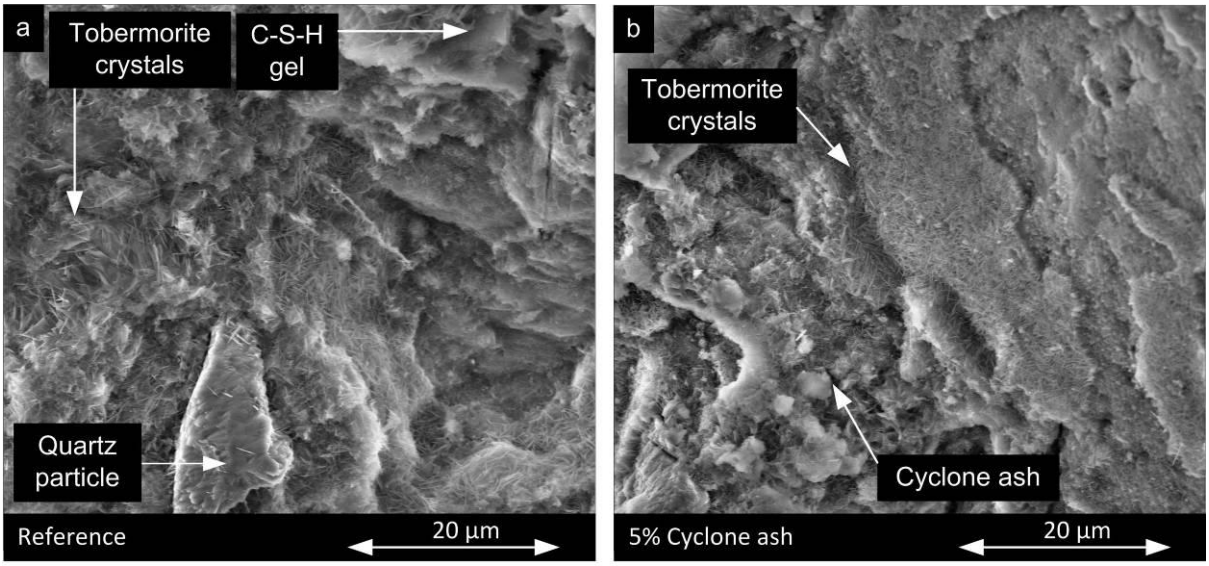

Figure 68: The microstructure of the fractured surface of 5 % substitution

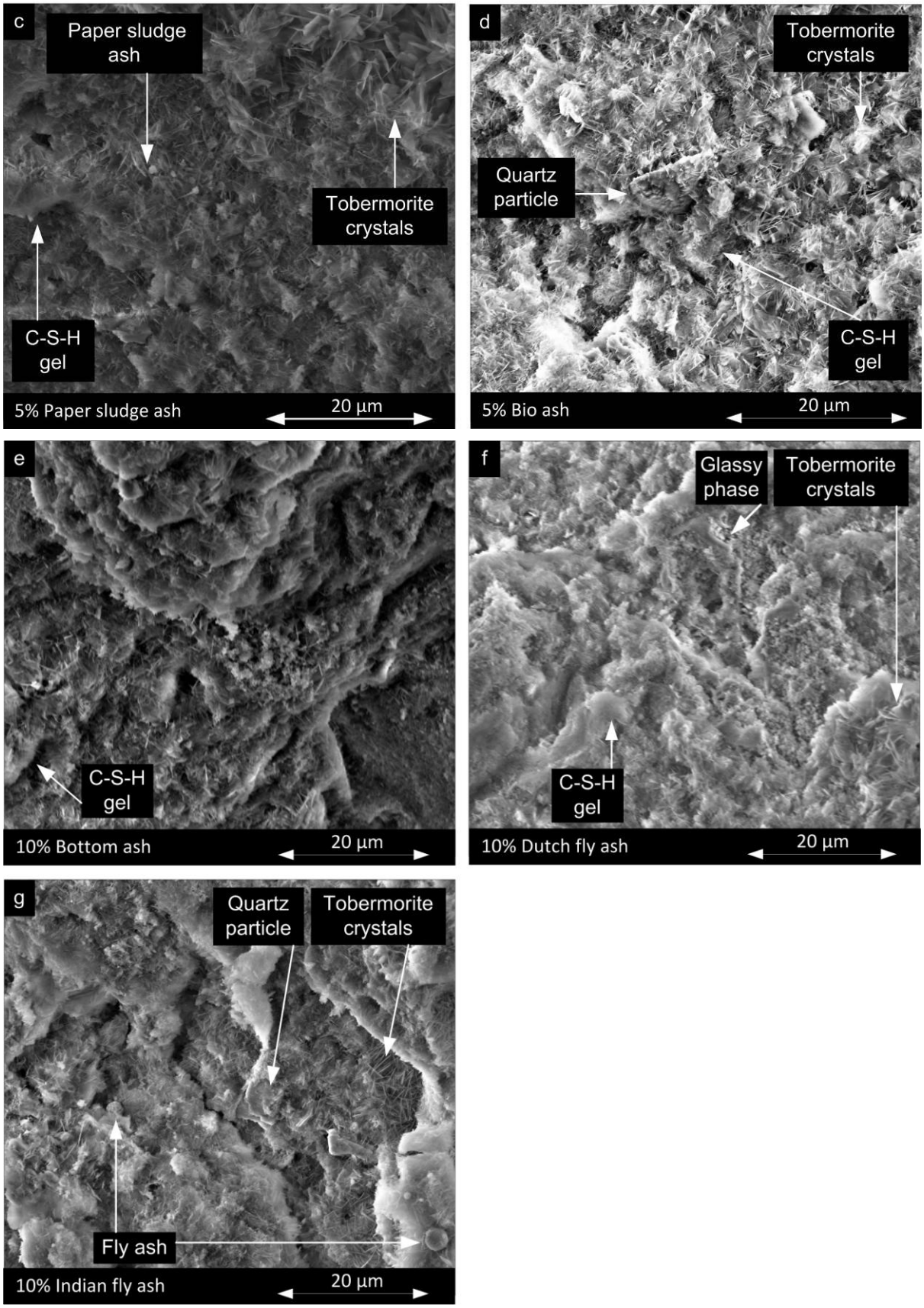

Figure 68: The microstructure of the fractured surface of 5 % substitution, cont.

Discussion 10 % substitution

The FESEM pictures of 10 % substitution of the matrix are summarized in Fig. 69a-g. The matrix of the 10 % cyclone ash contains a combination of remaining quartz particles, C-S-H gel, cyclone ash and tobermorite crystals as can be seen in Fig. 69b. These points to the likelihood that, the mixture is less homogeneous compared to the reference. Next, a very dense mix of C-S-H gel, tobermorite crystals and small traces of paper sludge ash were found in the matrix of 10 % paper sludge ash (Fig. 69c). In general, it appears that the matrix is relatively homogeneous. Furthermore, for 10 % bio ash different morphologies such as small and large tobermorite crystals with some traces of bio ash (Fig. 69d). Indian fly ash, Dutch fly ash and bottom ash illustrate just like the 10 % cyclone ash and the 10 % bio ash all kinds of calcium rich gel (Fig. 69e-g). However, the 10 % bottom ash and the Dutch fly ash show more C-S-H gel types and less crystallized tobermorite. Lastly, in both fly ashes samples were unreacted quartz particles detected (Fig. 69f-g).

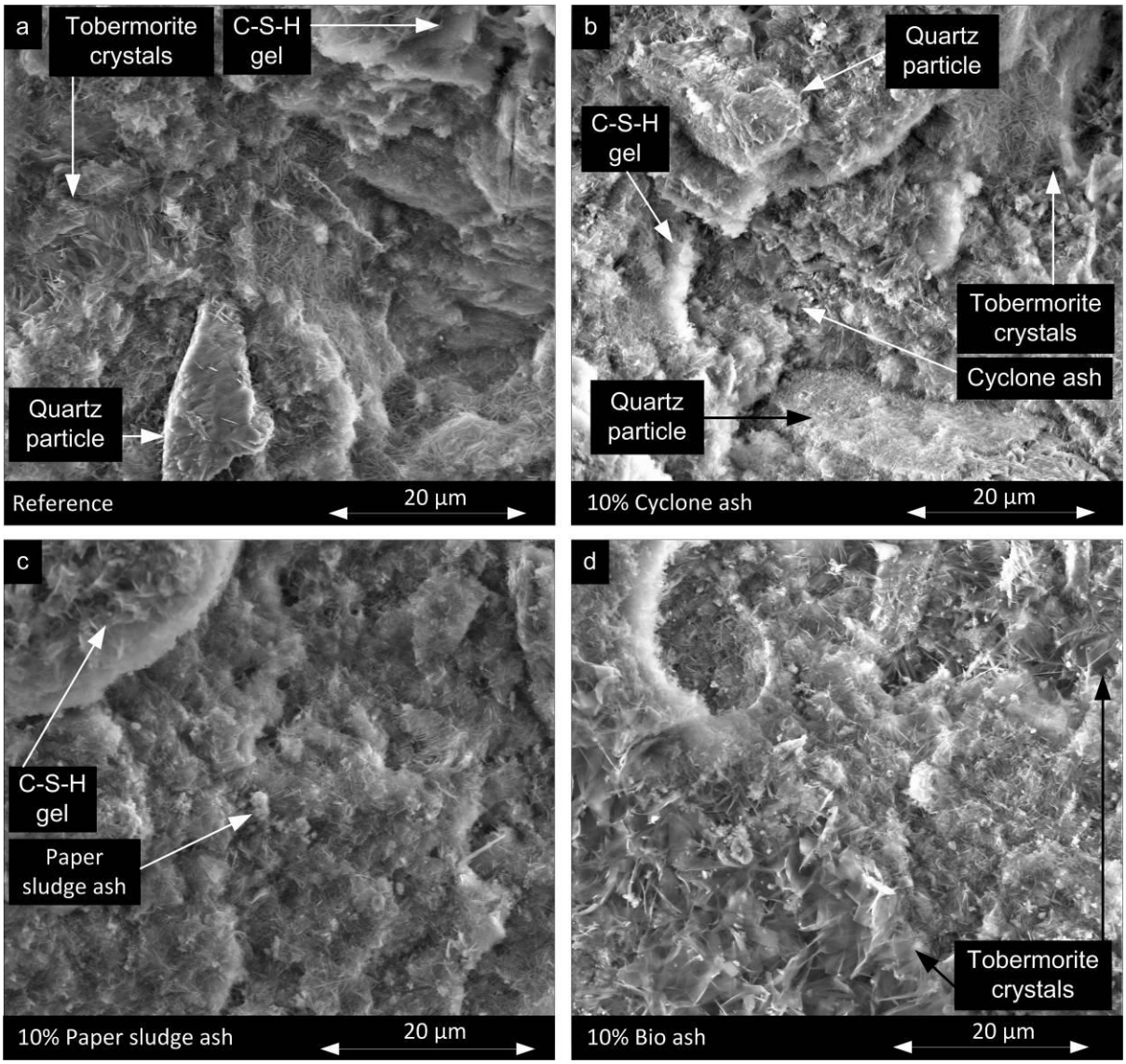

Figure 69: The morphology of the fractured matrix of 10 % substitution

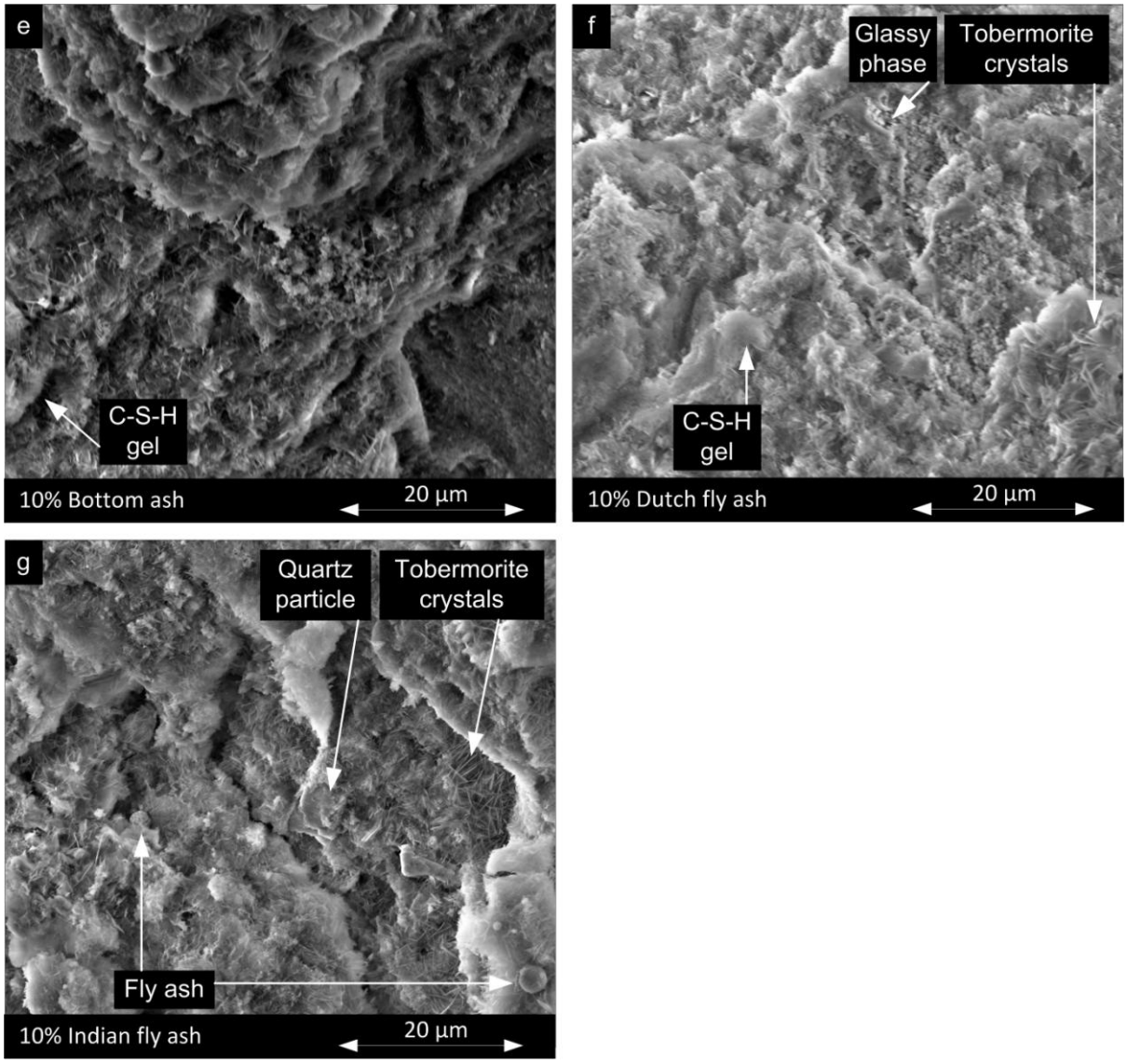

Figure 69: The morphology of the fractured matrix of 10 % substitution, cont.

Discussion 15 % substitution

The matrix of the fractured surfaces of the 15 % substitution can be indentified from Fig. 70a-d. Firstly, the reference demonstrates a more homogeneous structure compared to the substitution samples, which consist of a matrix with C-S-H gels and small and large tobermorite crystals. As can be observed in Fig. 70b, the 15 % paper sludge ash sample consists of a dense gel-like rich matrix. Furthermore, the bottom ash matrix seems to consist of a lot of separated particles, which did not react properly (see Fig. 70c). Also, multiple glassy-like particles remain as a result of the reaction of bottom ash. There is a definite possibility that a higher substitution of bottom ash is not favorable.

Lastly, inspection of Fig. 70d indicates that only the Indian fly ash has no big tobermorite crystal formation in the matrix. Nevertheless, big fly ash particles and quartz were spotted which have partly reacted. In general, in both the bottom ash, as the Indian fly ash samples multiple different particles did not properly dissolve or reacted. Finally, as a result it is assumed that a low filling effect occur which would confirm the less favorable physical properties of both samples.

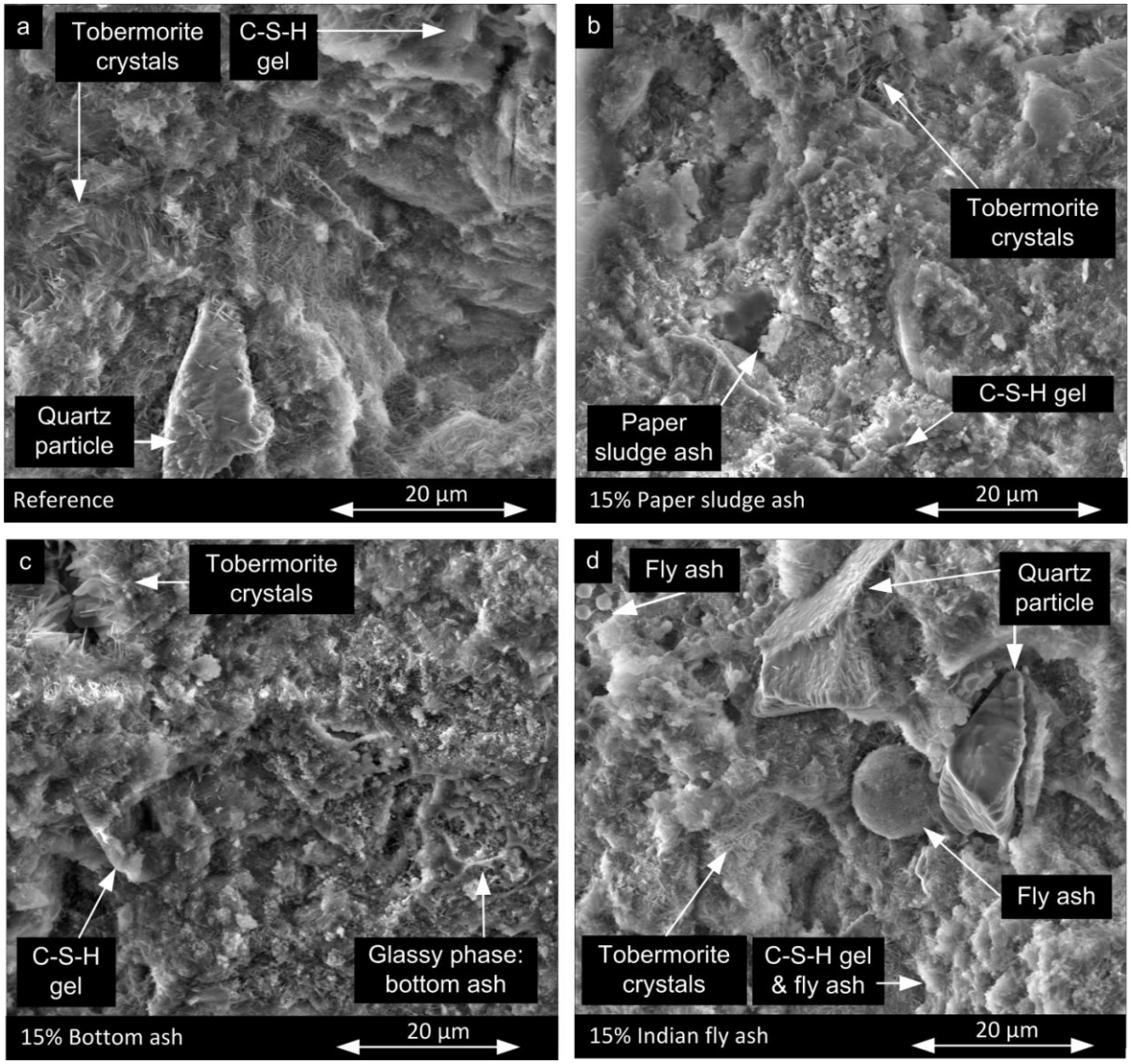

Figure 70: Matrix of 15 % substitution

8.2.3 TOBERMORITE CRYSTALS IN MACROPORE

DISCUSSION 5 % SUBSTITUTION

In general, the crystal formation is mainly depending on the local temperature, pressure, Ca/Si ratio, w/s ratio and aluminum amount. Fig. 71a-g reveals the inside microstructure of macropores. As can be seen from Fig. 71a well defined flower type or plate-like tobermorite is displayed. However, comparing the 5 % paper sludge ash sample (Fig. 71c) and 5 % bottom ash samples (Fig. 71b), it can be cleary seen that the microstructure is more dense with less defined crystals. The other samples, cyclone ash, bio ash and the fly ashes have similar crystal structure (Fig. 71a-b,d,f and g). Nevertheless, it could be noted that no causal relation based on these results can be made. It is assumed that small pores have in general more well defined crystals resulting possibly because of different pressure and temperature condition.

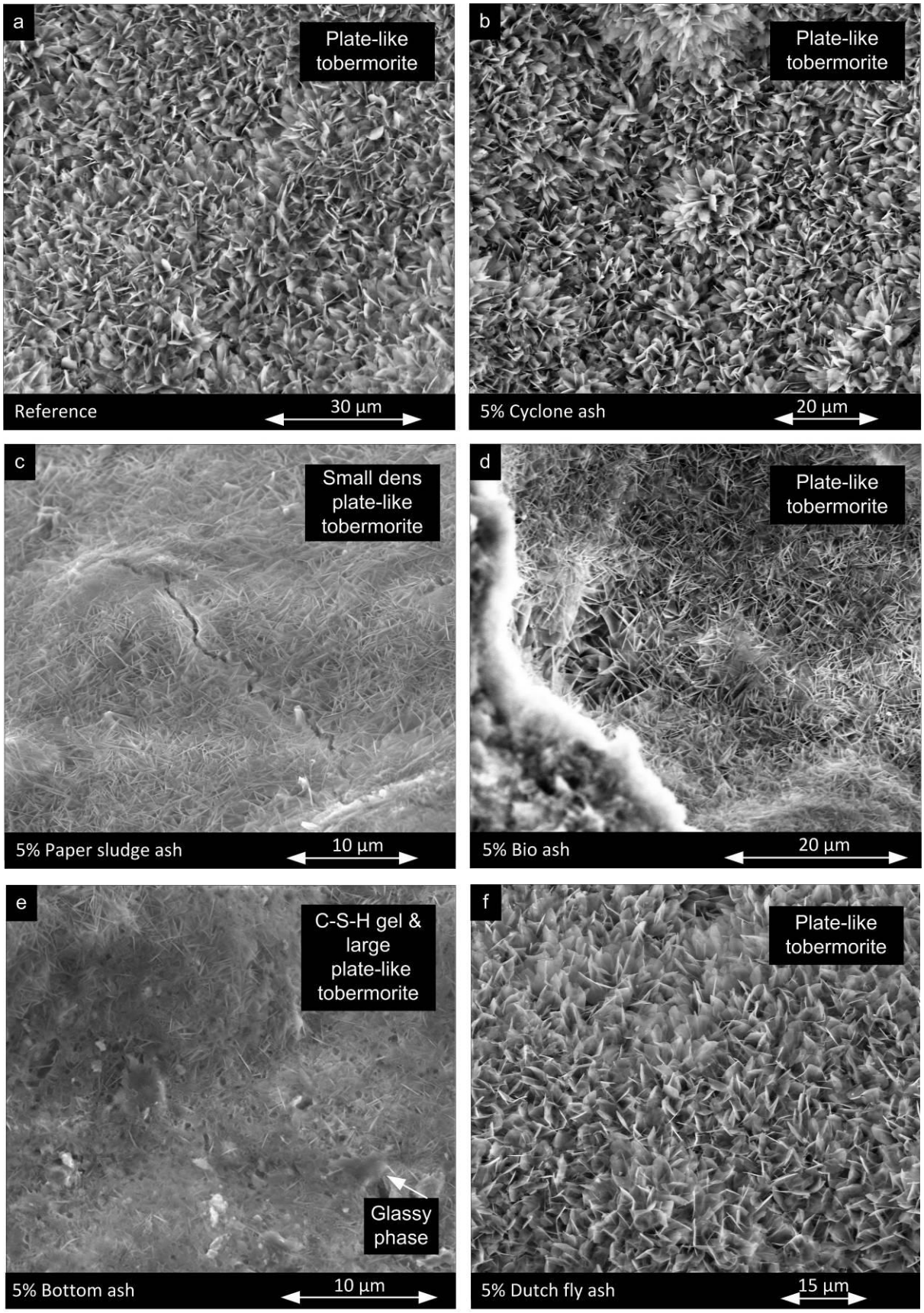

Figure 71: Crystal formation in a macropore of 5 % substitution

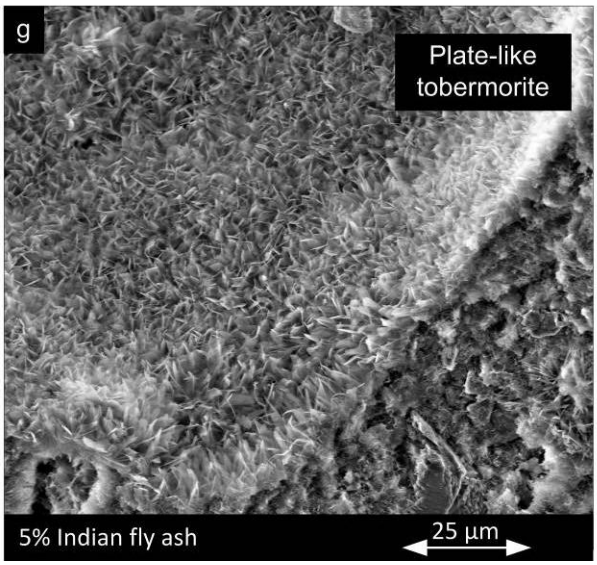

Figure 71: Crystal formation in a macropore of 5 % substitution, cont.

Discussion 10 % substitution

Fig. 72 shows the tobermorite crystals in a macropore. In 10 % cyclone ash, C-S-H with a fibrous-like structure (Fig. 72b) and various kinds of morphologies are seen in the macropore. It is suggested that the formation was retarded and probably a very low Ca/Si ratio tobermorite phase was formed. Furthermore, the morphology of the 10 % paper sludge ash sample contains more dense needle-like crystals (Fig. 72a).

The white particles, which are all over the images, are likely to be traces due to fracturing of the sample. The cyclone ash sample and the paper sludge ash sample have contradictory crystal structures to the reference (Fig. 72c). Furthermore, as can be found in Fig. 72d, the morphology of the bio ash sample is made of slightly fiber-like crystals, but comparable to the reference. It should be noted that the bio ash sample had the lowest w/s ratio.

Fig. 72e shows that 10 % bottom ash has multiple types of crystals inside the macropores. The 10 % Dutch fly ash sample reveals plate-like and grass-like crystal formations (Fig. 72f), the Indian fly ash presents thick flower-like crystals. Although, the fly ashes have similar oxide composition and density, only the Indian fly ash is slightly coarser in PSD. However, more additional aluminum powder and less water were added to the Indian fly ash sample. It could be that this led to a slightly higher CS.

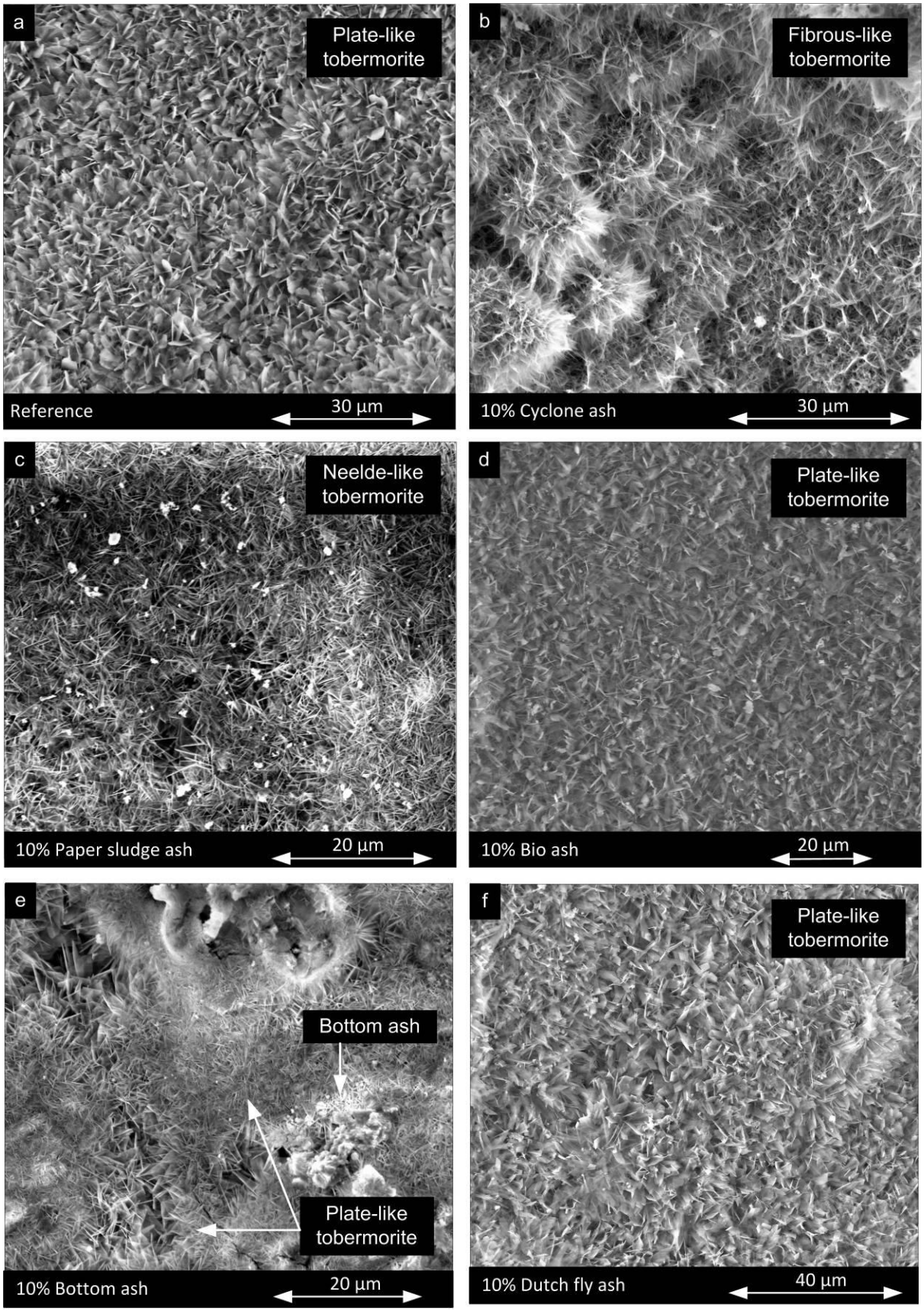

Figure 72: Crystal formation in a macropore of 10 % substitution

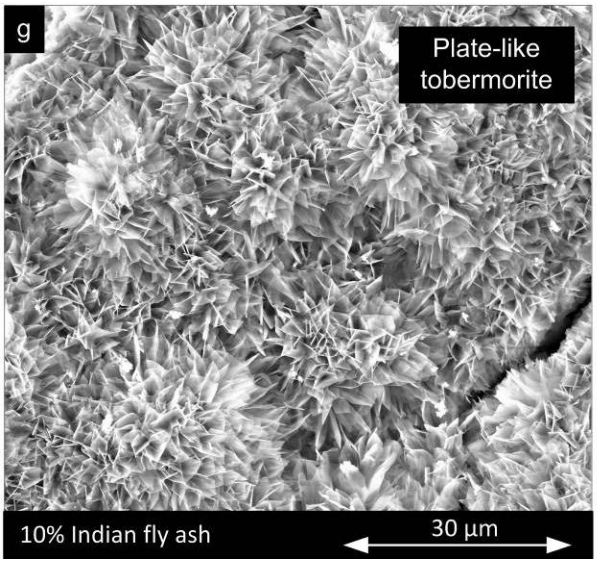

Figure 72: Crystal formation in a macropore of 10 % substitution, cont.

Discussion 15 % substitution

In Fig. 73a-d the inside of macropores is compared. The 15 % paper sludge ash sample show similar morphology of tobermorite crystals as the reference as can be observed in Fig. 73a-b. Next, both bottom ash and Indian fly ash show long grass-like crystals as represented in Fig. 73c and Fig. 73d. However, the XRD results show that both additives have comparable tobermorite level. Thus, the grass-like crystals which are also a good quality indication might be caused by slightly different temperature conditions. Nevertheless, the bottom ash sample has also pores with no grass-like tobermorite crystal morphology but with different kinds of dense C-S-H gel phases. Finally, it is recognized that the results of the 15 % paper sludge ash sample confirm the results of the XRD. Also, there is a strong possibility that the resemblance of crystal structure found with FESEM, is in line with the CS results.

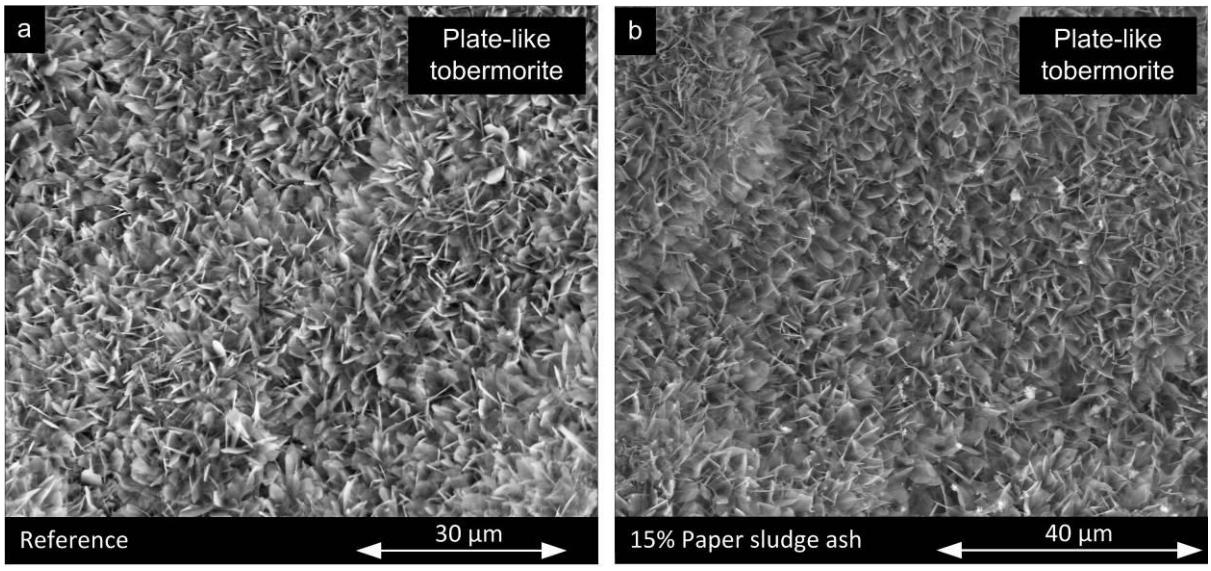

Figure 73: Crystal formation in a macropore of 15 % substitution

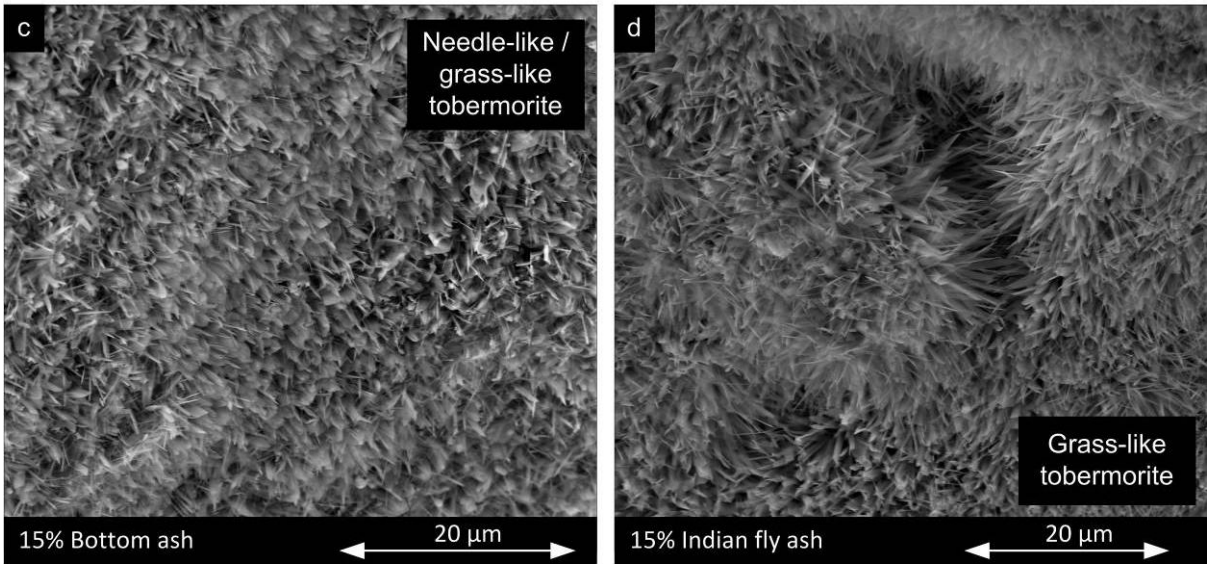

Figure 73: Crystal formation in a macropore of 15 % substitution, cont.

8.2.4 TOBERMORITE CRYSTALS IN DETAIL

DISCUSSION 5 % SUBSTITUTION

As illustrated by Fig. 74 plate-like tobermorite is produced from initially amorphous C-S-H in the matrix. The reference (Fig. 74a) contains well defined plate-like tobermorite crystals. Similar plate-like crystals were found in cyclone ash, bio ash, bottom ash and Dutch fly ash as can be seen in Fig. 74a-band Fig. 74d-f. Fig. 74c demonstrates that the 5 % paper sludge ash sample has a homogeneous formation of crystals, including very small and denser crystals. Empirically, it seems that, the crystals are in between amorphous and crystalline phases.

The density of the paper sludge ash itself is 2740 kg/m^3, which is in line with the bio ash and bottom ash. So density is not relevant. Furthermore, the formation of tobermorite crystals in the bottom ash sample are well defined. Lastly, the Indian fly ash samples showed similar small size crystal formation.

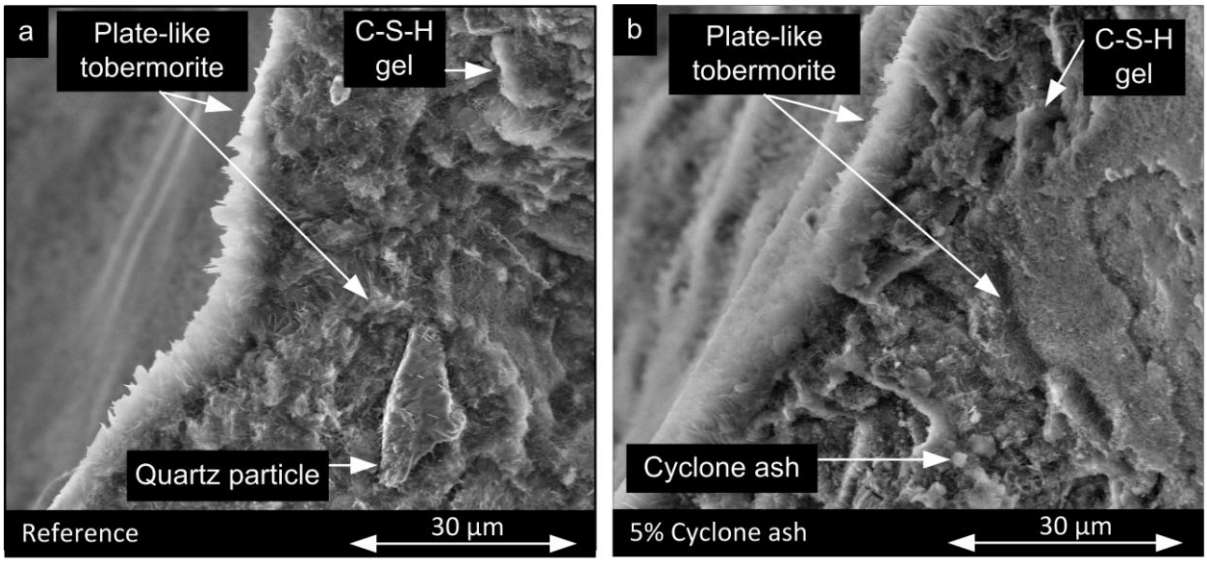

Figure 74: Detail of crystal formation of 5 % substitution

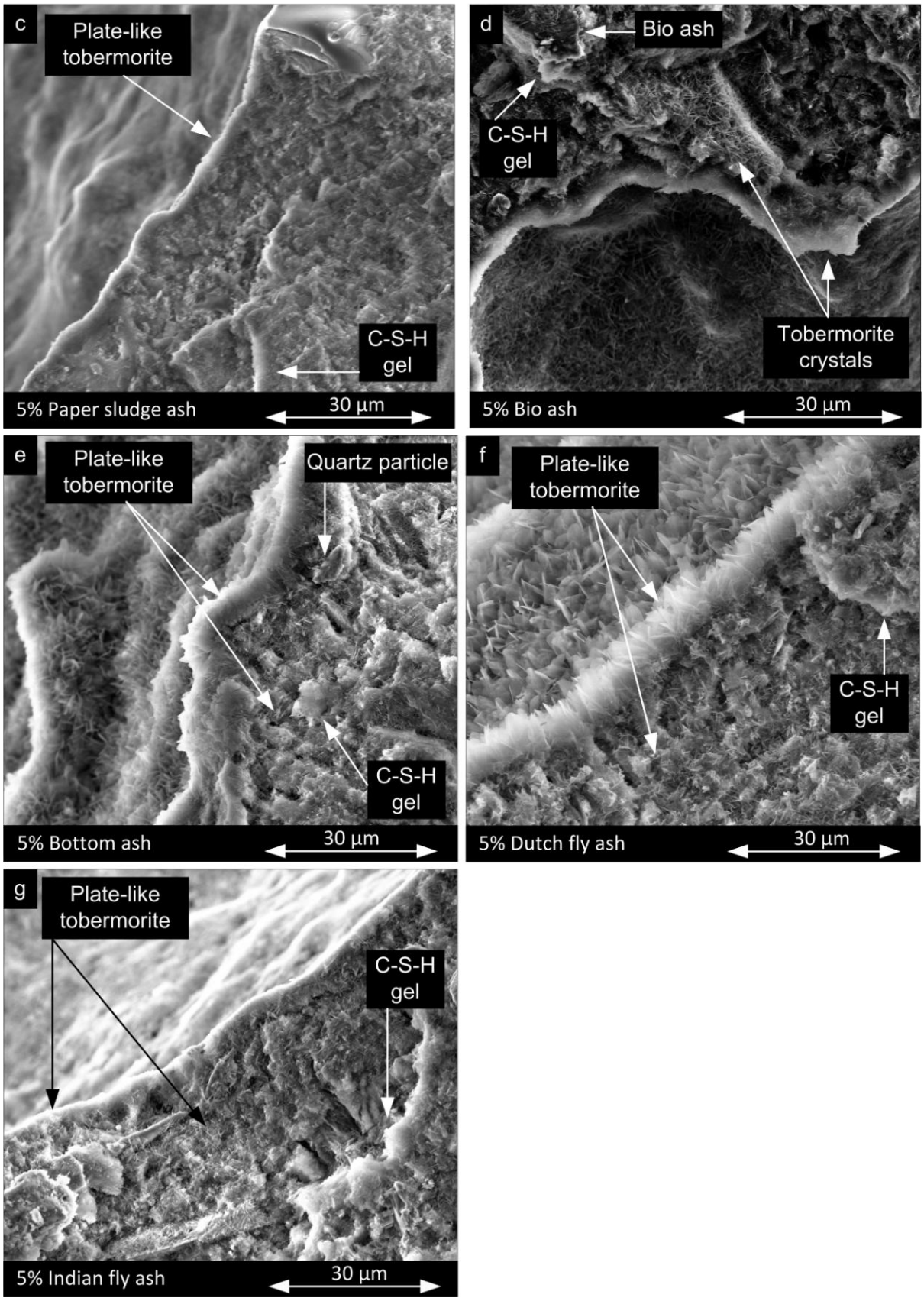

Figure 74: Detail of crystals formation of 5 % substitution, cont.

Discussion 10 % substitution

Fig. 75a-g display a tobermorite crystal structure inside a macropore. Firstly, the 10 % paper sludge ash has slightly smaller crystals. Secondly, similar crystal size and formation are shown in 10 % Indian fly ash sample. But, also different types of crystals are visible in other macropores. Furthermore, the 10 % cyclone ash has fairly large tobermorite crystals. The 10 % bottom ash has small, dense, not fully developed crystals in pores. However, the XRD results confirm that the 10 % bio ash sample has an almost similar tobermorite level.

Both, bio ash (Fig. 75d) and the bottom ash (Fig. 75e) show a similar dense crystal structure and dry density, but the bottom ash sample has a noticeable higher CS. Furthermore, in Fig. 75f plots a thin plate-like tobermorite crystals for the 10 % Dutch fly ash. This morphology was not seen elsewhere. Nevertheless, similar tobermorite levels for the Dutch fly ash as the references were obtained with the XRD. It seems that the crystal shape is not the only key parameter concerning CS.

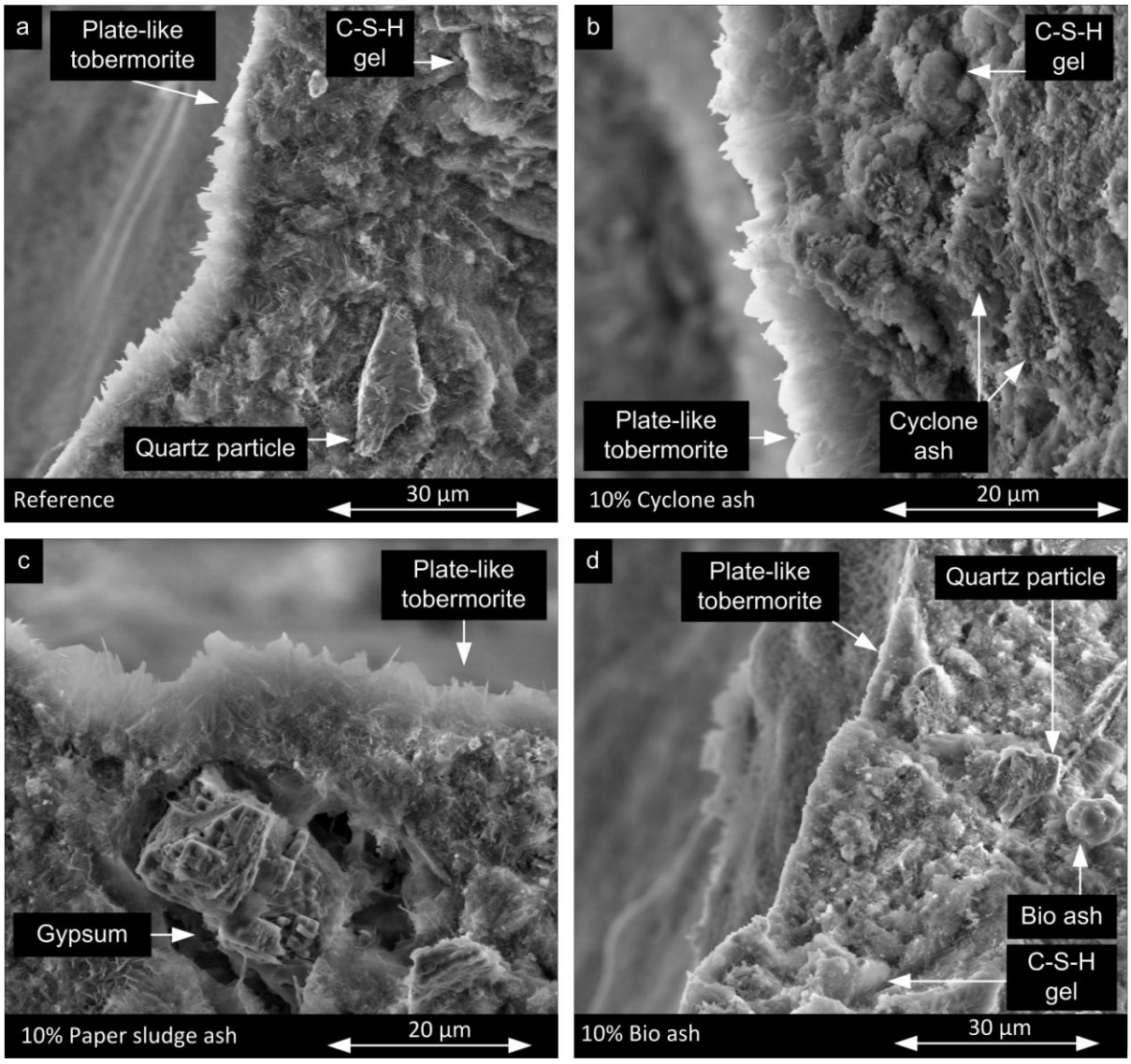

Figure 75: Detail of crystals formation of 10 % substitution

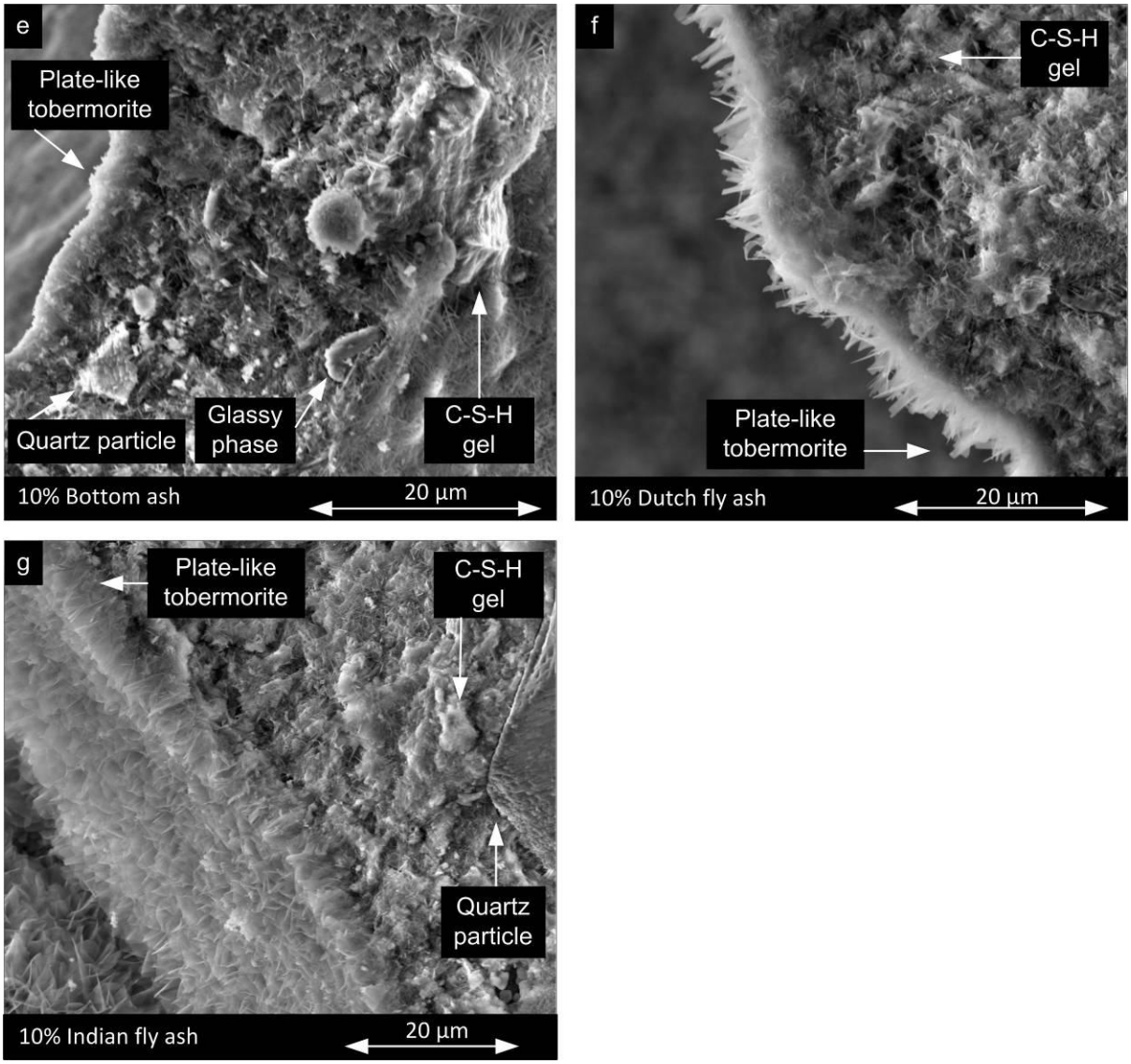

Figure 75: Detail of crystals formation of 10 % substitution, cont.

Discussion 15 % substitution

Fig. 76a-d illustrate the tobermorite crystals inside a macropore growing from the matrix. The size and shape of the tobermorite crystals of the reference and paper sludge ash sample are almost similar, see Fig. 76b. However, the crystal formation of the paper sludge ash looks denser. Next, both, the 15 % bottom ash and the 15 % Indian fly ash have no tobermorite crystals but a gel-like formation. It is assumed that this gel-like structure could be the starting phase of the formation of tobermorite crystals. Finally, based on the matrix structure and tobermorite crystal structure, paper sludge ash has the most similar morphology compared to the reference.

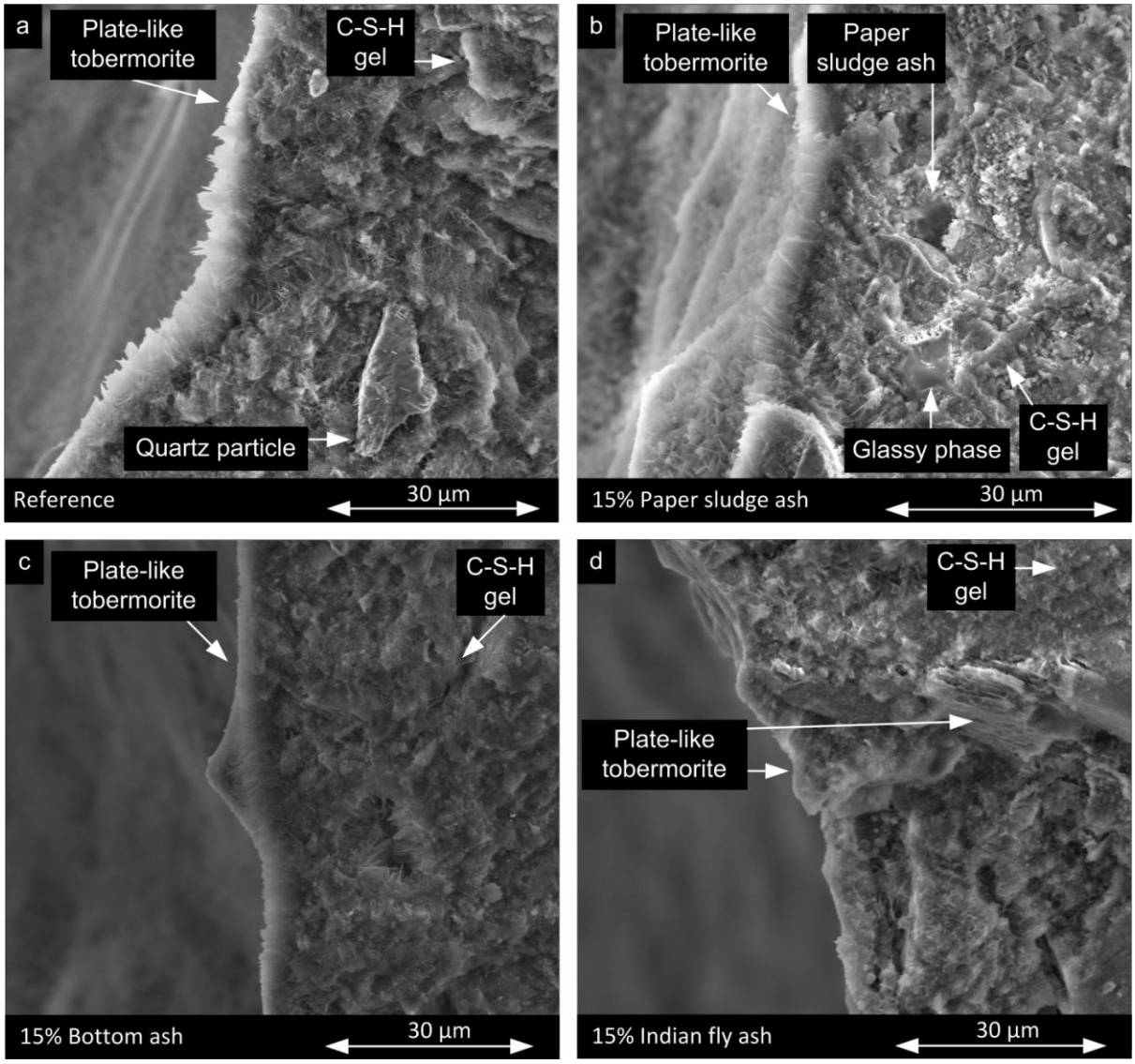

Figure 76: Detail of crystals formation of 15 % substitution

8.2.5 EXCEPTIONAL FINDINGS

TRACES OF GYPSUM AND ANHYDRITE

Several exceptional FESEM pictures are reported in Fig. 77-78. Firstly, the process where a calcium silicate nucleation starts to grow from a quartz grain can be seen from Fig. 77. In general, the autoclaving procedure is favourable for generating big gypsum crystals or calcium sulfate ($CaSO_4$) crystals.

Therefore, Fig. 78 presents five pictures with traces of gypsum and anhydrite ($CaSO_4$). These crystals are the result of a crystallization process. As is visible in Fig. 78a an agglomerate of gypsum particles is formed. It is suspected that this is due to bad mixing. Furthermore, large gypsum crystals are detected (confirmed by EDS) in the 5 % paper sludge ash sample (Fig. 79b). In general, a lot of gypsum crystals are growing inside the macropores of the paper sludge ash sample. The XRD results confirm a slightly higher anhydrite presence. Fig. 78c shows an agglomerate of gypsum. Finally, in Fig. 78d small crystals at the surface in the Dutch fly ash sample are plotted.

PARTLY DISSOLVED FLY ASH

Fig. 79 illustrates the findings of the partly dissolved Dutch fly ash and it reaction to form hydrates. It can be seen that reaction products (unreacted crystals) are visible at the surface (Fig. 79a) and in the fly ash itself (Fig. 79b-c) confirming, that Dutch fly ash is partially reactive. Finally, Fig. 79d represents a hollow Indian fly ash, in which are partly dissolved.

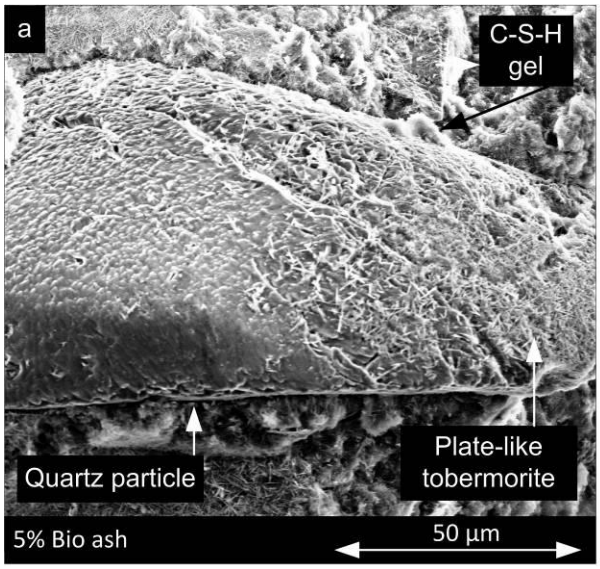

Figure 77: Matrix with dissolved quartz and gypsum particles

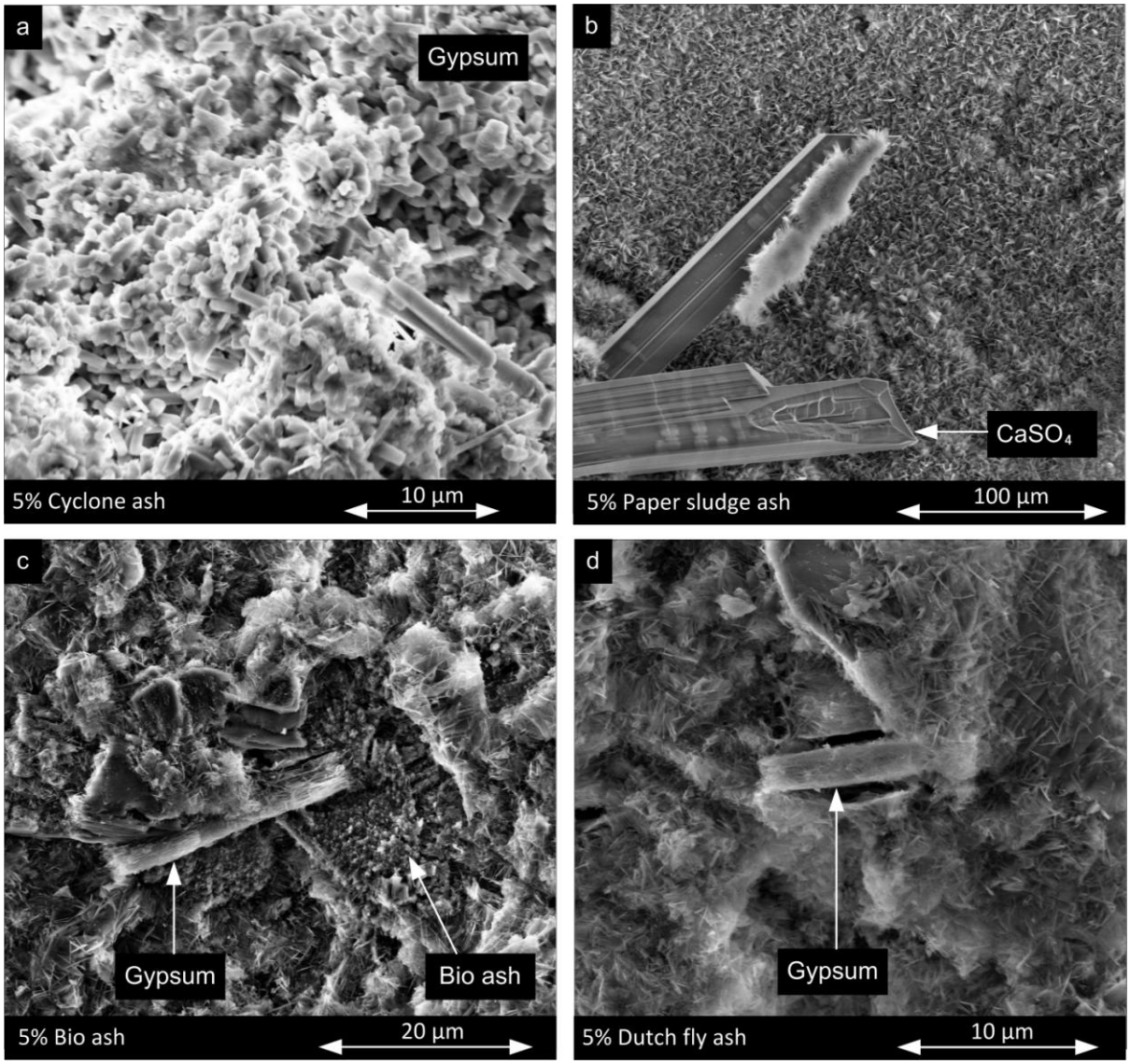

Figure 78: Matrix with dissolved quartz and gypsum particles

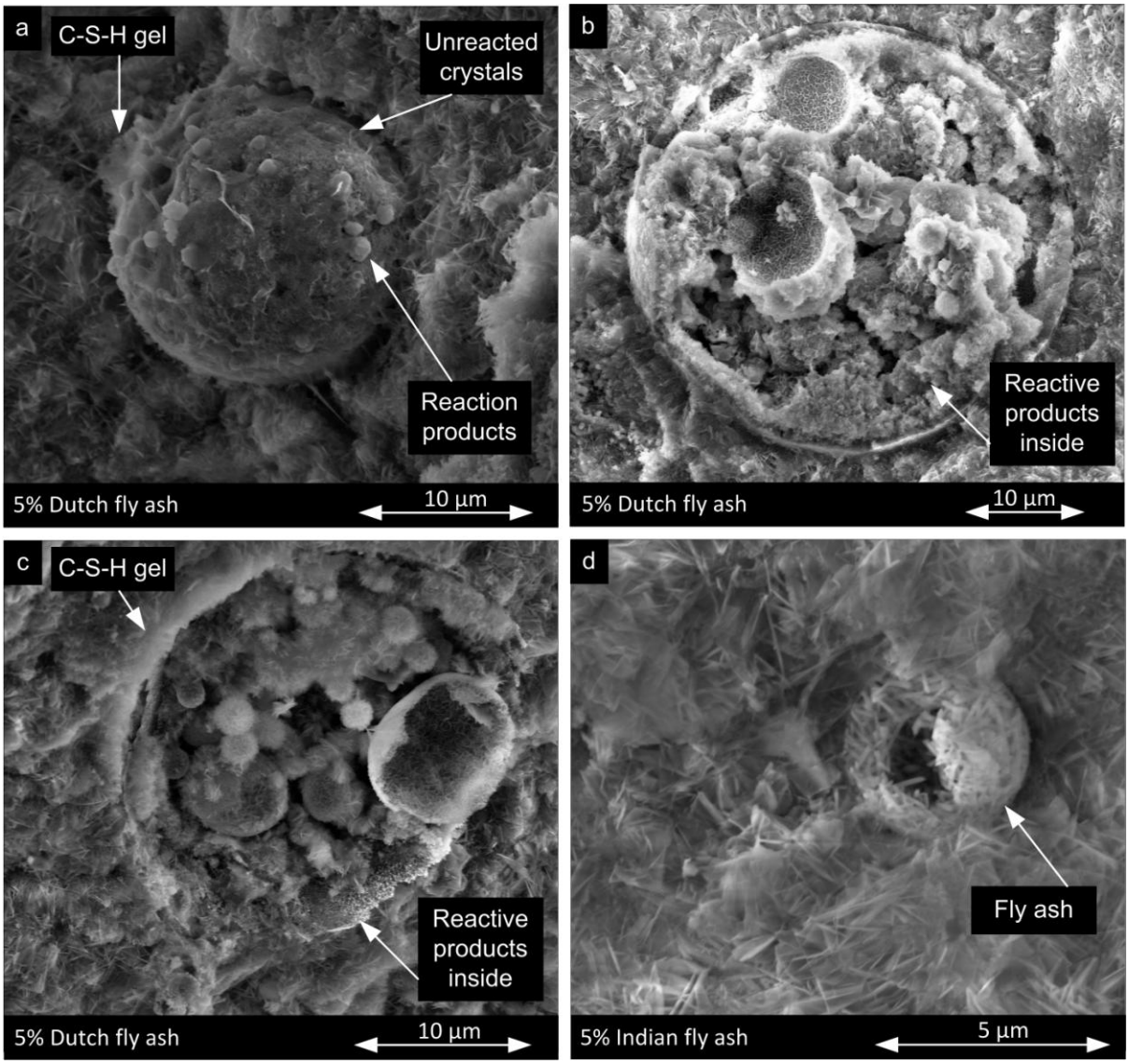

Figure 79: Fly ash particles

8.3 Conclusion

Overview macropores

The pore shape seems to have the highest influence on the strength. A large macropore distribution is visible in 10 % cyclone ash, resulting in a low CS. All paper sludge ash samples show a small macropores size distribution, resulting in a high CS.

Crystals in matrix

The strength of the crystal structure is determined by the compact structure of the adjacent crystals in the matrix.

1. The reference, 5 % paper sludge ash and 5 % cyclone ash display a dense crystal formation.
2. A less dense formation of crystals is illustrated in 5 % fly ashes and 5 % bio ash. There seems to be no direct relation between the different crystals structures and the CS, indicating weakening by porosity.
3. The crystal size in the matrix seems to be increased by an increase in substitution.

Crystals in macropore

1. The reference illustrates a less dense crystal structure at the surfaces and crystals grow in the macropore. This is comparable to 5 % cyclone ash and 5 % fly ashes which have a lower CS due to a larger macropore size distribution.
2. 5 % paper sludge ash and 5 % bottom ash show a high density crystal structure with no crystal growth in the macropores. Paper sludge ash shows a high CS due to a higher homogeneity of the macropores distribution.
3. 5 % bio ash and 10 % cyclone ash have no dense crystal structure because of the needle-like formed crystals. These crystals deliver a low CS, due to the low homogeneity of the macropores distribution.
4. The 10 % paper sludge ash has a no dense crystal structure due to the needle-like formed crystals, which deliver a low CS. This is compensated for by the higher homogeneity of the macropores distribution, resulting in higher CS.
5. The 10 % Indian fly ash shows large, well defined homogeneous crystal grow.
6. Large differences in local crystal morphology are seen in the 10 % bottom ash.
7. The 15 % bottom ash and 15 % Indian fly ash show grass-like and needle-like crystals, while the reference and the 15 % paper sludge ash show more plate-like crystals.

Crystals growing from the matrix

1. All samples illustrated different crystal structures at the surface of the macropore.
2. 5 % paper sludge ash, 5 % bio ash and 5 % Indian fly ash display a thin densely formed crystal layers. All crystals deliver a contribution to the matrix strength due to the absence of crystal grow in the macropore. The contrary can be stated for the other 5 % samples.
3. The 10 % bottom ash shows again a large variety of crystal morphology.

9. COLOR OF QUARTZ SUBSTITUTION

9.1 RESULTS AND DISCUSSION

Fig. 80 shows quartz replacement samples. The effects of the additives, bio ash (Fig. 80g-h) and bottom ash (Fig. 80i-k), on the final color are noticed visible. Next, larger pore size is significantly noticeable for the cyclone ash (Fig. 80b-c) and Dutch fly ash (Fig. 80l-m) substitution. A significant darker color is obtained due to the replacement of 15 % bottom ash (Fig. 80k) Also, a slightly smaller pore size are visible for the 15 % paper sludge ash sample (Fig. 80f).

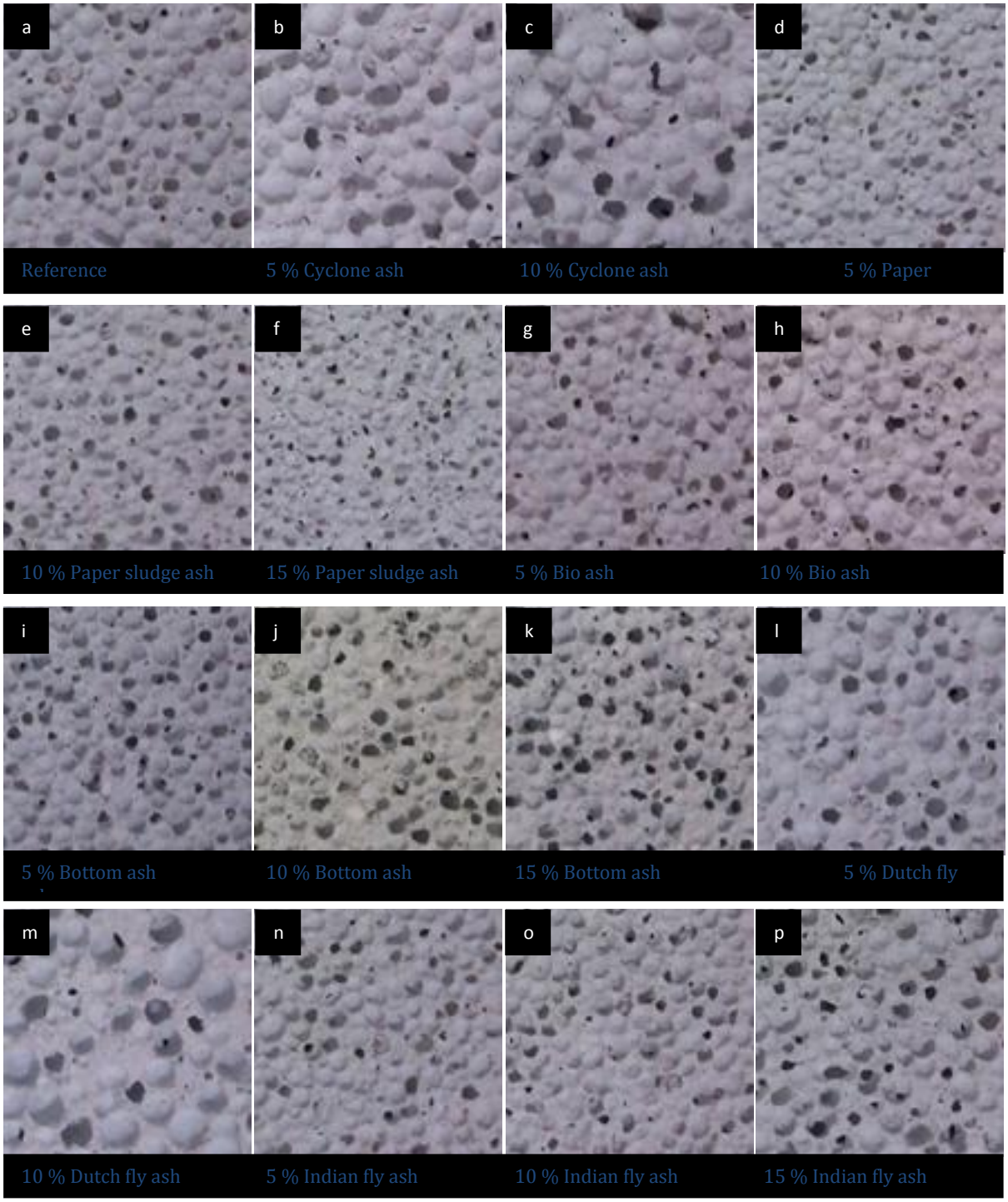

Figure 80: Shows all substitution samples at distance of 100 mm

A spectrophotometer is used for determining the color of the quartz substitution samples. This is a quantitative measurement of the reflection or transmission properties of a material as a function of wavelength. Fig. 81 shows the L*, a*, b* color scheme and Fig. 82 a* and b* color scheme. The results of the measurements are given in Fig. 83-84. All samples are slightly darker compared to the reference (Fig. 83). Fig. 83 shows that the bio ash and bottom ash substitutions samples have a noticeably less white appearance. Fig. 84 shows that the bio ash substitution samples are significantly reddish and the bottom ash substitution samples are greyish (Fig. 82). To conclude, the bio ash and bottom ash are less suitable because of their less white appearance.

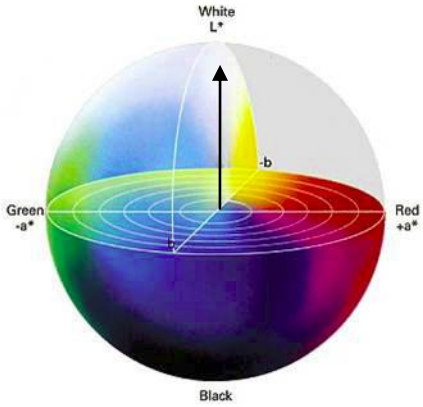

Figure 81: L*, a*, b* color scheme

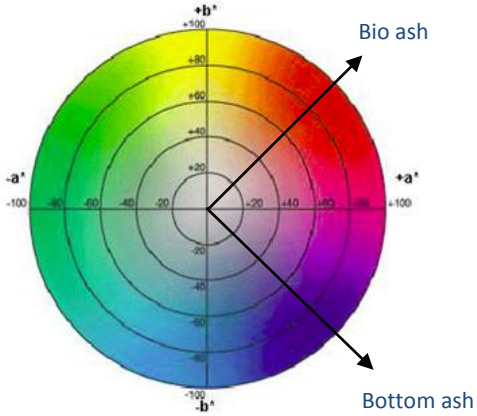

Figure 82: a*and b* color scheme

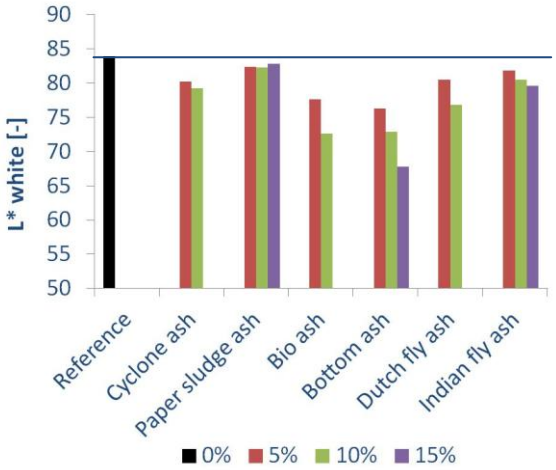

Figure 83: L*: white color of all substitutions

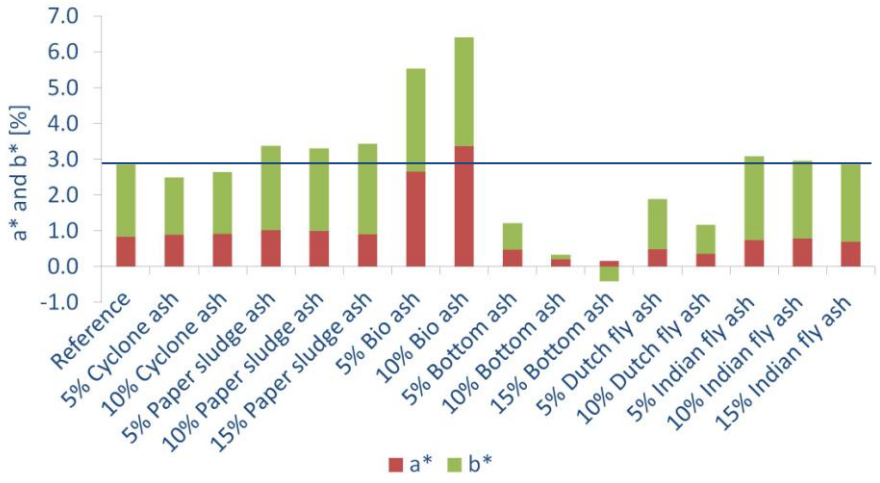

Figure 84: a* and B*: Red color of all substitutions

10. CONCLUSION OF QUARTZ SUBSTITUTION

Performance was defined by possibilities, restriction and economically aspect of the appliance of the additives in AAC.

GENERAL CONCLUSION

1. An optimal rising and stiffening development is essential for producing a potentially high CS AAC for all the additives.
2. Based on the impact of the additive on the quality and performance of CS and porosity, it is of major importance to have a constant (oxide) composition and PSD.
3. It is therefore important to have knowledge about the variability of the additives regarding composition and PSD.
4. All additives resulted in different crystal grow at the surface of the macropores. No conclusive relation between additives can be generated based on the FESEM analysis.

CYCLONE ASH

1. The XRD results show that the cyclone ash substitution contains a substantial amount of non-reacted calcite and anhydrite, indicating a non optimal mixture composition and reaction conditions (curing and autoclaving).
2. The low CS and porosity is directly related to insufficient reaction rate (dry density).
3. XRD results illustrate that a high tobermorite concentration in combination with a significant amount not reacted calcite and anhydrite indicates a substantial potential for improvement of the CS, by optimizing.
4. Substantial research is needed to optimize the reaction mixture and processing conditions during curing and autoclaving.
5. The color of the AAC samples with cyclone ash substitutions were similar to the reference.

BIO ASH

1. The presence of phosphates in bio ash decreased the viscosity of the mixture. Because of the high content of phosphates the bio ash is not suitable.
2. The imbalance between w/s ratio and aluminum powder concentration is not optimal for the mixture composition and reaction conditions (curing and autoclaving), resulting in a decreased CS.
3. The phosphates in bio ash should be recycled back in to the natural phosphate cycle due to the fore seen shortages of phosphate as a fertilizer.
4. So, phosphate should be removed from bio ash before applying it as an additive in AAC.
5. The presence of high concentrations of metal oxides can be a challenge.
6. Further research is needed to prove feasibility of bio ash in AAC.
7. The color of the AAC samples including substitution of bio ash were slightly reddish, due to the presence of excessive iron oxide.

PAPER SLUDGE ASH

1. Paper sludge ash seems to be the highest performing additive concerning CS, due to constant small macopores.
2. The advantage of paper sludge ash seems to be a product which is more specified compared to the other additives.
3. A restriction of paper sludge ash is the increased water demand resulting in a required adjustment of the mixture, with respect to w/s ratio an aluminum powder.
4. Paper sludge ash is a product made by one producer, which is more costly compared to the other additives.
5. The availability of paper sludge ash is questionable due to the broad application as a cement replacement.
6. The color of the AAC samples with paper sludge ash substitutions were identical to the reference.

Bottom ash

1. Bottom ash need to be milled to achieve the required PSD, therefore costs more.
2. All bottom ash substitution result in a relatively good CS.
3. Bottom ash is a good replacement for quartz. Bottom ash consists of more than 60 % of silicates.
4. The color of the AAC samples including substitutions of bottom ash were darker, due to the presence of coal-like components.

Dutch fly ash

1. The Dutch fly ash substitution resulted in similar porosity and density as the reference, but a substantially reduced CS.
2. XRD results show a comparable tobermorite concentration compared to the reference, which delivers insufficient CS.
3. The Dutch fly ash has less potential since the reaction rate is already optimal, but the CS is insufficient.
4. The color of the AAC samples with Dutch fly ash substitutions were similar to the reference color.

Indian fly ash

1. XRD results show a higher tobermorite intensity and also a high amount of anhydrite and calcite, indicating an insufficient reaction.
2. Substantial research is needed to optimize the reaction mixture and processing conditions during curing and autoclaving.
3. AAC samples with Indian fly ash substitutions have a similar color as the reference.

Economical aspect

The replacement of quartz seems only relevant with respect to sustainability (immobilizing solid waste, reducing landfill). Replacement of quartz for economical reasons is limited. Less quartz grinding versus marginally reduction of raw material costs.

Based on, this is the price, in €, per ton calculated. The reference recipe costs € 33.67 (see Appendix A.2.4 for detailed calculations). Only, the price of paper sludge ash is known, which is ± € 20.00 per ton. Paper sludge ash has the same price as quartz, so a substation from an economical point of view is not desirable. The price for the used additives was not known exactly. Two alternatives were selected to give an indication of the reduction price range. Alternative 1 has a price of € 10.00 per ton and alternative 2 has a price of € 5.00 per ton.

By using alternative 1, for a 15 % substitution of quartz, the total recipe price would have a reduction of € 1.50. The total recipe cost reduces with 4.7 %. The total recipe price reduction for alternative 2 for a 15 % substitution of quartz is about € 2.25. The total recipe cost for alternative 2 reduces with 7.2 %

Recommendation

1. It is recommended to adjust the composition of the mixture and reaction conditioned during the curing and autoclaving period, to improve the product by reduction of non-reacting anhydrides.
2. The results of the CS tests cannot be predicted based on the currently applied test on raw materials and information gathered during the curing period. It is always necessary to perform a CS test. Further research is needed to find a representative test on raw materials and a test during the curing period for a reliable prediction of the CS.

11. SUBSTITUTION OF PORTLAND CEMENT BY PAPER SLUDGE ASH

11.1 INTRODUCTION

The same methodology as for the quartz substitution is applied for all test.

MEASUREMENTS DURING CURING PERIOD

This chapter elucidates important influencing parameters and results obtained of test during the curing period for 10-50 % substitution of paper sludge ash. The main purpose of this chapter is to determine the reaction rate of all substitution ratios. Tab. 35 illustrates the reaction rate for all paper sludge ash substitutions.

Table 35: w/s ratio and amount of aluminum powder

Paper sludge ash substitution	w/s ratio	Aluminum powder
	[-]	[g]
0 %	0.580	14
10 %	0.580	14
20 %	0.580	14
30 %	0.580	14
40 %	0.595	14
50 %	0.608	14

The following tests were conducted for all samples: (I) the slump flow test, (II) rising development (of the mixture) test, (III) the temperature development and maximum temperature, (IV) the penetration depth test and, (V) the final product height. Appendix A.3.1 gives detailed measurements during curing period.

11.2 RESULTS DURING CURING PERIOD

DISCUSSION OF 0-30 % PAPER SLUDGE ASH SUBSTITUTION

At first, the w/s ratio was kept constant for 10-30 % paper sludge ash substitution. All results are compared to the reference. A declining slump width and accelerated stiffening development (Fig. 89 and Tab. 37) were observed in for a higher paper sludge ash substitution (Fig. 85). As a result of the accelerated stiffening development, the sinking effect occurred sooner, as is visible in Fig.86. This is due to quicker increased temperature in an early stage (till 180 min), expected for the 10 % substitution (Fig. 87-88 and Tab. 36). After 180 min, is also a lower temperature reported for both 20 % and 30 % substitution. However, the 10 % substitution has a reduced temperature forming the start, but the temperature development is still in line with the reference temperature development. Finally, the gradual decrease in final sample height is demonstrated in Fig. 90.

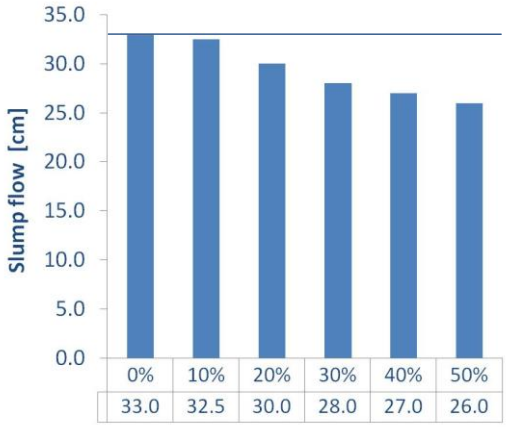

Figure 85: Slump width including all substitutions

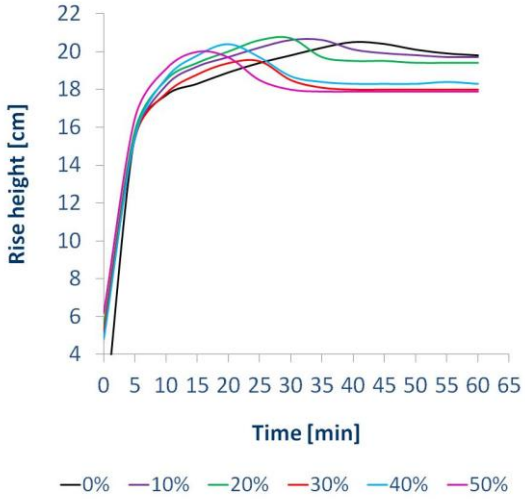

Figure 86: Rise height development including all substitutions

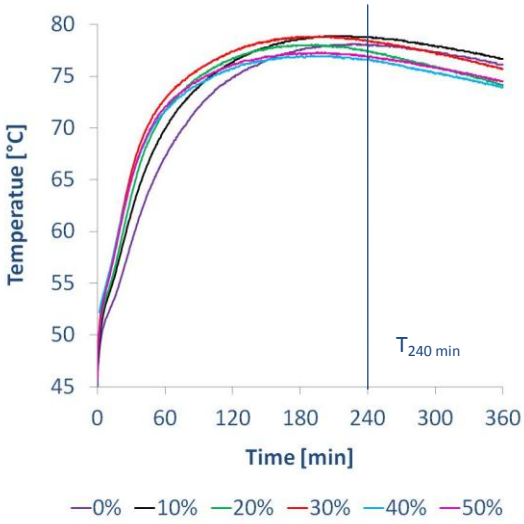

Figure 87: Temperature development including all substitutions

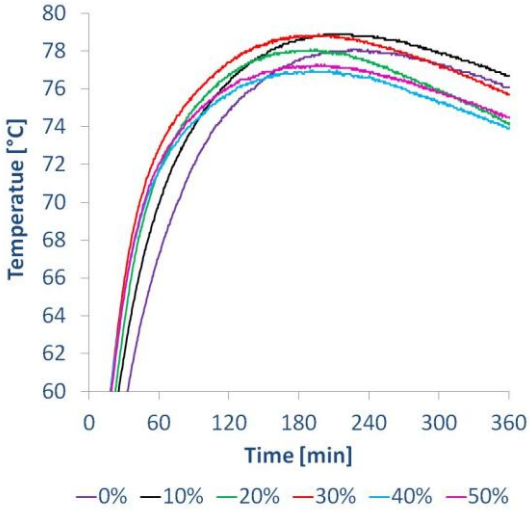

Figure 88: Magnification of temperature development including all substitutions

Table 36: Maximal temperature with occurred point of time

Paper sludge ash substitution	Max. temp. [°C]	Time [min]	$T_{240\ min}$ [°C]
0 %	78.1	223	78.1
10 %	78.9	202	78.8
20 %	78.1	190	77.4
30 %	78.8	173	78.4
40 %	77.0	190	76.6
50 %	77.3	195	76.9

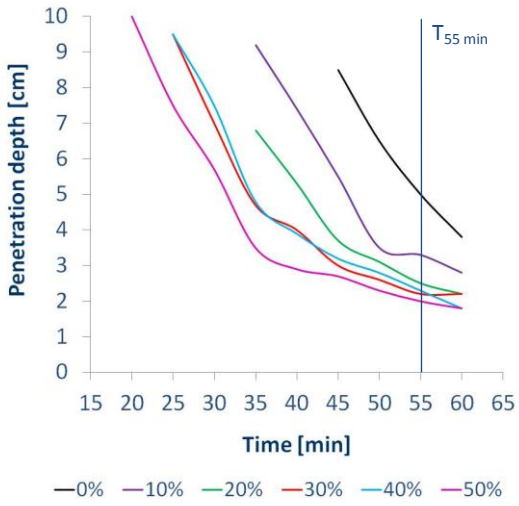

Figure 89: Penetration depth including all substitutions

Table 37: Results penetration depth at $T_{55\ min}$ including all substitutions

Paper sludge ash substitution	Penetration [cm]
0 %	5.0
10 %	3.3
20 %	2.6
30 %	2.4
40 %	2.2
50 %	2.0

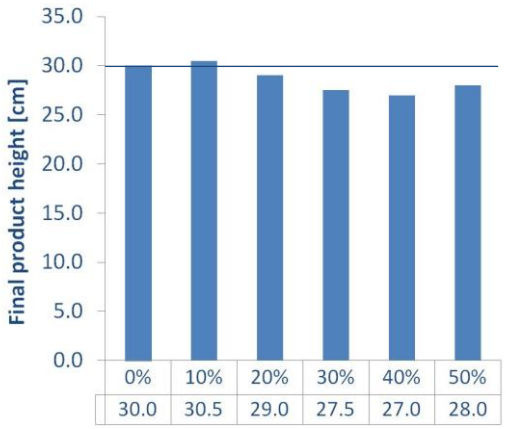

Figure 90: Rising height including all substitutions

Discussion of 40 % and 50 % paper sludge ash substitution

As mentioned previously, a higher substitution of paper sludge ash requires a higher w/s ratio. The w/s ratio for 40 % and 50 % are increased to 0.60 and 0.61. The 40 % and 50 % show a smaller slump width compared to 10-30 % (Fig. 85), but additional water caused a less extreme reduction. Next, in Fig. 86 the rising development increased in height during the first 15 min. Consequently, an earlier sinking and increased sinking effect occurred. Similar rising developments are seen for 30-50 % substitution, after 35 min.

Fig. 87-88 and Tab. 36 illustrated that a reduced maximum temperature for 40 % and 50 % compared to a lower substitutions and the reference. Meanwhile, a similar penetration depth for 30 % and 40 % can be indentified from Fig. 89. A further increased stiffening development is found for 50 %, as a result of increase binder effect. Lastly, the final height of the 50 % substitution is slightly increased compared to the 40 % substitution (Fig. 90).

The difference in maximum temperature is related to the slightly decreased binder content and w/s ratio. In the first 60 min all substitutions show an increased temperature causing a shorter stiffening time and rising time.

Conclusion

Large difference in the stiffening development shows the different reaction rate of paper sludge ash compared to the reference. This is probably caused by the difference in fast reacting components concentration between paper sludge ash substituted and the reference. Due to the way of substitution based on weight and not based on volume.

11.3 PHYSICAL PROPERTIES RESULTS

DISCUSSION OF ALL SUBSTITUTIONS

Similar behaviour is seen in all cases: a higher substitution results in an increased density and increased CS, a reduced lambda are seen in Fig. 91-92 and Fig. 94. Only, the porosity did not change significantly (Fig. 93). The CCS decreased marginally for a higher paper sludge ash substitution (Fig. 94). The 10 % substitution fulfils the ρ 4.5 requirements and 20 % till 50 % meet the ρ 5 requirements. In general, the lambda results are in line with the porosity results (Fig. 93 and Fig. 95). All lambda substitution results are higher compared to the reference. The 30 % substitution sample has a lower porosity resulting in an increased lambda. Further details regarding physical properties measurements can be found in Appendix A.3.2.

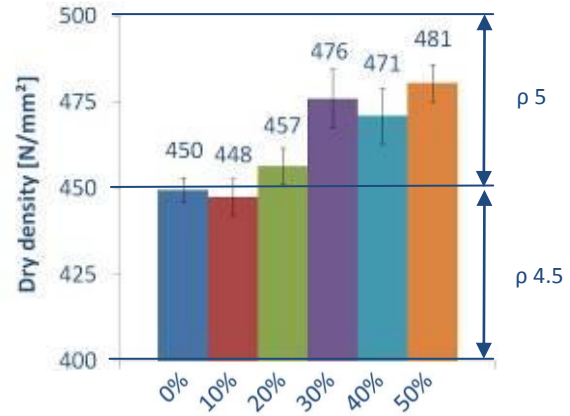

Figure 91: Dry density including all substitutions including

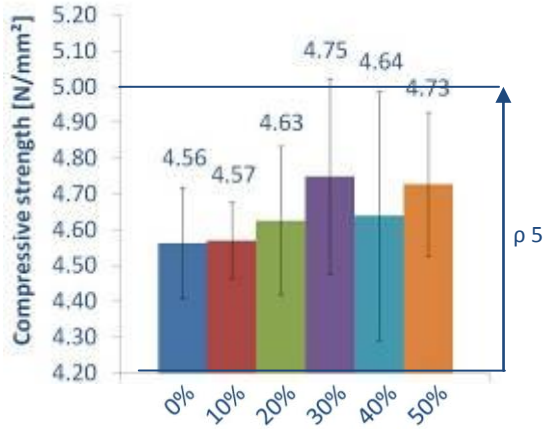

Figure 92: CS including all substitutions

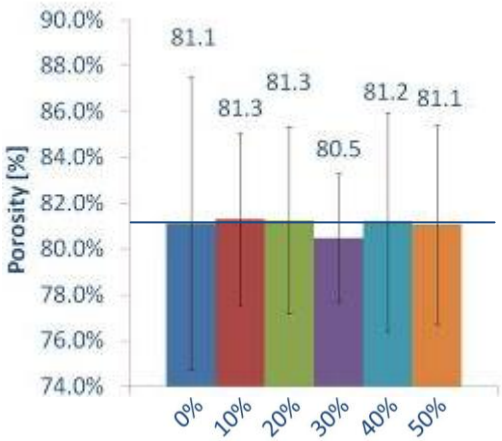

Figure 93: Porosity including all substitutions

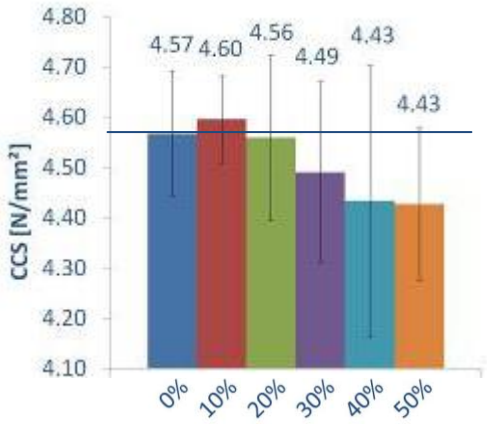

Figure 94: Influence of the paper sludge ash addition, in mass % on the CCS

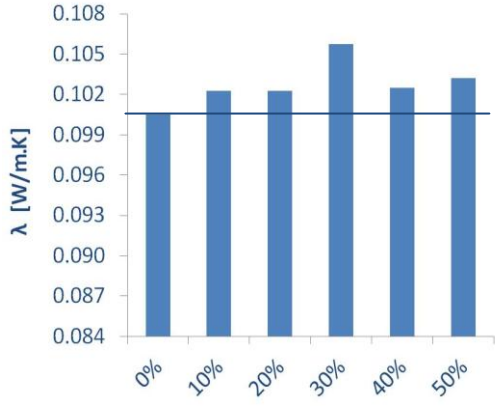

Figure 95: Lambda including all substitutions

COMPARISON

Fig. 96 clearly displays the relation between CS, density, paper sludge ash substitutions (0-30 %). The 40 % and 50 % are excluded since more water was added. Next, Fig. 96 illustrates the porosity as function of 0-30 % substitution levels. It is possible to create an almost constant porosity with a different ratio of paper sludge ash substitutions. It is assumed that the constant porosity is the reason for the high correlation in Fig. 96. Based on the optical inspection of the constant porosity it plausible that more uniform small macropores are present (Fig. 97).

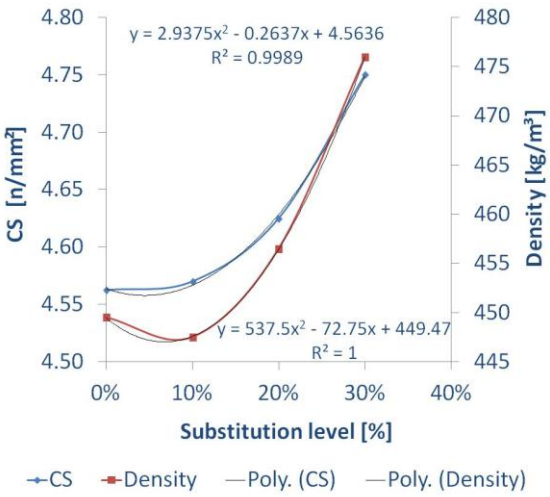

Figure 96: CS and density versus paper sludge ash substitution

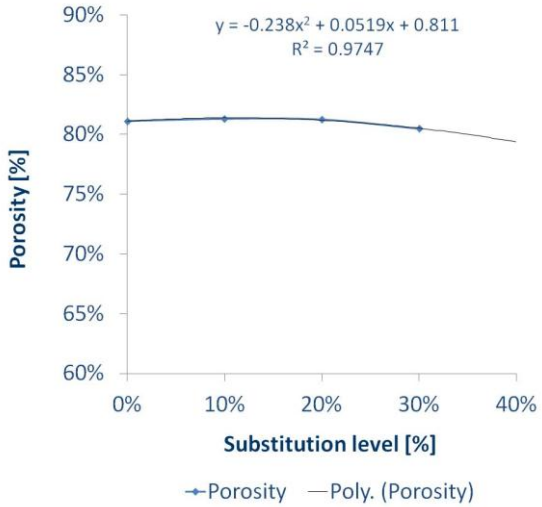

Figure 97: Porosity versus paper sludge ash substitution

CONCLUSION

Based on the results of the physical properties of the paper sludge ash substitution the following conclusions can be drawn:

1. The 10 % and 20 % samples showed similar results for all physical properties compared to the reference.
2. The highest average CS was obtained for the 30 % replacement.
3. It can be concluded that a constant porosity and simultaneously an increase in CS is produced. This is a positive result.
4. The results could be improved by adding more water.
5. The obtained lambda is comparable to the reference.

11.4 MINERAL PHASES ANALYSES

Fig. 98 illustrates the intensity of calcite and lime. As can be seen in Fig. 99 the 20 % and 40 % substitution contain more undissolved quartz compared to the other substitutions. The reason for this behaviour is unknown. The tobermorite level at 3.08 Å is lower for the 20 % and 40 %, compared to the other substitutions (Fig. 101). However, the tobermorite level at 11.30 Å is only significantly reduced for the 20 % substitution (Fig. 100). As can be seen in Fig. 99 and Fig. 101, more quartz dissolved and increased the tobermorite level at 3.08 Å. Furthermore, Fig. 102-103 display the calcite and anhydrite levels for all substitution levels. Both figures do not present a correlation between the mineral phase and the substitution level. As mentioned in chapter 7, possible errors regarding anhydrite and calcite levels could have been introduced resulting in not representative samples and/or dosing deviations. Appendix A.3.3 Mineral phase analysis shows the XRD measurements.

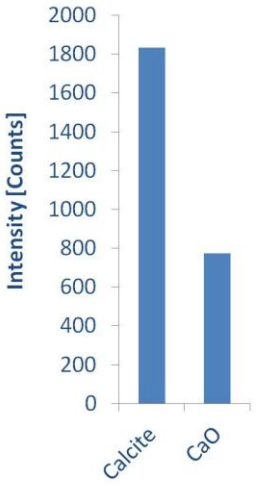

Figure 98: XRD measured calcite and CaO levels of paper sludge ash

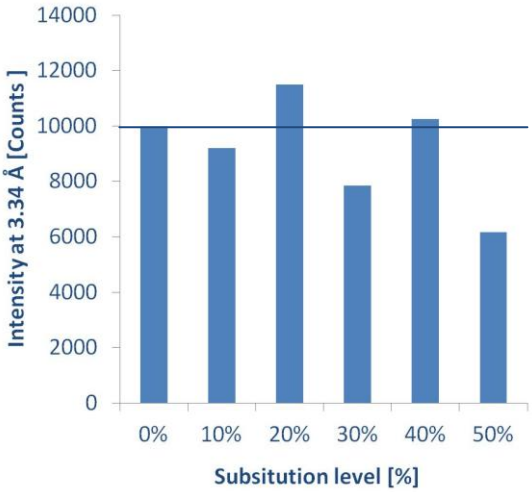

Figure 99: Intensity of quartz for all substitution levels

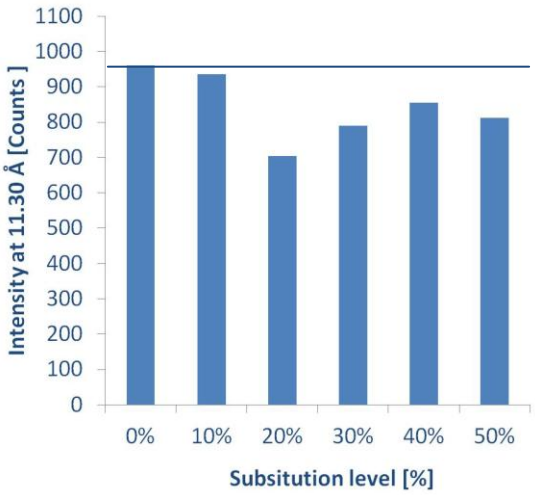

Figure 100: Intensity of tobermorite at 11.30 Å for all substitution levels

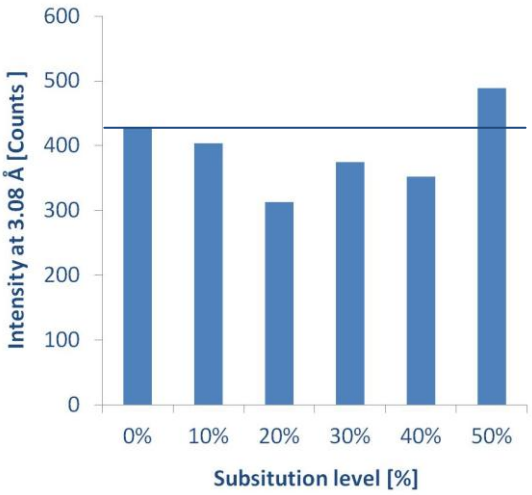

Figure 101: Intensity of tobermorite at 3.08 Å for all substitution levels

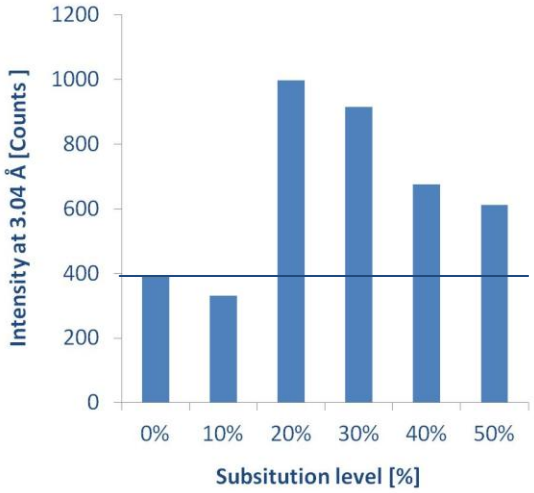

Figure 102: Intensity of calcite at 3.04 Å for all substitution levels

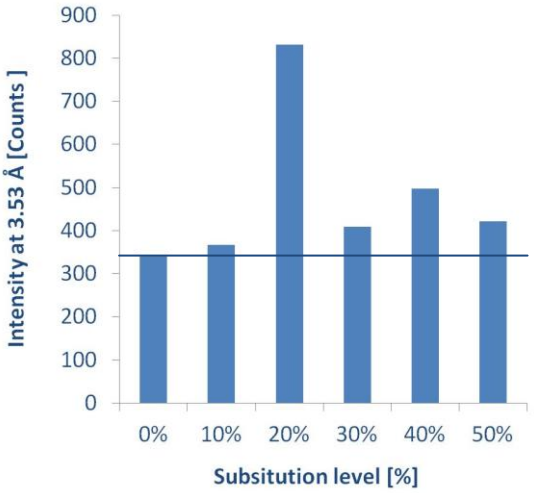

Figure 103: Intensity of anhydrite at 3.53 Å for all substitution levels

CONCLUSION

1. The substitution of cement by paper sludge ash shows no linear relations with the remaining quartz, tobermorite, calcite and anhydrite concentrations.
2. No correlation between CS and the tobermorite quantity and quality.
3. The current procedure is no guarantee for optimal quartz dissolving and production of tobermorite.
4. All substitution ratio's of paper sludge ash to a level of 50 % result in a slightly high CS.

11.5 FIELD EMISSION SCANNING ELECTRON MICROSCOPY

11.5.1 DISCUSSION AND RESULTS

DISCUSSION MACROPORE FORMATION

Fig. 104a-f gives the macropore formation of 0 till 50 % paper sludge ash substitution. The macropore formation of all substitution are more or less comparable to the reference.

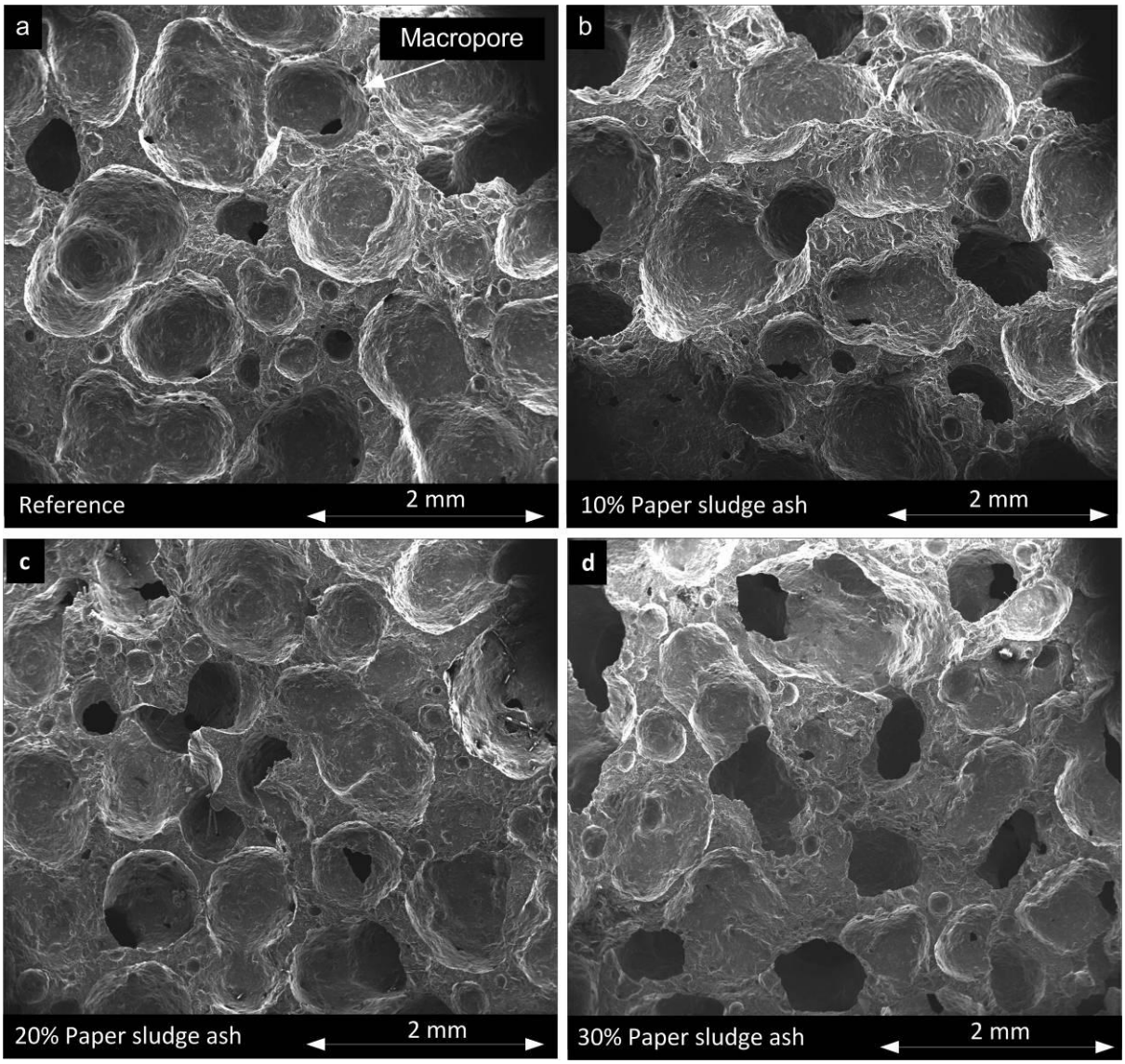

Figure 104: Overview of macropore distribution of all paper sludge ash substitution

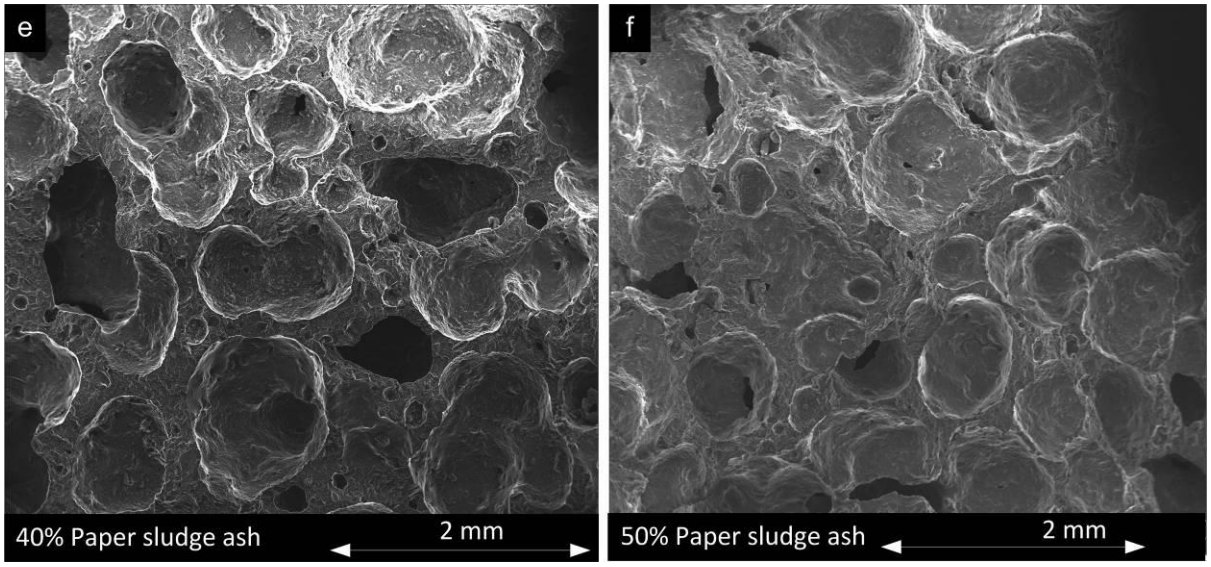

Figure 104: Overview of macropore distribution of all paper sludge ash substitution, cont.

Discussion fractured matrix

Based on, Fig. 105a-f the comparison of the matrix was made for all paper sludge ash substitutions. In all matrixes tobermorite crystals were indentified. A combination of large and small crystals were found in all paper sludge ash samples. Furthermore, Fig. 105a-g shows the presence of C-S-H I gels as white areas which is the initial phase of forming tobermorite. Next, the 30 % paper sludge ash has a denser matrix with homogeneous nucleation on site (see Fig. 105d). Therefore, a slightly higher volume is shared and as a result more nuclei were formed with smaller crystals size.

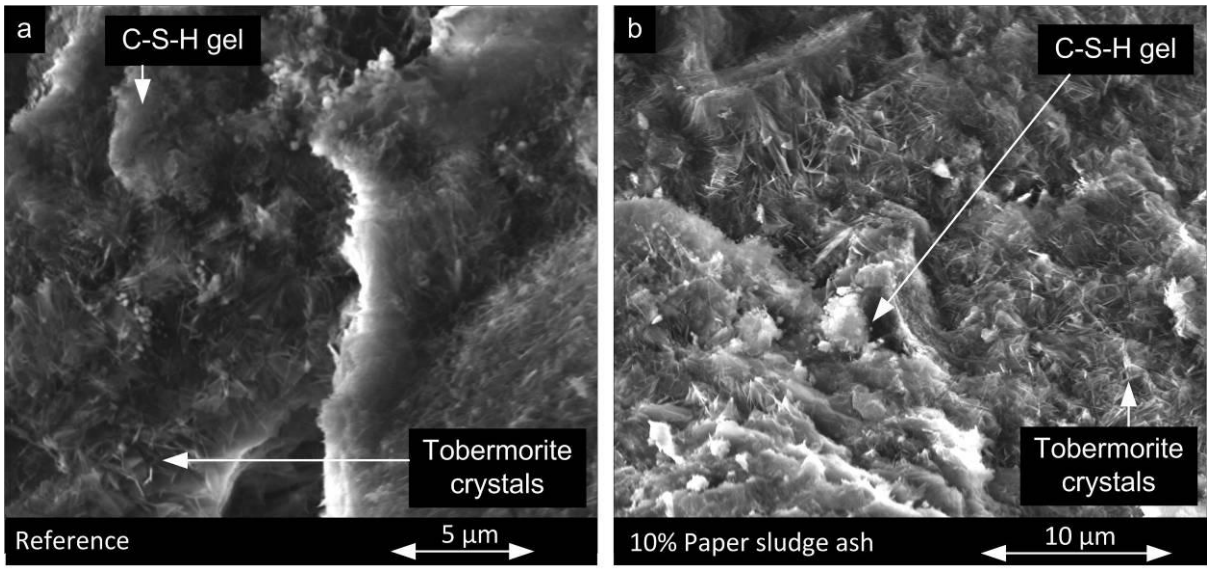

Figure 105: The matrix of all paper sludge ash substitution

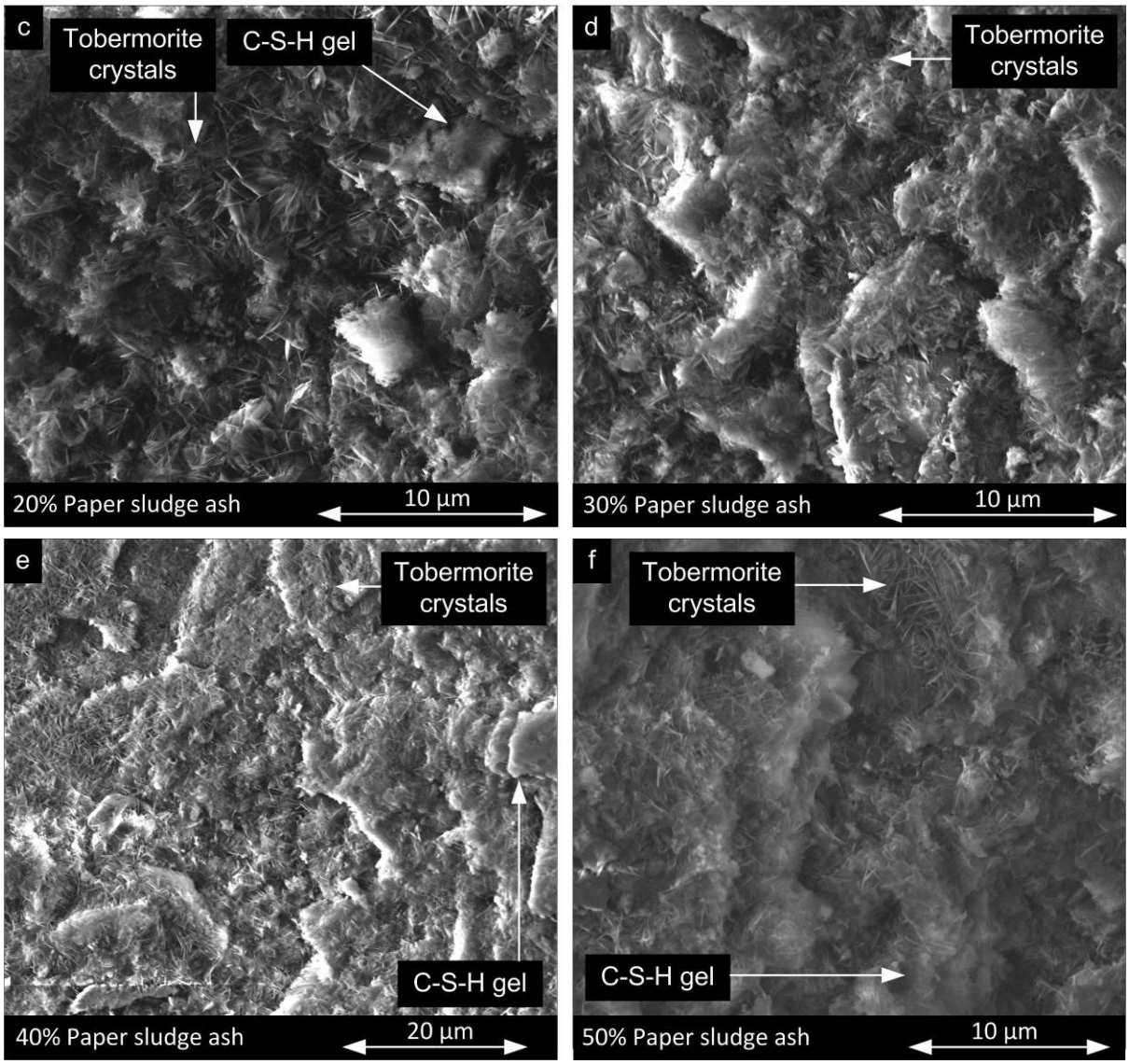

Figure 105: The matrix of all paper sludge ash substitution, cont.

Discussion tobermorite crystals in macropore

Fig. 106a-f summarizes the microstructure inside the marcopore, with the initially formed amorphous C-S-H gel and plate-like tobermorite. Firstly, comparing Fig. 106b-d, it seems that the 10 % and 30 % paper sludge ash samples have more crystalline needle-like crystals compared to 20 % paper sludge ash samples, which contain slightly more grass-like tobermorite. Secondly, larger well defined crystals are visible for the 40 % paper sludge ash sample compared to the reference given in Fig. 106a and Fig. 106e.

In general, the inside of small and large macropores has similar microstructure, based on the observation of multiple pores. Overall, the smaller pores have bigger more well defined crystals due to supposedly presence of a higher water level and/or perhaps a different local temperature and/or pressure (internal environment).

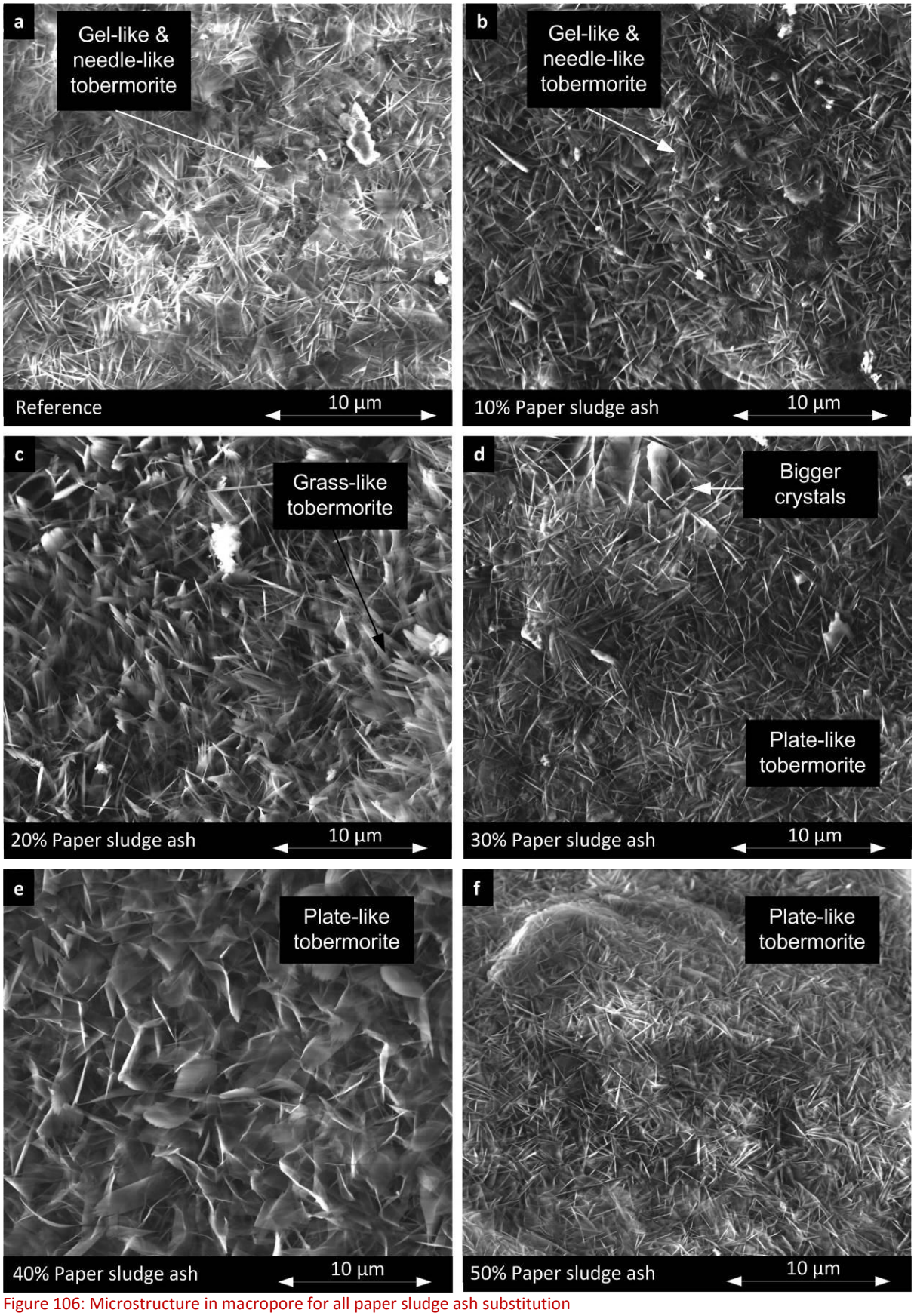

Figure 106: Microstructure in macropore for all paper sludge ash substitution

Discussion tobermorite crystals in detail

Fig. 107 shows the FESEM micrographs of fractured surfaces with tobermorite crystals growing from the matrix towards the inside of the macropores. According to Fig. 107a-c and Fig. 107e it can be observed that slightly smaller crystals at the interface are found for the reference compared to 10, 20 and 40 % paper sludge ash substitution. The 10 % paper sludge ash substitution shows the sample closely resembles the reference (Fig. 107a-b). It is suggested that this is consistent with the dissolving of the slightly lower quartz amount as a result of an almost similar tobermorite level as the reference (supported by XRD).

Furthermore, comparing Fig. 107a, Fig. 107c and Fig. 107e with the reference, large crystals can be seen for the 20 % and 40 % paper sludge ash substitutions. It is assumed that this is due to the lowest amount of dissolved quartz and the lower tobermorite level for these samples. Lastly, larger well defined crystals were spotted for the 40 % substitution compared to the 20 % substitution (Fig. 107c and Fig. 107e). It is suggested that more quartz dissolved for the 40 % substitution compared to the 20 % substitution and as a result a higher tobermorite level was obtained (similar to 30 % and 50 %). This seems to imply that well defined crystals can be related to higher tobermorite level validated by XRD. However, as mentioned in chapter 7, that links between FESEM and XRD can be accidental.

Next, the smallest more dense crystals were obtained for 30 % and 50 % substitution of paper sludge ash (Fig. 107d-f). It is evident that the 30 % and 50 % substitution have significantly more dissolved quartz compared to the reference and other paper sludge ash substitutions. Nevertheless, no higher tobermorite levels were obtained. The evidence points to the likelihood, that a higher substitution a higher w/s ratio is needed since paper sludge ash absorbs fairly more water. It seems that a slightly lower w/s ratio results in crystals structure which is denser and more well defined.

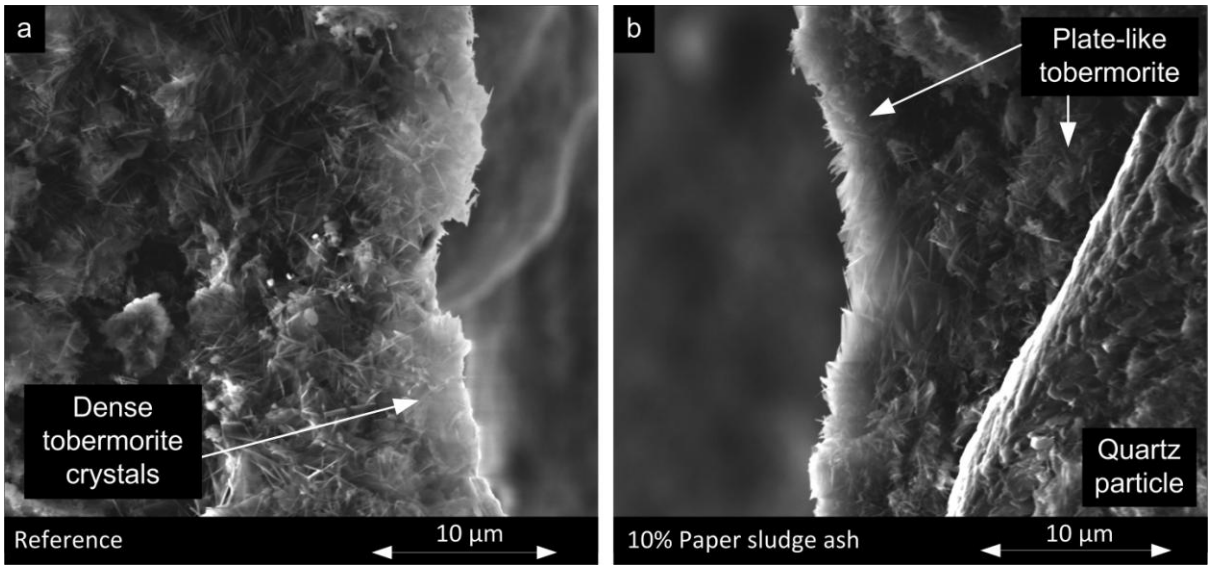

Figure 107: Crystal formations in macropores of all paper sludge ash substitution

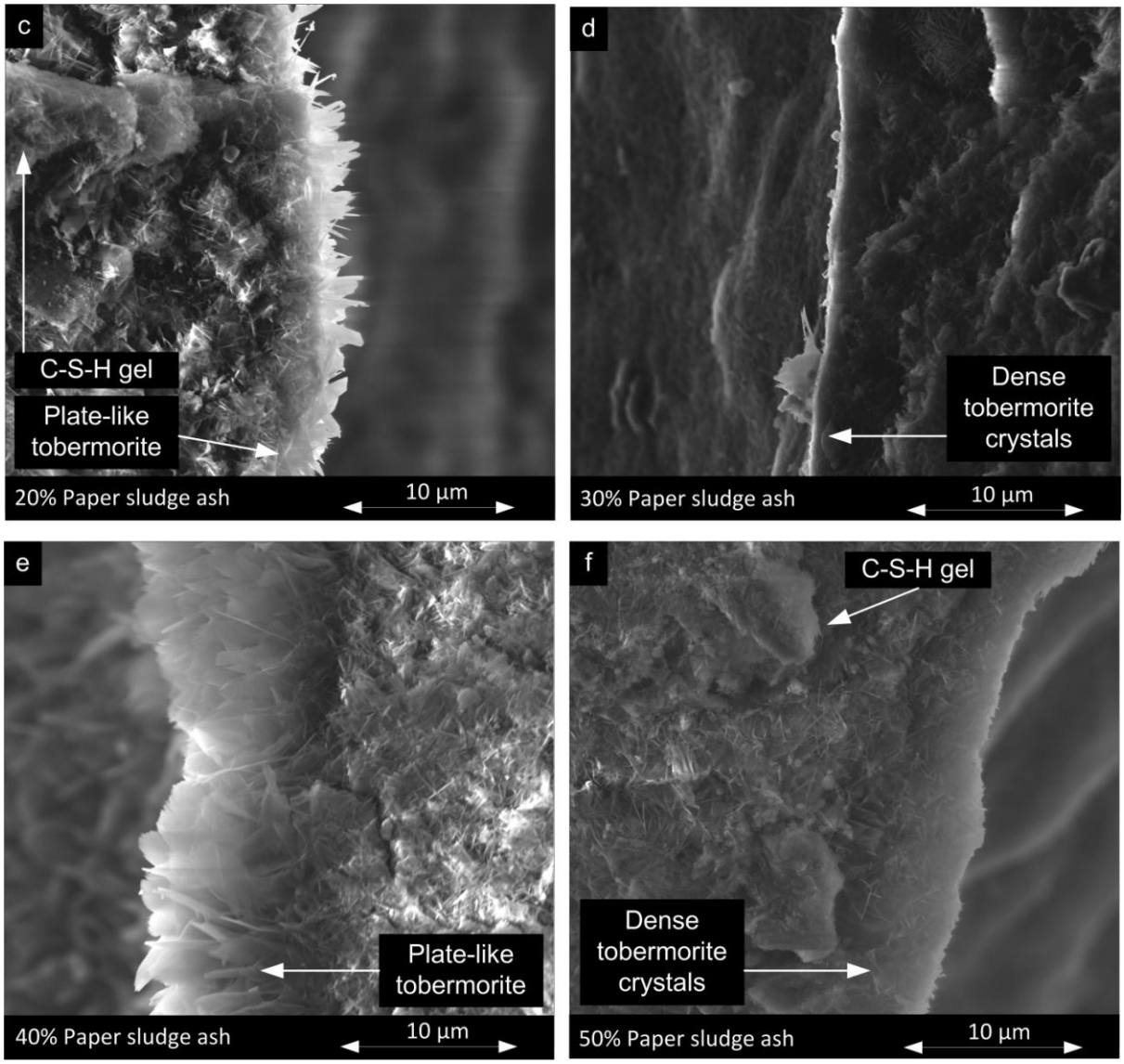

Figure 107: Crystal formations in macropores of all paper sludge ash substitution, cont.

Discussion exceptional findings

In Fig. 108a-c can be seen that the dissolved quartz reacts with calcium-rich particles creating tobermorite crystals in the surface.

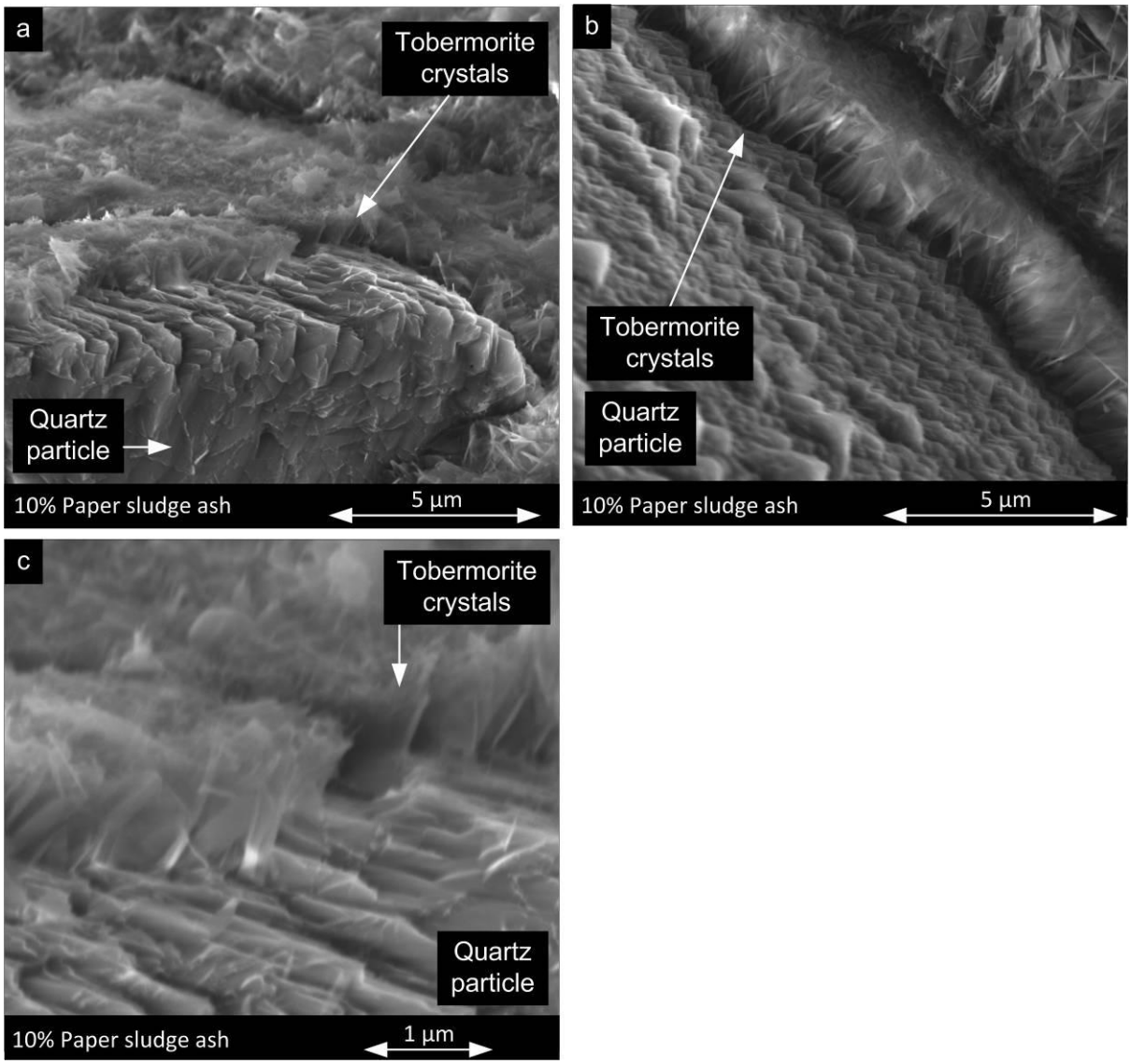

Figure 108: The dissolving of quartz particle producing tobermorite crystals

Discussion dissolving of gypsum

As represented in Fig. 109a, several gypsum clusters reacts to produce products (Fig. 109b). It is clearly visible that, in between the clusters of gypsum ettringite needles are present. As indentified from Fig. 109a it is assumed that this local spot, which is photographed, has a low filling effect.

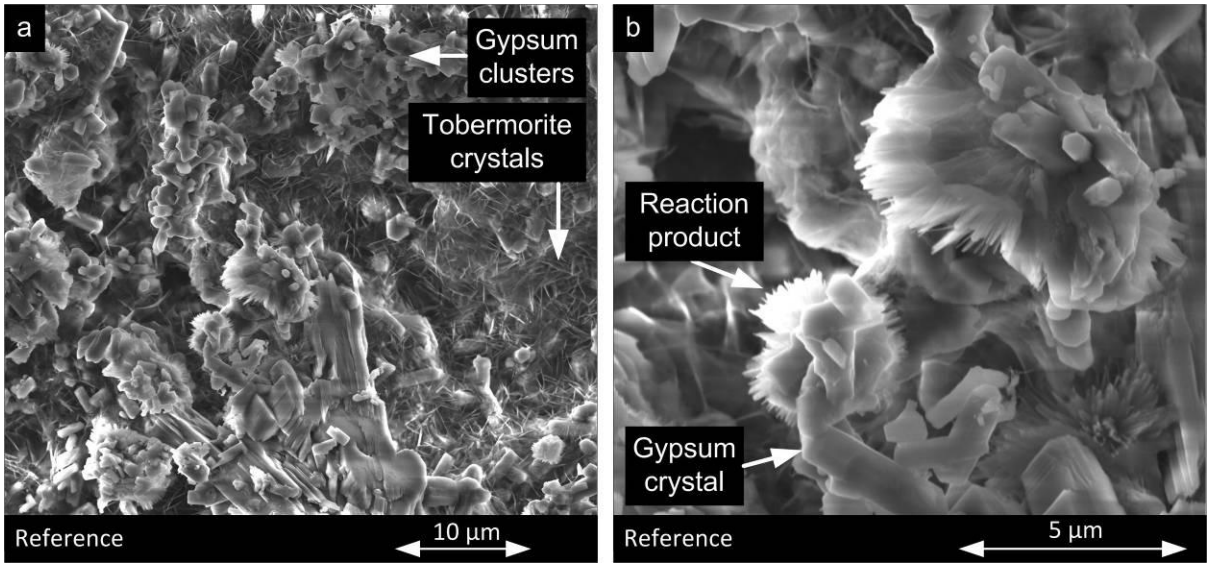

Figure 109: Gypsum clusters in the reference

11.5.2 Conclusion

The overall conclusion of all FESEM pictures is as followed:

1. All paper sludge ash samples show a homogeneous and small size macropore. It is assumed that this is the cause for a high CS.
2. In general, several types of tobermorite formation are found in macropores of 20 %, 30 % and 40 % substitution.

11.6 Color

Figure 110 shows no differences in color for the paper sludge ash substitution samples compared to the reference. Therefore no measurement with the spectrophotometer were performed.

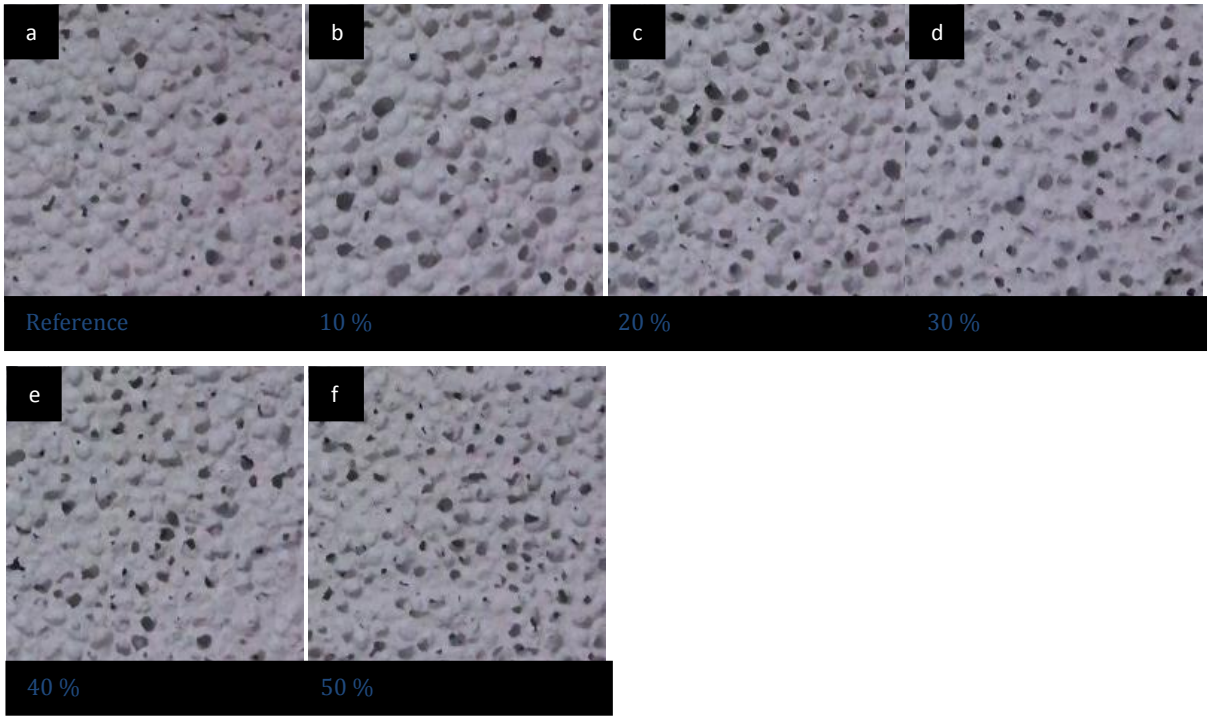

Figure 110: Color indication of paper sludge ash substitution

11.7 Overall conclusion of Portland cement substitution

Based on the present work the following conclusions can be made:

1. To conclude from results, paper sludge ash can replace Portland cement at least till 50 %, based on similar CS with slightly higher density, compared to the reference.
2. The replacement of paper sludge ash reduces the carbon dioxide emission during production of the raw materials of AAC. It is thereby assumed that paper sludge ash is a by-product of paper combustion.
3. Based on, XRD results it can be seen that the tobermorite concentration is not the only factor to define the CS.
4. The high homogeneity seems to be a dominant factor with respect to the CS of the paper sludge ash substitutes.
5. All paper sludge ash substitution levels deliver comparable results to the reference

Sustainable aspect

The substitution of paper sludge ash reduces the carbon dioxide footprint during the production of the Portland cement.

Economical aspect

The substitution of Portland cement by paper sludge ash is lucrative for economical reasons. The reference recipe costs € 33.67 (see Appendix A.3.4 Economic aspect, for more details). The price of paper sludge ash is ± € 20.00 per ton and the price for Portland cement is ± € 80.00 per ton. A 50 % substitution of Portland cement with paper sludge ash could result in, a reduction of € 6.00 for the total recipe price. The total raw materials cost can be reduced with 18 %.

12. RECOMMENDATION FOR FURTHER RESEARCH

Based on the present work four main recommendations can be formulated:

1. The most constant additive regarding composition and PSD and the most economic additive should be chosen.
   - 1a. The variability of the composition and PSD of the different additives should be determine.
   - 1b. The overall economical benefits of the different additives should be examined (including production costs, investment costs etc).

2. Paper sludge ash is the most promising additive for partly replacing Portland cement and quartz. The following action points should be undertaken:
   - 2a. First, the reaction rate of the mixture needs to be optimized, with respect to density and porosity, maintaining the CS at a 50 % replacement.
   - 2b. Secondly, higher substitution levels should be investigated and optimized.
   - 2c. The concentration variation of industrially produced paper sludge ash additions should be examined.
   - 2d. It is advised to develop a new test procedure to monitor and control the critical parameters during the curing period specially for paper sludge ash.
   - 2e. The feasibility of the production of specified AAC density and CS within the variation of the paper sludge ash parameters need to be evaluated.
   - 2f. It is recommended to use paper sludge ash as a substitute at a low concentration in industrial AAC production.
   - 2g. Combining the research information with the industrial operational knowledge of the higher substitution levels could result in a faster application.

3. Cyclone ash has the highest potential to partly substitute quartz.
   - 3a. First, it is advised to optimize the reaction rate of the mixture, with respect to CS, density and porosity, at a 10 % replacement.
   - 3b. Secondly, higher substitution levels should be investigated and optimized.
   - 3c. It is recommended to determine the concentration variation of industrially produced cyclone ash.
   - 3d. Furthermore, It is advised to develop a new specified test procedure to monitor and control the critical parameters during the curing period.
   - 3e. The feasibility of the production of specified - density and CS - AAC within the variation of the cyclone ash parameters need to be evaluated.

4. Finally, it is recommended to investigate the opportunity to use both paper sludge ash and cyclone ash as substitutes for Portland cement and quartz, in order to obtain a higher sustainability and lower costs and thereby achieving maximum substitution of raw materials.

13. WORKS CITED

A

Alexanderson, J. (1979). Relations between structure and mechanical properties of autoclaved aerated concrete. *Cement and Concrete research , 9*, pp. 507-514.
Aroni, S. (1993). *Autoclaved areated concrete: properties, testing and design.* Taylor & Francis.

B

Boesten, E. (2012). *Preliminary study autoclaved aerated concrete*. Graduation report for master degree. Eindhoven: Eindhoven University of Technology.

C

Chan, C., Sakiyama, M., & Mitsuda, T. (1987). Kinetics of the CaO, Quartz - H_2O reaction at 120 °C to 180 °C in suspensions. *Cement and Concrete Research , 8*, pp. 1-6.
Crennan, J., El-Hemaly, S., & Taylor, H. (1977). Autoclaved lime-quartz materials I. some factors influencing strength. *Cement and concrete research , 7*, 493-502.

H

Hauser, A., Eggenberger, U., & Mumenthaler, T. (1999, November 2). Fly ash from cellulose industry as secondary raw material in autoclaved aerated concrete. *Cement and Concrete Research , 29*, pp. 297-302.
HCV. (2011). *http://www.hvcenergie.nl/duurzaam/biomassa*.
Heinz, L. (2012, January). composition of the reference recipe and substitution level of additives. (E. Boesten, Interviewer)
Holt, E., & Raivio, P. (2005, May 3). Use of gasification residues in aerated autoclaved concrete. *Cement and Concrete Research , 35*, pp. 796-802.
Huang, X., Ni, W., Cui, W., Wang, Z., & Zhu, L. (2011). Preparation of autoclaved aerated concrete using copper tailings and blast furnace slag. *Construction and Building Materials, 27*, pp. 1-5.

I

Isu, N., Ishida, H., & Mitsuda, T. (1995). Influence of quartz particle size on the chemical and mechanical properties of autoclaved aerated concrete tobermorite formation. *Cement and Concrete Research , 25* (2), pp. 243-248.

J

Jing, Z., Jin, F., Hashida, T., Yamasaki, N., & Ishida, H. (2008, January 8). Influence of additions of coal fly ash and quartz on hydrothermal solodofocation of blast furnace slag. *Cement and Concrete Research , 38*, pp. 976-982.

K

Klimesch, D., & Ray, A. (1998). Hydrogarnet formation during autoclaving at 180 C in unstirred metakaoline-lime-quartz slurries. *Cement and Concrete Research , 28* (8), pp. 1109-1117.
Kondo, R. (1967). Autoclaved Calcium Silicate Building Products. *Society of Chemical Industry , 92*.
Kurama, H., Topcu, I., & Karakurt, C. (2009, February 24). Properties of the autoclaved aerated concrete produced from coal bottom ash. *Journal of materials procesing technology , 209*, pp. 767-773.

M

Mitsuda, T., Sasaki, K., & Ishida, H. (1992, July 7). Phase evolution during autoclaving process of aerated concrete. *Journal of the American Ceramic Society , 75* (7), pp. 1858-1863.
Mostafa, N. (2005). Influence of air-cooled slag on physicochemical properties of autoclaved aerated concrete. *Cement and Concrete Research, 35*, pp. 1349-1357.

O

Okada, Y., Shimoda, M., Mitsuda, T., & Toraya, H. (1990). Synthesis of tobermorite: NMR spectroscopy and analytical electron microscopy. *Onoda Company Report , 42,* pp. 123-131.

R

Report Institute. (2012). *Assessment of Potential Phosphate Ion-Concrete Interactions.*

S

Siddique, R. (2003). Effect of fine aggregate replacement with class F fly ash on the mechanical properties of concrete. *Cement and Concrete Research , 33* (4), pp. 539-547.

T

Thomas, J., & Jennings, H. (2008). iti.northwestern.edu.
The Countertop Institute. (2012). *http://www.concretecountertopinstitute.com/*

V

Vliegasunie. (2011) *http://www.vliegasunie.nl/*

W

Wijs, J. (2008). *Report: Aanvullend onderzoek SVI-vliegas.* Sittard: Intron.

14. APPENDIX

A.1 CHARACTERIZATION OF ADDITIVES

A.1.1 MINERAL PHASES ANALYZES

Table 38: Mineral phases detected with XRD

	Additives	Phases	
1.	Cyclone ash	Potassium Carbonate	K_2CO_3
		Potassium Magnesium Phosphate	$KMgPO_4$
		Potassium Sodium Aluminum Hydride	K_2NaAlH_6
		Calcium Sulfate	$CaSO_4$
		Carbon	C
		Titanium	Ti
		Titanium Hydride	TiH
		Calcium Oxide	CaO
		Silicon Oxide	SiO_2
		Iron Oxide Hydrate	$Fe_2O_3 \cdot H_2O$
		Iron Oxide	Fe_2O_3
		Aluminum Iron Oxide	$Al_2Fe_2O_6$
		Iron Silicate	Fe_2SiO_4
		Iron Titanium Hydride	H_2FeTi
		Aluminum Magnesium	AlMg
		Sodium Aluminum Hydride	Na_3AlHx
		Aluminum Silicon	$Al_{3.2}Si_{0.47}$
		Calcium Aluminum Oxide	$Ca_3Al_2O_6$
		Sodium Calcium Hydrogen Silicate	$NaCaHSiO_4$
		Calcium Phosphate Silicate	$Ca_{15}(PO_4)_2(Si)$
		Sodium Aluminum Silicate	$Na_{1.16}Al_2Si_{77.4}O_{158.3}$
		Calcium Aluminum Carbonate Silicate	$Ca_4Al_6Si_6O$
2.	Paper sludge ash	Quartz alpha	SiO_2
		Calcite, syn	$CaCO_3$
		Lime, syn	CaO
		Portlandite, syn	$Ca(OH)_2$
		Silicon, syn	Si
		Calcium Aluminum Oxide	$Ca_3Al_2O_6$
		Calcium Aluminum Carbonate Hydroxide Hydrate	$Ca_6Al_2(CO_3)_3(OH)_{12} \cdot 26H_2O$
		alpha-Cholestane	$C_{27}H_{48}$
		Ravatite	$C_{14}H_{10}$
		Magnesium Aluminum Oxide	$MgAl_2O_4$
		Enstatite, syn	$MgSiO_3$
4.	Bio ash	Quartz, syn	SiO_2
		Anhydrite, syn	$CaSO_4$
		Lime, syn	CaO
		Calcium Iron Phosphate	$Ca_9Fe(PO_4)_7$
		Hematite, syn	Fe_2O_3
		Aluminum Phosphate	$AlPO_4$
		Maghemite-C, syn	Fe_2O_3
		Rodolicoite, syn	$FePO_4$
		Silicon Phosphate Oxide	$SiP_2O_7/SiO_2 \cdot P_2O_5$
		Graftonite, syn	$Fe_3(PO_4)_2$

3.	Bottom ash	Quartz low alpha	SiO_2
		Anhydrite	$Ca(SO_4)$
		Gehlenite, syn	$Ca_2Al_2SiO_7$
		Magnesium Sulfate Hydroxide	$Mg_3S_2O_8(OH)_2$ / $_2MgSO_4{\cdot}Mg(OH)_2$
		Gismondine	$CaAl_2Si_2O_8 \cdot 4H_2O$
		Calcium Aluminum Oxide	$Ca(AlO_2)_2$
		Calcium Magnesium Aluminum Silicate	Ca - Mg - Al - Si - O
		Calcium Oxide	CaO
		Fayalite	Fe_2SiO_4
5.	Dutch fly ash	Quartz alpha	SiO_2
		Hematite, syn	Fe_2O_3
		Mullite, syn	$Al_5 Si_1 O_{10}$
		Spinel	$(Mg_{0.4} Al_{0.6})Al_{1.8} O_4)$
6.	Indian fly ash	Quartz alpha	SiO_2
		Lime	CaO
		Mullite, syn	$Al_{4.7} 5Si_{1.25} O_{9.63}$
		Hematite, syn-alpha	Fe_2O_3
		Magnetite	$Fe_{2.9} O_4$
		Potassium Aluminum Hydride	$K_3 Al H_6$

A.1.2 Density of Additives

Table 39: Density of additives

		Cyclone ash	Paper sludge ash 1	Bio ash	Bottom ash
Empty cup	[g]	2.1687	2.1687	2.1687	2.1685
Filled cup	[g]	8.9356	5.2933	8.4352	10.5184
Content	[g]	6.7669	3.1246	6.2665	8.3499
Volume 1	[cm³]	1.9580	1.1401	2.1857	3.1205
Volume 2	[cm³]	1.9600	1.1401	2.1826	3.1203
Volume 3	[cm³]	1.9620	1.1416	2.1853	3.1231
Volume 4	[cm³]	1.9585	1.1398	2.1854	3.1220
Volume 5	[cm³]	1.9635	1.1407	2.1865	3.1221
Volume 6	[cm³]	1.9620	1.1420	2.1852	3.1252
Volume 7	[cm³]	1.9620	1.1399	2.1839	3.1223
Volume 8	[cm³]	1.9613	1.1416	2.1856	3.1253
Volume 9	[cm³]	1.9613	1.1400	2.1863	3.1218
Volume 10	[cm³]	1.9620	1.1405	2.1846	3.1241
Average	[cm³]	1.9611	1.1406	2.1851	3.1227
SDV	[%]	0.17	0.08	0.12	0.17
Dry density (m/V)	[g/cm³]	3.4506	2.7394	2.8678	2.6740
Dry density (m/V)	[kg/m³]	3451	2739	2868	2674

Table 40: Density of additives, cont.

		Dutch fly ash	Indian fly ash	Paper sludge ash 2
Empty cup	[g]	2.168	2.1678	2.1687
Filled cup	[g]	9.9255	10.9834	5.2982
Content	[g]	7.7575	8.8156	3.1295
			3.9749	
Volume 1	[cm³]	3.3739	3.9773	1.1212
Volume 2	[cm³]	3.3761	3.9757	1.1238
Volume 3	[cm³]	3.3736	3.9768	1.1212
Volume 4	[cm³]	3.3735	3.9759	1.1232
Volume 5	[cm³]	3.3745	3.9751	1.1212
Volume 6	[cm³]	3.3756	3.9769	1.1236
Volume 7	[cm³]	3.3750	3.9767	1.1219
Volume 8	[cm³]	3.3779	3.9767	1.1230
Volume 9	[cm³]	3.3744	3.9750	1.1228
Volume 10	[cm³]	3.3754	3.9742	1.1225
Average	[cm³]	3.3750	3.9760	1.1224
SDV	[%]	0.13	0.10	0.10
Dry density (m/V)	[g/cm³]	2.2985	2.2172	2.7881
Dry density (m/V)	[kg/m³]	2299	2217	2788

A.2 QUARTZ SUBSTITUTION RESULTS

A.2.1 MEASUREMENTS DURING CURING PERIOD

A.2.1.1 RISING HEIGHT, TEMPERATURE OF HYDRATION AND PENETRATION DEPTH

Table 41: Rising height, temperature of hydration and penetration depth of all additive substitutions

	Additives	Slump flow	Final product height	w/s ratio	Aluminum amount
		[cm]	[cm]	[-]	[g]
0 %	Reference	34.0	28.5	0.58	14
5%	Cyclone ash	34.0	32.5	0.58	15
10 %	Cyclone ash	36.0	27.0	0.58	14
5%	Paper sludge ash	30.0	27.5	0.58	14
10 %	Paper sludge ash	28.0	27.5	0.58	14
15 %	Paper sludge ash	22.0	26.5	0.59	14
5%	Bio ash	34.0	29.0	0.58	14
10 %	Bio ash	34.0	27.5	0.54	15
5%	Bottom ash	34.0	29.5	0.58	14
10 %	Bottom ash	32.0	28.5	0.55	15
15 %	Bottom ash	29.5	29.5	0.53	16
5%	Dutch fly ash	34.6	29.0	0.58	14
10 %	Dutch fly ash	35.0	28.5	0.58	14
5%	Indian fly ash	34.0	29.5	0.58	14
10 %	Indian fly ash	30.0	29.5	0.55	15
15 %	Indian fly ash	29.0	30.0	0.52	16

Table 42: Rising height, temperature of hydration and penetration depth of reference

Reference

Time	Rising height	Temperature	Penetration depth
[min]	[cm]	[°C]	[cm]
0	6.2	42.0	
5	16.5	49.0	
10	17.2	49.8	
15	17.7	50.7	
20	17.8	51.9	
25	18.2	53.3	
30	18.5	54.3	
35	18.8	56.4	>>10
40	18.9	57.9	8.3
45	18.9	59.3	6.3
50	18.9	60.6	5.0
55	18.9	62.0	4.0
60	18.8	63.0	3.2

Table 43: Rising height, temperature of hydration and penetration depth of 5 % cyclone ash

5 % Cyclone ash

Time	Rising height	Temperature	Penetration depth
[min]	[cm]	[°C]	[cm]
0	5.5	41.2	
5	16.8	48.8	
10	19.0	50.0	
15	19.9	51.0	
20	20.5	52.1	
25	21.2	53.3	
30	21.2	54.9	
35	21.4	56.4	>>10
40	-	58.2	>>10
45	-	59.7	10
50	-	61.5	7.5
55	-	62.5	5.8
60	-	64.9	4.8

Table 44: Rising height, temperature of hydration and penetration depth of 10 % cyclone ash

10 % Cyclone ash

Time	Rising height	Temperature	Penetration depth
[min]	[cm]	[°C]	[cm]
0	4.0	44.8	
5	11.1	50.0	
10	13.0	51.2	
15	13.8	52.2	
20	14.7	53.1	
25	15.6	54.3	
30	16.6	55.8	
35	17.5	57.4	
40	18.5	59.0	
45	19.4	60.5	>> 10
50	18.3	62.0	-
55	16.7	63.4	8.5
60	16.3	64.7	7.0

Table 45: Rising height, temperature of hydration and penetration depth of 5 % paper sludge ash

5 % Paper sludge ash

Time	Rising height	Temperature	Penetration depth
[min]	[cm]	[°C]	[cm]
0	5.8	45.3	
5	15.6	50.0	
10	17.1	51.4	
15	17.9	52.8	
20	18.4	54.5	
25	18.8	56.4	
30	19.0	58.6	-
35	18.5	60.7	6.7
40	18.1	62.5	5.6
45	18.0	64.0	3.3
50	18.0	65.5	3.0
55	18.0	66.7	2.2
60	18.0	68.0	1.9

Table 46: Rising height, temperature of hydration and penetration depth of 10 % paper sludge ash

10 % Paper sludge ash

Time	Rising height	Temperature	Penetration depth
[min]	[cm]	[°C]	[cm]
0	4.5	45.5	
5	16.2	50.3	
10	18.1	52.0	
15	18.6	53.3	
20	19.0	55.4	
25	18.8	57.7	-
30	18.5	60.2	6.0
35	18.3	62.5	3.9
40	18.3	54.6	3.0
45	18.3	66.5	2.5
50	18.3	68.1	2.0
55	18.3	69.4	1.7
60	18.4	70.8	1.5

Table 47: Rising height, temperature of hydration and penetration depth of 15 % paper sludge ash

15 % Paper sludge ash

Time	Rising height	Temperature	Penetration depth
[min]	[cm]	[°C]	[cm]
0	6.7	43.9	
5	16.7	49.7	
10	18.6	51.6	
15	18.6	53.4	
20	18.0	55.6	
25	17.5	58.3	4.8
30	17.4	60.5	3.4
35	17.4	63.0	2.6
40	17.4	64.9	2.0
45	17.4	66.4	1.6
50	17.4	68.3	1.6
55	17.4	69.5	1.0
60	17.4	70.6	0.0

Table 48: Rising height, temperature of hydration and penetration depth of 5 % bio ash

5 % Bio ash

Time	Rising height	Temperature	Penetration depth
[min]	[cm]	[°C]	[cm]
0	6.7	45.4	
5	16.6	49.7	
10	18.2	51.0	
15	19.1	53.1	
20	19.5	55.7	
25	19.7	56.5	
30	19.9	57.2	-
35	20.2	59.1	8.8
40	20.2	60.8	7.0
45	19.9	62.3	6.0
50	19.8	63.8	4.3
55	-	-	-
60	-	-	-

Table 49: Rising height, temperature of hydration and penetration depth of 10 % bio ash

10 % Bio ash

Time	Rising height	Temperature	Penetration depth
[min]	[cm]	[°C]	[cm]
0	3.5	40.0	
5	13.5	44.2	
10	16.7	45.6	
15	17.6	46.2	
20	17.9	46.6	
25	18.1	46.9	
30	18.2	47.3	
35	18.2	47.6	
40	18.3	47.9	
45	18.4	48.3	>>10
50	18.4	48.7	-
55	18.4	48.9	8.8
60	18.4	49.3	8.5

Table 50: Rising height, temperature of hydration and penetration depth of 5 % bottom ash

5 % Bottom ash

Time	Rising height	Temperature	Penetration depth
[min]	[cm]	[°C]	[cm]
0	5.5	43.6	
5	15.8	50.0	
10	18.6	51.1	
15	18.8	52.8	
20	19.4	54.6	
25	19.8	56.9	
30	20.3	58.4	
35	20.7	60.1	
40	20.8	61.8	-
45	20.5	63.3	6.3
50	20.3	64.6	4.8
55	20.2	65.9	3.7
60	20.1	67.0	3.0

Table 51: Rising height, temperature of hydration and penetration depth of 10 % bottom ash

10 % Bottom ash

Time	Rising height	Temperature	Penetration depth
[min]	[cm]	[°C]	[cm]
0	4.2	42.9	
5	15.5	47.7	
10	18.5	49.7	
15	19.4	50.8	
20	19.8	52.0	
25	20.2	53.8	
30	20.6	55.5	-
35	20.7	57.0	8.3
40	20.2	58.8	6.5
45	20.1	60.6	5.4
50	19.9	62.0	4.0
55	19.9	63.2	3.4
60	19.9	64.5	3.0

Table 52: Rising height, temperature of hydration and penetration depth of 15 % bottom ash

15 % Bottom ash

Time	Rising height	Temperature	Penetration depth
[min]	[cm]	[°C]	[cm]
0	4.5	43.5	
5	16.2	49.5	
10	19.7	51.5	
15	20.9	52.9	
20	20.1	54.7	
25	20.9	56.8	
30	20.1	59.0	
35	19.6	61.1	5.1
40	19.5	63.0	4.1
45	19.5	64.7	3.0
50	19.5	66.0	2.9
55	19.5	67.2	2.2
60	19.5	68.4	2.0

Table 53: Rising height, temperature of hydration and penetration depth of 5 % Dutch fly ash

5 % Dutch fly ash

Time	Rising height	Temperature	Penetration depth
[min]	[cm]	[°C]	[cm]
0	5.4	44.5	
5	15.3	49.1	
10	17.1	50.3	
15	17.6	51.3	
20	17.8	52.4	
25	18.2	54.3	
30	18.6	55.6	
35	19.9	57.2	>>10
40	19.1	58.9	-
45	19.3	60.4	7.9
50	19.2	61.9	6.2
55	19.1	63.2	4.6
60	19.1	64.4	3.7

Table 54: Rising height, temperature of hydration and penetration depth of 10 % Dutch fly ash

10 % Dutch fly ash

Time	Rising height	Temperature	Penetration depth
[min]	[cm]	[°C]	[cm]
0	4.5	43.6	
5	15.8	49.0	
10	17.7	50.5	
15	17.9	51.6	
20	18.2	53.0	
25	18.6	54.7	
30	18.9	56.6	>>10
35	19.3	58.5	9.5
40	19.6	60.2	7.8
45	19.4	61.8	6.5
50	19.3	63.3	5.5
55	19.3	64.7	4.4
60	19.3	65.5	3.2

Table 55: Rising height, temperature of hydration and penetration depth of 5 % Indian fly ash

5 % Indian fly ash

Time	Rising height	Temperature	Penetration depth
[min]	[cm]	[°C]	[cm]
0	4.9	45.5	
5	16.5	50.8	
10	18.4	52.6	
15	19.0	53.9	
20	19.4	55.6	
25	19.9	57.7	
30	20.3	59.6	
35	20.5	61.2	9.0
40	20.4	62.9	7.3
45	20.1	64.4	5.5
50	20.1	65.6	4.2
55	19.9	66.8	3.7
60	19.9	67.6	3.0

Table 56: Rising height, temperature of hydration and penetration depth of 10 % Indian fly ash

10 % Indian fly ash

Time	Rising height	Temperature	Penetration depth
[min]	[cm]	[°C]	[cm]
0	5.0	46.7	
5	16.8	51.9	
10	19.0	53.7	
15	19.8	55.4	
20	20.5	57.8	
25	20.9	59.9	10.0
30	20.7	62.1	8.5
35	20.1	64.0	6.0
40	19.8	65.5	5.0
45	19.8	67.2	3.3
50	19.7	68.0	3.0
55	19.8	69.0	2.5
60	19.8	69.9	2.0

Table 57: Rising height, temperature of hydration and penetration depth of 15 % Indian fly ash

15 % Indian fly ash

Time	Rising height	Temperature	Penetration depth
[min]	[cm]	[°C]	[cm]
0	5.1	43.1	
5	18.3	49.4	
10	20.2	51.2	
15	20.8	52.5	
20	21.1	54.0	
25	21.3	56.9	
30	21.1	57.8	
35	20.8	59.7	6.5
40	20.6	61.5	4.8
45	20.5	63.0	3.7
50	20.5	64.4	3.2
55	20.5	65.6	2.7
60	20.5	66.7	2.2

A.2.2 Physical properties measurements

A.2.2.1 Dry density

Table 58: Dry density measurements of all additive substitutions

Dry density

	Additives	Sample 1	Sample 2	Sample 3	Sample 4	Average	STD
		[kg/m³]	[kg/m³]	[kg/m³]	[kg/m³]	[kg/m³]	[%]
0 %	Reference	458	462	454	460	458.5	3.42
5 %	Cyclone ash	400	408	398	402	402.0	4.32
10 %	Cyclone ash	394	376	390	374	383.5	9.98
5 %	Paper sludge ash	472	482	470	482	476.5	6.40
10 %	Paper sludge ash	470	478	468	476	473.0	4.76
15 %	Paper sludge ash	490	500	492	504	496.5	6.61
5 %	Bio ash	454	460	454	458	456.5	3.00
10 %	Bio ash	438	442	436	442	439.5	3.00
5 %	Bottom ash	450	456	450	456	453.0	3.46
10 %	Bottom ash	446	454	442	454	449.0	6.00
15 %	Bottom ash	442	454	440	454	447.5	7.55
5 %	Dutch fly ash	454	458	452	458	455.5	3.00
10 %	Dutch fly ash	459	460	454	462	458.8	3.40
5 %	Indian fly ash	452	454	448	454	452.0	2.83
10 %	Indian fly ash	448	456	448	456	452.0	4.62
15 %	Indian fly ash	436	444	436	440	439.0	3.83

A.2.2.2 Compressive strength (CS) and compensated compressive strength (CCS)

Table 59: CS and CCS measurements of all additive substitutions

		CS						CCS
	Additives	Sample 1	Sample 2	Sample 3	Sample 4	Average	STD	
		[N/mm²]	[N/mm²]	[N/mm²]	[N/mm²]	[N/mm²]	[-]	[N/mm²]
0 %	Reference	4.47	4.86	4.94	5.04	4.83	0.25	4.47
5 %	Cyclone ash	3.65	3.91	3.69	3.71	3.74	0.12	3.65
10 %	Cyclone ash	3.1	3.08	2.91	2.84	2.98	0.13	3.1
5 %	Paper sludge ash	4.87	5.21	5.16	5.41	5.16	0.22	4.87
10 %	Paper sludge ash	4.75	5.3	4.43	5.23	4.93	0.41	4.75
15 %	Paper sludge ash	4.97	5.2	4.93	5.25	5.09	0.16	4.97
5 %	Bio ash	4.7	4.77	4.26	4.49	4.56	0.23	4.7
10 %	Bio ash	3.08	3.17	2.92	3.08	3.06	0.10	3.08
5 %	Bottom ash	4.33	4.61	4.45	4.56	4.49	0.12	4.33
10 %	Bottom ash	4.23	4.48	4.18	4.56	4.36	0.19	4.23
15 %	Bottom ash	4.04	4.17	4.15	4.41	4.19	0.16	4.04
5 %	Dutch fly ash	4.35	4.34	4.29	4.42	4.35	0.05	4.35
10 %	Dutch fly ash	3.53	3.39	3.62	3.49	3.51	0.10	3.53
5 %	Indian fly ash	4.01	4.15	3.88	4.02	4.02	0.11	4.01
10 %	Indian fly ash	3.74	4.01	3.49	4.00	3.81	0.25	3.74
15 %	Indian fly ash	3.33	3.14	3.33	3.42	3.31	0.12	3.33

A.2.2.3 SPECIFIC DENSITY AND POROSITY

Table 60: Specific density and porosity measurements of all additive substitutions

	Additives	Specific density	Dry density	Pore vol. (dry density/ specific density)	Porosity	STD
		[kg/m³]	[kg/m³]	[%]	[%]	[%]
0 %	Reference	2348	458.5	19.5	80.5	1.4
5 %	Cyclone ash	2388	402.0	16.8	83.2	0.6
10 %	Cyclone ash	2337	383.5	16.4	83.6	0.9
5 %	Paper sludge ash	2331	476.5	20.4	79.6	1.9
10 %	Paper sludge ash	2292	473.0	20.6	79.4	0.8
15 %	Paper sludge ash	2367	496.5	21.0	79.0	1.6
5 %	Bio ash	2367	456.5	19.3	80.7	1.6
10 %	Bio ash	2452	439.5	17.9	82.1	8.7
5 %	Bottom ash	2377	453.0	19.1	80.9	1.3
10 %	Bottom ash	2373	449.0	18.9	81.1	0.7
15 %	Bottom ash	2424	447.5	18.5	81.5	0.9
5 %	Dutch fly ash	2334	455.5	19.5	80.5	0.8
10 %	Dutch fly ash	2376	458.8	19.3	80.7	1.8
5 %	Indian fly ash	2354	452.0	19.2	80.8	1.5
10 %	Indian fly ash	2328	452.0	19.4	80.6	6.0
15 %	Indian fly ash	2409	439.0	18.2	81.8	1.7

SPECIFIC DENSITY MEASUREMENTS WITH PYCNOMETER

Table 61: Specific density measurements of the reference

Reference

3 samples		Sample 1	Sample 2	Sample 3
Weight content	[g]	22.7908	22.7527	22.661
Density 1	[g/cm³]	2.3830	2.3878	2.3216
Density 2	[g/cm³]	2.3697	2.3772	2.3134
Density 3	[g/cm³]	2.3635	2.3685	2.3048
Density 4	[g/cm³]	2.3747	2.3644	2.3027
Density 5	[g/cm³]	2.3725	2.3588	2.2967
Density 6	[g/cm³]	2.3728	2.3595	2.2959
Density 7	[g/cm³]	2.3740	2.3743	2.2945
Density 8	[g/cm³]	2.3737	2.3704	2.2929
Density 9	[g/cm³]	2.3728	2.3701	2.2928
Density 10	[g/cm³]	2.3760	2.3660	2.2918
Average	[cm³]	2.3733	2.3697	2.3007
SDV	[%]	0.49	0.86	1.00
Average density	[g/cm³]	2.34		
Average density	[kg/m³]	2347		

Table 62: Specific density measurements of 5 % cyclone ash

5 % Cyclone ash

3 samples		Sample 1	Sample 2	Sample 3
Weight content	[g]	19.5447	19.2961	19.8873
Density 1	[g/cm³]	2.4095	2.3719	2.3925
Density 2	[g/cm³]	2.4084	2.3661	2.3975
Density 3	[g/cm³]	2.4030	2.3699	2.3938
Density 4	[g/cm³]	2.3965	2.373	2.3917
Density 5	[g/cm³]	2.4003	2.3694	2.3942
Density 6	[g/cm³]	2.4065	2.3678	2.3917
Density 7	[g/cm³]	2.4020	2.3668	2.3882
Density 8	[g/cm³]	2.3996	2.3673	2.3919
Density 9	[g/cm³]	2.3993	2.3677	2.3884
Density 10	[g/cm³]	2.4016	2.3640	2.3877
Average	[cm³]	2.4027	2.3684	2.3918
SDV	[%]	0.42	0.27	0.31
Average density	[g/cm³]	2.39		
Average density	[kg/m³]	2387		

Table 63: Specific density measurements of 10 % cyclone ash

10 % Cyclone ash

3 samples		Sample 1	Sample 2	Sample 3
Weight content	[g]	19.5309	19.3452	19.2525
Density 1	[g/cm³]	2.2960	2.3351	2.3937
Density 2	[g/cm³]	2.2782	2.3127	2.4097
Density 3	[g/cm³]	2.2854	2.3267	2.4070
Density 4	[g/cm³]	2.2832	2.3289	2.4077
Density 5	[g/cm³]	2.2821	2.3274	2.4063
Density 6	[g/cm³]	2.2794	2.3271	2.4076
Density 7	[g/cm³]	2.2794	2.3232	2.4038
Density 8	[g/cm³]	2.2824	2.3204	2.4038
Density 9	[g/cm³]	2.2783	2.3196	2.4003
Density 10	[g/cm³]	2.2771	2.3258	2.4029
Average	[cm³]	2.2822	2.32469	2.40428
SDV	[%]	0.55	0.61	0.46
Average density	[g/cm³]	2.3370		
Average density	[kg/m³]	2337		

Table 64: Specific density measurements of 5 % paper sludge ash

5% Paper sludge ash

3 samples		Sample 1	Sample 2	Sample 3
Weight content	[g]	23.5137	22.8519	22.7494
Density 1	[g/cm³]	2.3622	2.3377	2.3622
Density 2	[g/cm³]	2.3472	2.3273	2.3521
Density 3	[g/cm³]	2.3427	2.3215	2.3434
Density 4	[g/cm³]	2.3354	2.3181	2.3374
Density 5	[g/cm³]	2.3327	2.3149	2.3376
Density 6	[g/cm³]	2.3383	2.3107	2.3363
Density 7	[g/cm³]	2.3323	2.3085	2.3317
Density 8	[g/cm³]	2.3278	2.3088	2.3328
Density 9	[g/cm³]	2.3231	2.3064	2.3322
Density 10	[g/cm³]	2.3258	2.3055	2.3344
Average	[cm³]	2.3368	2.3159	2.3400
SDV	[%]	1.16	1.04	0.99
Average density	[g/cm³]	2.33		
Average density	[kg/m³]	2331		

Table 65: Specific density measurements of 10 % paper sludge ash

10% Paper sludge ash

3 samples		Sample 1	Sample 2	Sample 3
Weight content	[g]	23.3398	22.8984	22.6624
Density 1	[g/cm³]	2.3281	2.2706	2.3033
Density 2	[g/cm³]	2.3297	2.2577	2.2974
Density 3	[g/cm³]	2.3203	2.2579	2.2973
Density 4	[g/cm³]	2.3256	2.2551	2.2964
Density 5	[g/cm³]	2.3257	2.2565	2.2917
Density 6	[g/cm³]	2.3268	2.2548	2.2916
Density 7	[g/cm³]	2.3243	2.2531	2.2928
Density 8	[g/cm³]	2.3205	2.2529	2.2878
Density 9	[g/cm³]	2.3272	2.252	2.2917
Density 10	[g/cm³]	2.3261	2.2529	2.2888
Average	[cm³]	2.3254	2.25635	2.29388
SDV	[%]	0.30	0.54	0.47
Average density	[g/cm³]	2.2919		
Average density	[kg/m³]	2292		

Table 66: Specific density measurements of 15 % paper sludge ash

15 % Paper sludge ash

3 samples		Sample 1	Sample 2	Sample 3
Weight content	[g]	23.6715	24.6035	24.1910
Density 1	[g/cm³]	2.3624	2.4274	2.3721
Density 2	[g/cm³]	2.3558	2.4125	2.3588
Density 3	[g/cm³]	2.3527	2.4045	2.3540
Density 4	[g/cm³]	2.3559	2.4002	2.3469
Density 5	[g/cm³]	2.3557	2.3966	2.3427
Density 6	[g/cm³]	2.3556	2.3932	2.3421
Density 7	[g/cm³]	2.3556	2.3932	2.3403
Density 8	[g/cm³]	2.3482	2.3946	2.3399
Density 9	[g/cm³]	2.3496	2.3906	2.3376
Density 10	[g/cm³]	2.3497	2.3989	2.3375
Average	[cm³]	2.3541	2.40117	2.34719
SDV	[%]	0.42	1.12	1.12
Average density	[g/cm³]	2.3675		
Average density	[kg/m³]	2367		

Table 67: Specific density measurements of 5 % bio ash

5% Bio ash

3 samples		Sample 1	Sample 2	Sample 3
Weight content	[g]	22.7058	21.7644	21.4195
Density 1	[g/cm³]	2.4244	2.3331	2.3968
Density 2	[g/cm³]	2.4131	2.3205	2.3967
Density 3	[g/cm³]	2.4181	2.3113	2.3787
Density 4	[g/cm³]	2.4180	2.3104	2.3749
Density 5	[g/cm³]	2.4215	2.3036	2.3714
Density 6	[g/cm³]	2.4178	2.3018	2.3687
Density 7	[g/cm³]	2.4186	2.3042	2.3695
Density 8	[g/cm³]	2.4196	2.2991	2.3687
Density 9	[g/cm³]	2.4124	2.3037	2.3656
Density 10	[g/cm³]	2.4150	2.3002	2.3643
Average	[cm³]	2.4179	2.3088	2.3755
SDV	[%]	0.37	1.07	1.19
Average density	[g/cm³]	2.37		
Average density	[kg/m³]	2367		

Table 68: Specific density measurements of 10 % bio ash

10 % Bio ash

3 samples		Sample 1	Sample 2	Sample 3
Weight content	[g]	21.4028	21.4944	21.2415
Density 1	[g/cm³]	2.4350	2.4187	2.5059
Density 2	[g/cm³]	2.4224	2.4099	2.4945
Density 3	[g/cm³]	2.4415	2.3992	2.4868
Density 4	[g/cm³]	2.4421	2.3966	2.4826
Density 5	[g/cm³]	2.4389	2.4143	2.4808
Density 6	[g/cm³]	2.4368	2.3952	2.4786
Density 7	[g/cm³]	2.4372	2.3892	2.7560
Density 8	[g/cm³]	2.4381	2.4139	2.4781
Density 9	[g/cm³]	2.4344	2.4180	2.4967
Density 10	[g/cm³]	2.4320	2.4180	2.4768
Average	[cm³]	2.4358	2.4073	2.5137
SDV	[%]	0.56	1.11	8.57
Average density	[g/cm³]	2.4523		
Average density	[kg/m³]	2452		

Table 69: Specific density measurements of 5 % bottom ash

5% Bottom ash

3 samples		Sample 1	Sample 2	Sample 3
Weight content	[g]	21.4118	21.4019	21.2110
Density 1	[g/cm³]	2.4225	2.3884	2.3595
Density 2	[g/cm³]	2.4050	2.3885	2.3493
Density 3	[g/cm³]	2.3971	2.3841	2.3546
Density 4	[g/cm³]	2.3902	2.3844	2.3530
Density 5	[g/cm³]	2.3871	2.3809	2.3513
Density 6	[g/cm³]	2.3883	2.3853	2.3545
Density 7	[g/cm³]	2.3858	2.3827	2.3526
Density 8	[g/cm³]	2.3849	2.3871	2.3505
Density 9	[g/cm³]	2.3849	2.3766	2.3505
Density 10	[g/cm³]	2.3821	2.3809	2.3570
Average	[cm³]	2.3928	2.3839	2.3533
SDV	[%]	1.25	0.38	0.32
Average density	[g/cm³]	2.38		
Average density	[kg/m³]	2377		

Table 70: Specific density measurements of 10 % bottom ash

10 % Bottom ash

3 samples		Sample 1	Sample 2	Sample 3
Weight content	[g]	22.1095	21.7656	22.7317
Density 1	[g/cm³]	2.3665	2.3808	2.3888
Density 2	[g/cm³]	2.3626	2.3839	2.3716
Density 3	[g/cm³]	2.3626	2.3865	2.3785
Density 4	[g/cm³]	2.3607	2.3751	2.3718
Density 5	[g/cm³]	2.3568	2.3845	2.3745
Density 6	[g/cm³]	2.3604	2.3764	2.3766
Density 7	[g/cm³]	2.3547	2.3816	2.3743
Density 8	[g/cm³]	2.3596	2.3834	2.3733
Density 9	[g/cm³]	2.3597	2.3853	2.3738
Density 10	[g/cm³]	2.3584	2.3823	2.3777
Average	[cm³]	2.3602	2.3820	2.3761
SDV	[%]	0.33	0.37	0.50
Average density	[g/cm³]	2.3728		
Average density	[kg/m³]	2373		

Table 71: Specific density measurements of 15 % bottom ash

15 % Bottom ash

3 samples		Sample 1	Sample 2	Sample 3
Weight content	[g]	21.8757	21.6444	21.6939
Density 1	[g/cm³]	2.3766	2.4023	2.5261
Density 2	[g/cm³]	2.3572	2.3981	2.5227
Density 3	[g/cm³]	2.3593	2.3986	2.5162
Density 4	[g/cm³]	2.3616	2.3990	2.5099
Density 5	[g/cm³]	2.3567	2.3971	2.5108
Density 6	[g/cm³]	2.3603	2.3991	2.5133
Density 7	[g/cm³]	2.3580	2.3934	2.5125
Density 8	[g/cm³]	2.3561	2.3982	2.5111
Density 9	[g/cm³]	2.3617	2.3938	2.5115
Density 10	[g/cm³]	2.3631	2.3931	2.5080
Average	[cm³]	2.3611	2.3973	2.5142
SDV	[%]	0.59	0.30	0.58
Average density	[g/cm³]	2.4242		
Average density	[kg/m³]	2424		

Table 72: Specific density measurements of 5 % Dutch fly ash

5 % Dutch fly ash

3 samples		Sample 1	Sample 2	Sample 3
Weight content	[g]	22.2016	23.1187	21.2555
Density 1	[g/cm³]	2.2662	2.4015	2.3528
Density 2	[g/cm³]	2.2574	2.3933	2.3473
Density 3	[g/cm³]	2.2464	2.4004	2.3357
Density 4	[g/cm³]	2.2528	2.4067	2.3428
Density 5	[g/cm³]	2.2564	2.3990	2.3368
Density 6	[g/cm³]	2.2579	2.3998	2.3465
Density 7	[g/cm³]	2.2560	2.3995	2.3443
Density 8	[g/cm³]	2.2506	2.3968	2.3511
Density 9	[g/cm³]	2.2567	2.4017	2.3475
Density 10	[g/cm³]	2.2559	2.4006	2.3450
Average	[cm³]	2.2556	2.3999	2.3450
SDV	[%]	0.52	0.34	0.55
Average density	[g/cm³]	2.33		
Average density	[kg/m³]	2334		

Table 73: Specific density measurements of 10 % Dutch fly ash

10 % Dutch fly ash

3 samples		Sample 1	Sample 2	Sample 3
Weight content	[g]	22.1165	22.6446	22.6823
Density 1	[g/cm³]	2.3629	2.3856	2.4463
Density 2	[g/cm³]	2.3538	2.3757	2.4333
Density 3	[g/cm³]	2.3472	2.3743	2.4228
Density 4	[g/cm³]	2.3412	2.3699	2.4226
Density 5	[g/cm³]	2.3368	2.3632	2.4169
Density 6	[g/cm³]	2.3360	2.3629	2.4148
Density 7	[g/cm³]	2.3358	2.3627	2.4137
Density 8	[g/cm³]	2.3358	2.3570	2.4124
Density 9	[g/cm³]	2.3338	2.3581	2.4108
Density 10	[g/cm³]	2.3317	2.3556	2.4118
Average	[cm³]	2.3415	2.3665	2.4205
SDV	[%]	1.01	0.97	1.14
Average density	[g/cm³]	2.3762		
Average density	[kg/m³]	2376		

Table 74: Specific density measurements of 5 % Indian fly ash

5 % Indian fly ash

3 samples		Sample 1	Sample 2	Sample 3
Weight content	[g]	22.2545	22.3395	22.4341
Density 1	[g/cm³]	2.3323	2.3455	2.4301
Density 2	[g/cm³]	2.3280	2.3350	2.4328
Density 3	[g/cm³]	2.3188	2.3315	2.4220
Density 4	[g/cm³]	2.3120	2.3229	2.4229
Density 5	[g/cm³]	2.3136	2.3205	2.4221
Density 6	[g/cm³]	2.3109	2.3191	2.4180
Density 7	[g/cm³]	2.3157	2.3160	2.4139
Density 8	[g/cm³]	2.3089	2.3181	2.4217
Density 9	[g/cm³]	2.3090	2.3373	2.4155
Density 10	[g/cm³]	2.3084	2.3191	2.4109
Average	[cm³]	2.3158	2.3265	2.4210
SDV	[%]	0.83	1.01	0.68
Average density	[g/cm³]	2.35		
Average density	[kg/m³]	2354		

Table 75: Specific density measurements of 10 % Indian fly ash

10 % Indian fly ash

3 samples		Sample 1	Sample 2	Sample 3
Weight content	[g]	22.0540	22.9158	21.9329
Density 1	[g/cm³]	2.3270	2.3967	2.3365
Density 2	[g/cm³]	2.3179	2.3866	2.3238
Density 3	[g/cm³]	2.3168	2.3815	2.3200
Density 4	[g/cm³]	2.3141	2.3800	2.1342
Density 5	[g/cm³]	2.3079	2.3789	2.3134
Density 6	[g/cm³]	2.3053	2.3732	2.3133
Density 7	[g/cm³]	2.3010	2.3733	2.3086
Density 8	[g/cm³]	2.2989	2.3698	2.3092
Density 9	[g/cm³]	2.2965	2.3689	2.3075
Density 10	[g/cm³]	2.3081	2.3724	2.3058
Average	[cm³]	2.3094	2.3781	2.2972
SDV	[%]	0.96	0.86	5.80
Average density	[g/cm³]	2.3282		
Average density	[kg/m³]	2328		

Table 76: Specific density measurements of 15 % Indian fly ash

15 % Indian fly ash

3 samples		Sample 1	Sample 2	Sample 3
Weight content	[g]	21.0909	21.0690	21.5559
Density 1	[g/cm³]	2.4213	2.4181	2.4396
Density 2	[g/cm³]	2.4114	2.4177	2.4322
Density 3	[g/cm³]	2.4076	2.4100	2.4185
Density 4	[g/cm³]	2.4010	2.4067	2.4176
Density 5	[g/cm³]	2.3989	2.4029	2.4140
Density 6	[g/cm³]	2.3955	2.4028	2.4098
Density 7	[g/cm³]	2.3961	2.4000	2.4100
Density 8	[g/cm³]	2.3962	2.4227	2.4086
Density 9	[g/cm³]	2.3890	2.4022	2.4026
Density 10	[g/cm³]	2.3913	2.4181	2.4074
Average	[cm³]	2.4008	2.4101	2.4160
SDV	[%]	0.99	0.83	1.16
Average density	[g/cm³]	2.4090		
Average density	[kg/m³]	2409		

A.2.2.4 THERMAL CONDUCTIVITY

Table 77: Measurement of thermal conductivity of all additive substitutions

		Thermal conductivity			
	Additives	Sample1	Sample 2	Average	STD
		[W/m.K]	[W/m.K]	[W/m.K]	[%]
0 %	Reference	0.0964	0.0971	0.0968	0.05
5 %	Cyclone ash	0.0885	0.0883	0.0884	0.01
10 %	Cyclone ash	0.0837	0.0831	0.0834	0.04
5 %	Paper sludge ash	0.1010	0.0963	0.0987	0.33
10 %	Paper sludge ash	0.0977	0.0988	0.0983	0.08
15 %	Paper sludge ash	0.1020	0.1020	0.1020	0.00
5 %	Bio ash	0.0994	0.0978	0.0986	0.11
10 %	Bio ash	0.0967	0.0939	0.0953	0.20
5 %	Bottom ash	0.0940	0.0956	0.0948	0.11
10 %	Bottom ash	0.0948	0.0947	0.0948	0.01
15 %	Bottom ash	0.0919	0.0944	0.0932	0.18
5 %	Dutch fly ash	0.0973	0.0983	0.0978	0.07
10 %	Dutch fly ash	0.0986	0.0983	0.0985	0.02
5 %	Indian fly ash	0.0961	0.0974	0.0968	0.09
10 %	Indian fly ash	0.1000	0.1000	0.1000	0.00
15 %	Indian fly ash	0.0925	0.0948	0.0937	0.16

A.2.3 MINERAL PHASES ANALYSIS

Table 78: Measurement of mineral phases of all additive substitutions

		Tobermorite		Quartz		Anhydrite	Calcite
		11.3 Å (Quantity)	3.08 Å (Quality)	3.34 Å (peak 1)	4.26 Å (peak 2)	3.53 Å (peak 1)	3.04 Å (peak 1)
		[counts]	[counts]	[counts]	[counts]	[counts]	[counts]
0 %	Reference	439	953	9368	1336	234	312
5 %	Cyclone ash	272	792	12799	1160	1387	661
10 %	Cyclone ash	467	1357	9111	1608	628	526
5 %	Paper sludge ash	381	998	6924	966	252	455
10 %	Paper sludge ash	473	1125	5926	1319	312	626
15 %	Paper sludge ash	473	1155	5024	1650	305	817
5 %	Bio ash	446	875	9022	1752	330	346
10 %	Bio ash	453	972	11336	1785	700	269
5 %	Bottom ash	386	1097	7842	1133	259	338
10 %	Bottom ash	376	931	10648	1711	302	580
15 %	Bottom ash	341	925	4975	1206	231	449
5 %	Dutch fly ash	538	1116	6886	1119	295	346
10 %	Dutch fly ash	599	1058	10117	1035	423	345
5 %	Indian fly ash	523	911	6415	1076	522	298
10 %	Indian fly ash	683	1508	10987	1551	511	592
15 %	Indian fly ash	462	1069	10591	1845	529	375

A.2.4 ECONOMIC ASPECT

Table 79: Percentage and price per ton of raw material in recipe

Price	[% of total recipe]	[€ per ton]
Quartz	66.67	€ 20.00
Lime	8.33	€ 10.00
Cement	20.00	€ 80.00
Gypsum	2.50	€ 70.00
Lime hydrate	2.50	€ 70.00
Alternative 1	5 - 10 - 15	€ 10.00
Alternative 2	5 - 10 - 15	€ 5.00
Paper sludge ash	5 - 10 - 15	€ 20.00

Table 80: Calculation recipe

Replace quartz

Quartz	Lime	Cement	Gypsum	Lime hydrate	**Additive (€5)**	**Total cost**
(€20 x 66.7%) + (€10 x 8.3%) + (€80 x 20%) + (€70 x 2.5 %) + (€70 x 2.5 %) =						€ 33.67
(€20 x 61.7%) + (€10 x 8.3%) + (€80 x 20%) + (€70 x 2.5 %) + (€70 x 2.5 %) + (€5 x 5%) =						€ 33.17
(€20 x 56.7%) + (€10 x 8.3%) + (€80 x 20%) + (€70 x 2.5 %) + (€70 x 2.5 %) + (€5 x 10%) =						€ 32.67
(€20 x 51.7%) + (€10 x 8.3%) + (€80 x 20%) + (€70 x 2.5 %) + (€70 x 2.5 %) + (€5 x 15%) =						€ 32.17

Table 81: Price recipe and reduction

	Additive 1 (€ 10.00 p. ton)			Additive 2 (€ 5.00 p. ton)		
	Price	Reduction	Reduction	Price	Reduction	Reduction
	[€]	[€]	[%]	[€]	[€]	[%]
Reference	33.67	-	-	33.67	-	-
5 %	33.17	0.50	1.5	32.92	0.75	2.3
10 %	32.67	1.00	3.1	32.17	1.50	4.7
15 %	32.17	1.50	4.7	31.42	2.25	7.2

A.3 PORTLAND CEMENT SUBSTITUTION RESULTS

A.3.1 MEASUREMENTS DURING CURING PERIOD

A.3.1.1 RISING HEIGHT, TEMPERATURE OF HYDRATION AND PENETRATION DEPTH

Table 82: Measurements of rising height, temperature of hydration and penetration depth of all substitutions
Specifications for the different substitutions

Substitution level	Slump flow	Final product height	w/s ratio	Aluminum amount
[%]	[cm]	[cm]	[-]	[g]
0	33.0	30.0	0.580	14
10	32.5	30.5	0.580	14
20	30.0	29.0	0.580	14
30	28.0	27.5	0.580	14
40	27.0	27.0	0.595	14
50	26.0	28.0	0.608	14

Table 83: Rising height, temperature of hydration and penetration depth of reference
Reference

Time	Rising height	Temperature	Penetration depth
[min]	[cm]	[°C]	[cm]
0	-	-	
5	15.6	50.6	
10	17.7	52.1	
15	18.3	53.4	
20	18.9	55.0	
25	19.4	56.9	
30	19.8	58.6	
35	20.2	60.5	
40	20.5	62.1	>>10
45	20.4	63.6	8.5
50	20.1	65.0	6.5
55	19.9	66.1	5.0
60	19.8	67.1	3.8

Table 84: Rising height, temperature of hydration and penetration depth of 10 % paper sludge ash
10 % Paper sludge ash

Time	Rising height	Temperature	Penetration depth
[min]	[cm]	[°C]	[cm]
0	5	46.4	
5	15.4	51.4	
10	18.2	53.6	
15	19.2	55.3	
20	19.7	57.3	
25	20.2	59.4	
30	20.6	61.7	>>10
35	20.6	63.4	9.2
40	20.1	65.1	7.4
45	19.9	66.5	5.5
50	19.8	67.7	3.5
55	19.7	68.8	3.3
60	19.7	69.9	2.8

Table 85: Rising height, temperature of hydration and penetration depth of 20 % paper sludge ash

20 % Paper sludge ash

Time	Rising height	Temperature	Penetration depth
[min]	[cm]	[°C]	[cm]
0	5.5	47.5	
5	15.8	52.1	
10	18.5	54.1	
15	19.4	56.0	
20	20.0	58.3	
25	20.6	60.7	
30	20.7	63.0	>>10
35	19.7	65.3	6.8
40	19.5	66.9	5.3
45	19.5	68.5	3.7
50	19.4	69.6	3.1
55	19.4	70.6	2.5
60	19.4	71.5	2.2

Table 86: Rising height, temperature of hydration and penetration depth of 30 % paper sludge ash

30 % Paper sludge ash

Time	Rising height	Temperature	Penetration depth
[min]	[cm]	[°C]	[cm]
0	5.2	47.7	
5	15.5	53.3	
10	17.8	55.5	
15	18.8	57.6	>>10
20	19.4	60.3	-
25	19.5	62.9	9.5
30	18.5	65.3	7.0
35	18.1	67.7	4.7
40	18.0	68.8	4.0
45	18.0	70.2	3.0
50	18.0	71.3	2.6
55	18.0	72.0	2.2
60	18.0	72.8	2.2

Table 87: Rising height, temperature of hydration and penetration depth of 40 % paper sludge ash

40 % Paper sludge ash

Time	Rising height	Temperature	Penetration depth
[min]	[cm]	[°C]	[cm]
0	4.8	46.5	
5	15.5	52.2	
10	18.6	54.5	
15	19.8	56.6	>>10
20	20.4	58.9	>>10
25	19.7	61.5	9.5
30	18.7	63.6	7.5
35	18.4	65.6	4.8
40	18.3	67.1	3.9
45	18.3	68.5	3.2
50	18.3	69.6	2.8
55	18.4	70.5	2.3
60	18.3	71.3	1.8

Table 88: Rising height, temperature of hydration and penetration depth of 50 % paper sludge ash

50 % Paper sludge ash

Time	Rising height	Temperature	Penetration depth
[min]	[cm]	[°C]	[cm]
0	6.2	45.8	
5	16.5	52.9	
10	19.1	55.9	
15	20.0	57.8	>>10
20	19.7	59.8	10.0
25	18.5	62.3	7.5
30	18.0	64.6	5.7
35	17.9	66.6	3.5
40	17.9	68.3	2.9
45	17.9	69.4	2.7
50	17.9	70.3	2.3
55	17.9	71.2	2.0
60	17.9	72.0	1.8

A.3.2 PHYSICAL PROPERTIES MEASUREMENTS

A.3.2.1 DRY DENSITY

Table 89: Dry density measurements of all paper sludge ash substitutions

	Dry density					
Paper sludge ash	Sample 1	Sample 2	Sample 3	Sample 4	Average	STD
[%]	[kg/m³]	[kg/m³]	[kg/m³]	[kg/m³]	[kg/m³]	[%]
0	448	450	446	454	449.5	3.4
10	444	452	442	452	447.5	5.3
20	452	460	452	462	456.5	5.3
30	468	480	470	486	476.0	8.5
40	464	478	464	478	471.0	8.1
50	476	486	476	484	480.5	5.3

A.3.2.2 COMPRESSIVE STRENGTH AND COMPENSATED COMPRESSIVE STRENGTH

Table 90: CS and CCS measurements of all paper sludge ash substitutions

	CS						CCS
Paper sludge ash	Sample 1	Sample 2	Sample 3	Sample 4	Average	STD	
[%]	[N/mm²]	[N/mm²]	[N/mm²]	[N/mm²]	[N/mm²]	[%]	[N/mm²]
0	4.49	4.66	4.38	4.72	4.56	15.6	4.57
10	4.49	4.53	4.53	4.73	4.57	10.8	4.60
20	4.60	4.79	4.34	4.77	4.63	20.8	4.56
30	4.51	4.79	4.58	5.12	4.75	27.4	4.49
40	4.26	4.72	4.50	5.08	4.64	34.8	4.43
50	4.58	4.78	4.56	4.99	4.73	20.1	4.43

A.3.2.3 SPECIFIC DENSITY AND POROSITY

Table 91: Specific density and porosity measurements of all paper sludge ash substitutions

	Dry density	Specific density	Pore vol. (dry density/ specific density)	Porosity
	[kg/m³]	[kg/m³]	[%]	[%]
0%	449.5	2382	18.9	81.1
10%	447.5	2395	18.7	81.3
20%	456.5	2436	18.7	81.3
30%	476.0	2440	19.5	80.5
40%	471.0	2502	18.8	81.2
50%	480.5	2538	18.9	81.1

SPECIFIC DENSITY MEASUREMENTS WITH PYCNOMETER

Table 92: Specific density measurements of reference

Reference

3 samples		Sample 1	Sample 2	Sample 3
Weight empty cup	[g]	36.5008	36.4985	36.5142
Weight filled cup	[g]	59.1172	59.6833	59.2825
Weight content	[g]	22.6164	23.1848	22.7683
Volume 1	[cm³]	9.4838	9.7373	9.4394
Volume 2	[cm³]	9.4942	9.7513	9.5052
Volume 3	[cm³]	9.5005	9.7731	9.5409
Volume 4	[cm³]	9.5247	9.7061	9.5746
Volume 5	[cm³]	9.5113	9.6946	9.6069
Volume 6	[cm³]	9.5233	9.7037	9.5925
Volume 7	[cm³]	9.4724	9.6997	9.5643
Volume 8	[cm³]	9.5264	9.7258	9.5964
Volume 9	[cm³]	9.4952	9.7121	9.5900
Volume 10	[cm³]	9.5451	9.7128	9.6129
Average	[cm³]	9.5077	9.7217	9.5623
SDV	[%]	2.2	2.5	5.4
Density (m/V)	[g/cm³]	2.379	2.385	2.381
Density (m/V)	[kg/m³]	2379	2385	2381
Average density	[g/cm³]	2382		

Table 93: Specific density measurements of 10 % paper sludge ash

10 % Paper sludge ash

3 samples		Sample 1	Sample 2	Sample 3
Weight empty cup	[g]	36.5003	36.5003	36.5008
Weight filled cup	[g]	58.8446	58.7507	58.7385
Weight content	[g]	22.3443	22.2504	22.2377
Volume 1	[cm³]	9.2179	9.2859	9.2859
Volume 2	[cm³]	9.264	9.306	9.2853
Volume 3	[cm³]	9.262	9.3221	9.2812
Volume 4	[cm³]	9.2699	9.3217	9.2947
Volume 5	[cm³]	9.2812	9.3392	9.289
Volume 6	[cm³]	9.294	9.3439	9.2965
Volume 7	[cm³]	9.2873	9.3539	9.3064
Volume 8	[cm³]	9.2851	9.3452	9.3078
Volume 9	[cm³]	9.3029	9.3417	9.3135
Volume 10	[cm³]	9.3085	9.362	9.3234
Average	[cm³]	9.2773	9.3322	9.2984
SDV	[%]	2.6	2.3	1.4
Density (m/V)	[g/cm³]	2.408	2.384	2.392
Density (m/V)	[kg/m³]	2408	2384	2392
Average density	[g/cm³]	2395		

Table 94: Specific density measurements of 20 % paper sludge ash

20 % Paper sludge ash

3 samples		Sample 1	Sample 2	Sample 3
Weight empty cup	[g]	36.5008	36.4993	36.4997
Weight filled cup	[g]	58.9816	58.4324	58.4575
Weight content	[g]	22.4808	21.9331	21.9578
Volume 1	[cm³]	9.2059	8.9890	8.9811
Volume 2	[cm³]	9.2232	8.9908	9.0053
Volume 3	[cm³]	9.2453	9.0367	8.9662
Volume 4	[cm³]	9.2447	8.9969	8.9559
Volume 5	[cm³]	9.2455	9.0102	9.0628
Volume 6	[cm³]	9.2394	9.0096	8.9927
Volume 7	[cm³]	9.2396	9.0096	9.0128
Volume 8	[cm³]	9.2366	9.0670	9.0171
Volume 9	[cm³]	9.2389	9.0316	9.0122
Volume 10	[cm³]	9.2458	9.0067	8.9816
Average	[cm³]	9.2365	9.0148	8.9988
SDV	[%]	1.3	2.4	3.1
Density (m/V)	[g/cm³]	2.434	2.433	2.440
Density (m/V)	[kg/m³]	2434	2433	2440
Average density	[g/cm³]	2436		

Table 95: Specific density measurements of 30 % paper sludge ash

30 % Paper sludge ash

3 samples		Sample 1	Sample 2	Sample 3
Weight empty cup	[g]	36.4999	36.5004	36.5002
Weight filled cup	[g]	59.8366	60.3045	60.3795
Weight content	[g]	23.3367	23.8041	23.8793
Volume 1	[cm³]	9.5314	9.6747	9.8750
Volume 2	[cm³]	9.4896	9.7010	9.9041
Volume 3	[cm³]	9.5276	9.6701	9.9052
Volume 4	[cm³]	9.5235	9.6806	9.9002
Volume 5	[cm³]	9.5067	9.6440	9.8999
Volume 6	[cm³]	9.5242	9.6792	9.9167
Volume 7	[cm³]	9.5127	9.7128	9.9032
Volume 8	[cm³]	9.5064	9.6975	9.9021
Volume 9	[cm³]	9.5490	9.6883	9.9227
Volume 10	[cm³]	9.5272	9.6868	9.9155
Average	[cm³]	9.5198	9.6835	9.9045
SDV	[%]	1.6	1.9	1.3
Density (m/V)	[g/cm³]	2.451	2.458	2.411
Density (m/V)	[kg/m³]	2451	2458	2411
Average density	[g/cm³]	2440		

Table 96: Specific density measurements of 40 % paper sludge ash

40 % Paper sludge ash

3 samples		Sample 1	Sample 2	Sample 3
Weight empty cup	[g]	36.5005	36.499	36.5002
Weight filled cup	[g]	59.0902	58.8523	59.6082
Weight content	[g]	22.5897	22.3533	23.1080
Volume 1	[cm³]	9.0907	8.9676	9.2336
Volume 2	[cm³]	9.0097	8.9394	9.2707
Volume 3	[cm³]	9.0244	8.9045	9.2334
Volume 4	[cm³]	9.0256	8.8732	9.2129
Volume 5	[cm³]	8.9984	8.9379	9.2554
Volume 6	[cm³]	9.0083	8.9390	9.2422
Volume 7	[cm³]	9.0481	8.9009	9.2789
Volume 8	[cm³]	9.0131	8.9005	9.2443
Volume 9	[cm³]	9.0319	8.9623	9.2886
Volume 10	[cm³]	9.0080	8.8914	9.2388
Average	[cm³]	9.0258	8.9217	9.2499
SDV	[%]	2.7	3.2	2.3
Density (m/V)	[g/cm³]	2.503	2.506	2.498
Density (m/V)	[kg/m³]	2503	2506	2498
Average density	[g/cm³]	2502		

Table 97: Specific density measurements of 50 % paper sludge ash

50 % Paper sludge ash

3 samples		Sample 1	Sample 2	Sample 3
Weight empty cup	[g]	36.5011	36.5003	36.4996
Weight filled cup	[g]	58.7023	59.6232	58.5046
Weight content	[g]	22.2012	23.1229	22.0050
Volume 1	[cm³]	8.6928	9.1290	8.7096
Volume 2	[cm³]	8.7420	9.1400	8.6382
Volume 3	[cm³]	8.7309	9.1639	8.6484
Volume 4	[cm³]	8.7229	9.1498	8.6423
Volume 5	[cm³]	8.7061	9.1152	8.6418
Volume 6	[cm³]	8.6907	9.1313	8.6617
Volume 7	[cm³]	8.7277	9.1417	8.6603
Volume 8	[cm³]	8.7619	9.2049	8.6467
Volume 9	[cm³]	8.7728	9.1323	8.6867
Volume 10	[cm³]	8.7420	9.1413	8.6772
Average	[cm³]	8.7290	9.1449	8.6613
SDV	[%]	2.7	2.5	2.3
Density (m/V)	[g/cm³]	2.543	2.528	2.541
Density (m/V)	[kg/m³]	2543	2528	2541
Average density	[g/cm³]	2537		

A.3.2.4 THERMAL CONDUCTIVITY

Table 98: Thermal conductivity measurements of all paper sludge ash substitutions

	Thermal conductivity			
	Measurement 1	Measurement 2	Average	STD
	[W/m.K]	[W/m.K]	[W/m.K]	[%]
0 %	0.0998	0.1020	0.1009	0.16
10 %	0.1020	0.1010	0.1015	0.07
20 %	0.1020	0.1010	0.1015	0.07
30 %	0.1060	0.1070	0.1065	0.07
40 %	0.1030	0.1040	0.1035	0.07
50 %	0.1040	0.1030	0.1035	0.07

A.3.3 MINERAL PHASES ANALYSIS

Table 99: Mineral phases analysis of all paper sludge ash substitutions

	Tobermorite		Quartz		Anhydrite	Calcite
	11.3 Å (Quantity)	3.08 Å (Quality)	3.34 Å (peak 1)	4.26 Å (peak 2)	3.53 Å (peak 1)	3.04 Å (peak 1)
	[counts]	[counts]	[counts]	[counts]	[counts]	[counts]
0 %	960	428	9963	1671	341	390
10 %	936	404	9206	1176	367	331
20 %	704	313	11482	1521	832	997
30 %	789	375	7843	1164	409	914
40 %	855	352	10252	1485	498	675
50 %	812	489	6174	1821	421	611

A.3.4 ECONOMIC ASPECT

Table 100: Economic measurements all paper sludge ash substitutions

Paper sludge ash (€ 20.00 p. ton)

	Price	Reduction	Reduction
	[€]	[€]	[%]
0 %	33.67	-	-
10 %	32.47	1.2	4
20 %	31.27	2.4	7
30 %	30.07	3.6	11
40 %	28.87	4.8	14
50 %	27.67	6.0	18

Table 101: Calculation recipe

Quartz	Lime	Cement	Gypsum	Anhydrite	Paper sludge ash	Total cost
(€20 x 66.7%) + (€10 x 8.3%) + (€80 x 20%) + (€70 x 2.5 %) + (€70 x 2.5 %) =						€ 33.67
(€20 x 66.7%) + (€10 x 8.3%) + (€80 x 18%) + (€70 x 2.5 %) + (€70 x 2.5 %) + (€20 x 2%) =						€ 32.47
(€20 x 66.7%) + (€10 x 8.3%) + (€80 x 16%) + (€70 x 2.5 %) + (€70 x 2.5 %) + (€20 x 4%) =						€ 31.27
(€20 x 66.7%) + (€10 x 8.3%) + (€80 x 14%) + (€70 x 2.5 %) + (€70 x 2.5 %) + (€20 x 6%) =						€ 30.07
(€20 x 66.7%) + (€10 x 8.3%) + (€80 x 12%) + (€70 x 2.5 %) + (€70 x 2.5 %) + (€20 x 8%) =						€ 28.87

Filename:	part3_final_24-08-2012
Directory:	C:\Program Files\Microsoft Office\Office12
Template:	C:\Users\s091425\AppData\Roaming\Microsoft\Templates\Normal.dotm
Title:	New recipe for Autoclaved Aerated Concrete (AAC)
Subject:	
Author:	Student
Keywords:	
Comments:	
Creation Date:	8/24/2012 9:35:00 PM
Change Number:	5
Last Saved On:	8/25/2012 3:01:00 PM
Last Saved By:	Student
Total Editing Time:	3 Minutes
Last Printed On:	8/27/2012 11:38:00 AM
As of Last Complete Printing	
Number of Pages:	27
Number of Words:	5,895 (approx.)
Number of Characters:	33,603 (approx.)